信州大学審査学位論文

Iodine Utilization for Functionalizations of High Performance Fibers

September, 2011

Ummul Khair Fatema

Acknowledgements

The guidance of my advisor, Dr. Yasuo Gotoh, Associate Professor, Shinshu University, has immensely valuable in my development as a researcher, as a professional, and as a person. I would like to express my sincere gratitude to him to confer me into his research group and work with this interesting topic. My accomplishments were made possible by his sincere support, insightful feedback, tireless care and stimulating interest of this subject matter throughout my research. Without his invaluable advice with a continuous stream of suggestions, this dissertation would not have been completed. I am appreciative of all that I have learned under his mentorship, and I am confident that his teaching will benefit me throughout my career.

I would like to thank my thesis committee members Prof. Fujio Okino, Prof. Hisanao Usami, Prof. Yutaka Ohkoshi and Prof. Hideaki Morikawa of Shinshu University and Prof. Yoshifumi Aoi of Ryukoku University for their commitment to my education and for their significant contributions to my research.

I gratefully appreciate the financial support of Ministry of Education, Culture, Sports, Science, and Technology (MEXT), Japan that gave opportunity to carry out my research in Shinshu University, Japan.

I have been fortunate to work with several talented co-workers Dr. Ahmed Jalal Uddin, Dr. Takuya Tetsumoto, Mr. Yamamoto, Ms. Tomizawa, Mr. Ishikawa and Mr. Ueamura. I really owe for their spontaneous support and assistance in laboratory. I am also grateful to all other members of Gotoh Laboratory for their good collaboration and being so kind during my research. Their hard work and creativity were critical to the completion of this research.

Finally I am very grateful to my parents for their dedication, endless support, and encouragement during the long years of study, with a particular thanks to my beloved husband Mr. Matiul Islam for his confidence in my research ability and his patience. Without their loving support the present work would be impossible to be finished.

Ummul Khair Fatema

September, 2011

Contents

Chapter 1

General introduction

1.1 Overview of iodine

Iodine is a shiny, blue-black nonmetallic element, which derives its name from the Greek word 'iodes' that means 'violet' in reference to its color. It is a micronutrient element that is fundamental to a living body and is essential for the subsistence and the growth of humans and animals, and thus considered as a life and wisdom element. In the past decade, the organic chemistry of iodine has experienced a rapid development. This growing interest in iodine compounds is mainly due to the mild and highly selective oxidizing properties of hypervalent iodine reagents, combined with their benign environmental character and commercial availability. Organic iodine(III) and iodine(V) derivatives are now routinely used in organic syntheses for various selective oxidative transformations of complex organic molecules.

The world-wide total production of iodine per year is roughly 28 thousand metric tons and the production is dominated by Chile (50%) and Japan (35%), with smaller amounts produced in the USA (5%) and the CIS (5%) [1–3]. Iodine profound areas in Japan are Chiba, Niigata and Miyazaki prefecture; of which Chiba prefecture accounts for 90% of the total production. From an industrial standpoint, it can only be extracted as iodine containing resources. Iodine is a precious resource for Japan. Here, iodine is obtained from seaweed, seawater, minerals, marine organisms and brines. Seawater contains only about 0.05 part per million iodine, but some species of seaweed, brine are able to concentrate this iodine manyfold, so that commercial extraction of the iodine is possible. The manufacture of iodine from brine usually follwed the following two methods [4]:

1. Blowing-out method

This method takes advantage of the easy vaporization property of iodine and is suited to processing brine at high temperature. First, sand and impurities in the brine are settled out and removed. An oxidizing agent is added and the brine is oxidized. The oxidized brine diffuses to the top of a blowing-out tower and iodine vaporizes. This vapor is then drawn into an absorption tower where it comes into contact with an absorbing agent, which absorbs and concentrates the iodide. Chlorine is added to the iodide solution to crystallize the iodine. These crystals are melted and refined before iodine can be delivered to customers.

2. Ion-Exchange Resin method

Sand and impurities in brine are removed through settling and filtering. An oxidizing agent is added and the brine is oxidized. The resultant brine is passed through a column packed with an ion-exchange resin that absorbs the iodine, which is in the form of a poly-iodide. The resin is then removed and transferred to an elution column where the poly-iodide is eluted with a sulfite solution. Chlorine is added to the eluted solution and iodine crystallized out and these crystals are melted and refined.

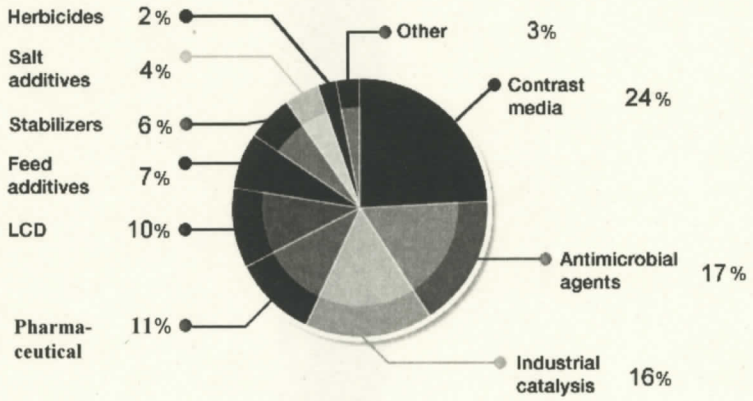

Fig. 1.1 Some advance application fields of iodine.

Iodine is epitomized and exemplified for its highly flexible applications and rightly considered as an essential element for the human well-being. Its rarity in many soils has led to many deficiency problems in land animals and inland human populations. So, iodine compounds are added to the table salt and fed to treat and prevent iodine deficiency symptom. Furthermore, it is used as raw material to create bio- and organic iodides as good activators for many chemical reactions. The usage of iodine is now extending to the most advanced fields; some of them are illustrated in. Fig. 1.1. The usage of iodine is closely linked to our daily lives. The products include a medicated gargle, X-ray contrast media, antimicrobial agent, a fire extinguisher, and replacement of chlorofluorocarbons with fluoroiodocarbons [1–4]. In addition, iodine has useful many applications in the field of agriculture. Recently, the demand for iodine has grown in high-tech fields such as optical polarizing film (OPF) for liquid crystal display (LCD) and etching agents for semiconductors. The increased production of OPF for LCD screen in fast emerging

economies of Asia-Pacific, is displaying continued growth and demand for iodine and its derivatives, and now accounts for almost 40% of the total iodine consumption. Some recent reports postulated that the demand of iodine is forecasted to rise by 3.5% per year [2] and expected to reach 28.11 thousand metric tons by the year 2015 [3]. Several technological advancements such as organic synthesis and advanced applications are opening up the enormous importance of iodine.

Table 1.1 General properties of iodine

Characteristics		Characteristics	
Name, symbol, number	iodine, I, 53	Phase	solid
Chemical series	halogens	Density	4.933 $g \cdot cm^{-3}$
Group, period, block	17, 5, p	Melting point	113.7 °C
Appearance	violet-dark gray, lustrous	Boiling point	184.3 °C
Crystal structure	orthorhombic	Atomic weight	126.9
Magnetic ordering	nonmagnetic	Thermal conductivity	0.449 $W \cdot m^{-1} \cdot K^{-1}$
Bulk modulus	7.7 GPa	Electrical resistivity	$1.3 \times 10^{7} \Omega$ m (0 °C)

Table 1.2 Estimated world production of crude iodine, by country [a,b]

(Metric tons)

	2005	2006	2007	2008	2009
Chile[c]	15,346	16,494	15,473	15,503	17,399
Japan	8,095	8,724	9,282	9,500	9,600
United States	1,574	W	W	W	W
China	550	560	570	570	580
Azerbaijan	300	300	300	300	300
Russia	300	300	300	300	300
Turkmenistan	270	270	270	270	270
Indonesia	75	75	75	75	75
Uzbekistan	2	2	2	2	2
------ Total	26,500	26,700	26,300	26,500	28,500

W Withheld to avoid disclosing company proprietary data; not included in total.

[a] World totals, U.S. data, and estimated data are rounded to no more than three significant digits; may not add to totals shown.

[b] Table includes data available through June 24, 2010.

[c] Includes iodine production reported by Servicio Nacional de Geologia y Miner-a.

Source: United States Geological Survey Mineral Resources Program

The usage of iodine for functionalization and the fabrication of new polymeric and fibrous material have paid enormous attention since few decades. The Nobel Prize in chemistry in 1977 was dedicated for developing the important new field of electrically conductive polymers produced by doping polyacetylene film with iodine [5]. A coating of hexyl-polyvinylpyrrolidone was devised in Massachusetts Institute of Technology, USA that can kill 99% of common disease-causing organisms. Polyvinylpyrrolidone (PVP) polymers are dye-receptive agent, a binder, a complexing agent, a detoxicant, a film former, a stabilizer, a protective colloidal and suspending agent [6]. An asymmetric carbon-carbon bond-forming reaction has invented at the University of Lausanne, Switzerland that could be useful in synthesis. Methyl iodide is used in part of the reaction [7]. A chiral catalyst derived from 4-pyrrolidinopyridine and acylated azlactone exhibits correct reactivity for catalytic kinetic resolution of racemic primary amines [8]. International Specialty Products Corp. (ISP) offers a tablet disintegrator that is based on PVP technology similar to that used by pharmaceutical tablet formulators. The PVP swells on contact with water, which causes rapid tablet breakup and helps soap to dissolve quickly in the wash [9]. New uses of fluoroiodocarbon as halogen replacements may cause an increased demand for iodine. Hydrogen iodide gas showed superior characteristics for etching materials, such as indium tin oxide film, used for pixel electrodes of liquid crystal displays. Iodine-125 is the primary radionuclide for in vitro application due to its 60 day half-life and low energy photon emission [10].

Japan is also exploring the iodine-oriented researches because of the availability of iodine. An aluminumoxidation coating impregnated with an iodine compound was developed by an electrochemical method at Chiba Institute of Technology, and the bactericidal activities of the coatings were effective against various molds and bacteria [11]. The adsorption of iodine on single crystal electrodes is one of the most intensively studied electrochemical processes. Recent studies at Tohoku University disclosed a novel property of iodine-modified electrodes because of the adsorption of organic molecules formed highly ordered molecular arrays [12]. Carbonaceous materials with good yield have been successfully fabricated using iodine pretreatment from polymeric precursor [13]. In our laboratory, we reported the iodine doping techniques for the fabrication of polymer/metal iodide composites [14,15], the enhancement of mechanical properties of existing polymeric

fibers [16], the fabrication of carbon fiber from natural biopolymer *Bombyx mori* silk fibroin and development of graphite structure [17-20], carbon fiber from polymeric precursor [21,22], metallization of polymers for imparting functionalities etc. [23]. Considering the current research trend, it can be assumed that the usage of iodine will explore novel research opportunities and expected to pick up momentum in the forthcoming years.

1.2 Functionalization of textile materials

Recently functional and high-grade advanced fibers have shown over-proportional market growth besides of their conventional applications. With the development of science and technology, textile materials have been specially designed and engineered to meet the demands for a variety of applications ranging from wipes to smart clothes [24]. The importance of multifunctional fibers is closely connected with the recent changes in the textile industry. The role of multifunctional fibers seems to offer the textile and apparel industry new challenges and benefits for the future. Functional textile materials should meet consumer demands in terms of comfort, easy care, hygiene; while ensuring protection against mechanical, thermal, chemical and biological attacks. Furthermore, the functional fibers can considerably improve their applications and extend the range of utilization. The surface features of functional fiber affect conductivity, adhesion, friction, wettability, biocompatibility and electro-optical properties of the materials, and enable considerable improvements in performance and durability through tailored corrosion and flame resistance, electro-metallic shielding etc. for their technical applications, e.g., in automotive, railroad, aerospace and aviation engineering, in construction and for home textiles etc. [25,26].

The maintenance of current properties and the creation of new material properties are the most important concern for the functionalization of fibers. Generally the functionalization of textile materials can be achieved by not only new production technologies (e.g., 3D structures) but also new developments for the improvement of the fiber materials or for the modifications of the fiber surface. Some of the most important principles of fiber functionalization by material modification are as follows [27–28]:

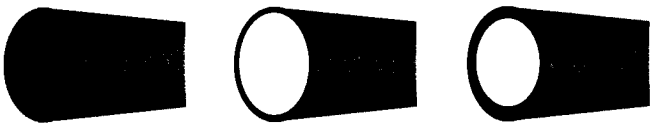

Fig. 1.2 Variants of fiber functionalization.

(a) *Incorporation of functional additives* (organic or biological compounds, inorganic particles, polymers) into the polymer melt or polymer solution before spinning. The advantage is the high permanence but drawbacks are low flexibility, the high non-textile portion, and also the procedure is not practicable for natural fibers.

(b) *Grafting of monomers* by photo induced or plasma techniques on the fiber surface directly or means of linkers. This effective method yields excellent permanent effects but is restricted to specific characteristics of fibers and additive structures.

(c) *Post-equipped textiles* (fiber, fabrics) with functional coatings. This universal method is very flexible with regard to coating technology and productive capacity, and is largely independent of fiber type. It requires low quantities of additive and enables the combination of different functions in a simple way. The ability to deposit well-controlled coatings on polymer fibers would change to both the physical and chemical properties of polymer fibers for wide range of applications.

In this thesis, we adopted the incorporation and coating techniques for functionalization of fibers.

1.2.1 Fabrication of carbon fibers with functions

Carbonaceous materials (carbon fiber, carbon nanofiber, carbon nanotube, carbon hollow fiber etc.) have attracted continuing attention because of their outstanding merits of high modulus, high strength, high electrical and thermal conductivity, and chemical- and bio-inertness over conventional fibrous materials [29,30]. Further, electrospun nanofibers have great potential for a wide range of applications because of a very large specific surface area, low density and high porosity. Carbon nanofibers made from electrospun polymeric precursors further expand the list of possible uses for nanofibers [31–35]. For instance, high performance materials from carbon and carbon nanofibers have been applied to functional

materials such as an electrode of lithium-ion battery [36] and transparent conductive films [37,38]. In our first approach, PVA nanofibers were prepared through electrospinning techniques and then converted to carbon nanofibers using iodine pretreatment and high temperature carbonization. Research on carbon-based materials in recent years has discovered several new forms of carbon structures such as fullerenes, carbon nanotubes, carbon nanofoams and colossal carbon tubes with unique properties and applications [39,40]. The hollow fibers based on carbon structure possess high specific surface area, extremely light weight with low density and high-pressure resistance besides the excellent properties of carbon fiber. The hollow carbon fibers (H-CFs) have shown their potential application in membrane-based gas separation technology, filtration, catalysis, electrodialysis, energy storage etc. [41,42]. The H-CFs are also proved its prominent application in radar in view of its hollow structure and microwave absorption properties [43]. Until today, many researchers have prepared H-CF from various polymeric materials based on polyacrylonitrile, polyimide, polysulfone, cellulose acetate, polyvinylidene chloride, polyfurfuryl alcohol and polyetherimide [42,44–50]. Generally melt spinning, wet spinning, dry spinning or dry/wet spinning are used for the fabrication of hollow polymeric precursor and then carefully controlled pyrolysis method is used usually to produce carbon hollow fibers derived from organic polymers. But these processes require multiple preparation steps and therfore are costly. Recently, a template method was also conducted using polypropylene hollow fiber membrane for the synthesis of H-CFs [51]. However, to authors' knowledge, there has been no report regarding the fabrication of hollow carbon structures from solid polymeric precursor. So, we attempted to fabricate the H-CFs from solid polymeric precursor poly(vinylalcohol) (PVA) filament using the iodine doping technique followed by stabilization and high heat treatment of carbonization.

1.2.2 Functionalization of high performance fibers

High performance fibers (HPFs) of poly(*p*-phenylene benzobisoxazole) (PBO) and poly(*p*-phenylene terephthalamide) (PPTA) are important engineering fibers with combination of high modulus and strength, light weight, high resistance to chemical reagents and flame and have been widely used in high performance textiles composites, military and aerospace industries since their production [52–54]. But the potential problems

of light degradation and moisture vulnerability makes questionable of their outdoor applications and storage [55–57]. Metallization of the fiber surface is a common method to protect and maintain of mechanical properties of fiber against light, rust and corrosion. In addition, new functionalities and surface properties can also be tailored, and their utilities in industrial or technical field would be enhanced. The metallization has usually been carried out by vacuum deposition, magnetron sputtering and electroless plating. The electroless plating refers to the autocatalytic or chemical reduction of metal ions and subsequent plating onto a substrate. We choose the electroless plating for present work due to its simplicity (no current needs to be applied) and flexibility of materials to be coated [58–61]. A variety of metals such as Au, Cu, Ag, Co, Pt, Pd, Ni, Pb and Sn etc. are used for the metallization of fibers. In our study, Cu, Ni and Ag for electroless metallization on PBO and PPTA fibers are chosen.

1.3 Strategies to utilize iodine for functionalization of fibers

1.3.1 Fabrication of carbon fibers

Carbon nanofibers and hollow carbon fibers were fabricated using iodine pretreatment and subsequent stabilization and carbonization of polymeric PVA nanofibers and solid filaments, respectively. PVA has relatively high carbon content among vinyl polymers and high molecular orientation in fiber form, but it melts below the carbonization temperature and is thermally decomposed into volatile low molecular weight molecules, which results in an unsustainable form of fiber and considerably low carbon yield [62]. Therefore, it is challenging to fabricate carbon fibers from PVA precursors without pretreatment or additives. Some researchers have reported that the dehydration of PVA induced by iodine treatment enhances the thermal stability of PVA during carbonization [15, 21, 22,63]. Possibly, cross linking among the PVA chains occurs during thermostabilization process forming a water insoluble polyene-type structure, which converts into cyclic polyaromatic structures withstanding the high temperature of carbonization. These processes extremely enhanced the carbon yield and enabled to obtain intact carbon fiber. Similarly, the controlled iodination of fiber surface and its oxidization during stabilization makes the outer surface stable and infusible. During carbonization by high-temperature exposure, while the inner non-iodinated part was thermally decomposed and a hollow inside the fiber

was formed keeping outer layer intact and resulted in the formation of hollow carbon fiber from solid polymeric precursor fiber.

1.3.2 Metallization of fibers

Electroless plating of polymer materials generally requires coarseness of smooth surfaces by etching with oxidative agents or strong acids followed by a catalyzation process including sensitization and activation steps [64–67]. PBO and PPTA fibers possess a chemically inert surface, which brings about poor interfacial adhesion between the fiber and the plated layer after electroless plating. Therefore, some catalyst fixation process that enables to impart high interfacial adhesion is necessary. Moreover, conventional chemical etching process for catalyzation leads to drastic loss of mechanical properties of substrate, especially for high modulus and high strength fibers. Accordingly, it is important to develop an efficient and etchant free activation process without mechanical loss. Several new attempts have been investigated using supercritical carbon dioxide (Sc. CO_2), silane modification, plasma induced graft polymerization etc. for activation prior to electroless plating on different fibers, which require special techniques and hence are costly [68–74]. Gotoh et al. have previously reported a method to impart metal iodides into a polymer matrix by utilizing iodine pretreatment to various polymers to prepare organic/inorganic composites [14,15]. This method is effective to introduce metal component into polymer matrix and is facile to control the amount of introduced metal iodides. Metal iodides formed in and on a polymer matrix are easily reduced to metal nanoparticles, which can act as a catalyst for plating. In this work, we developed an efficient method to attach Ag^{+} and Pd^{2+} species on the surface of HPFs and reduce the ions to metal Ag and Pd particles, respectively, for subsequent plating process using iodine pretreatment technique, as illustrated in Fig. 1.3.

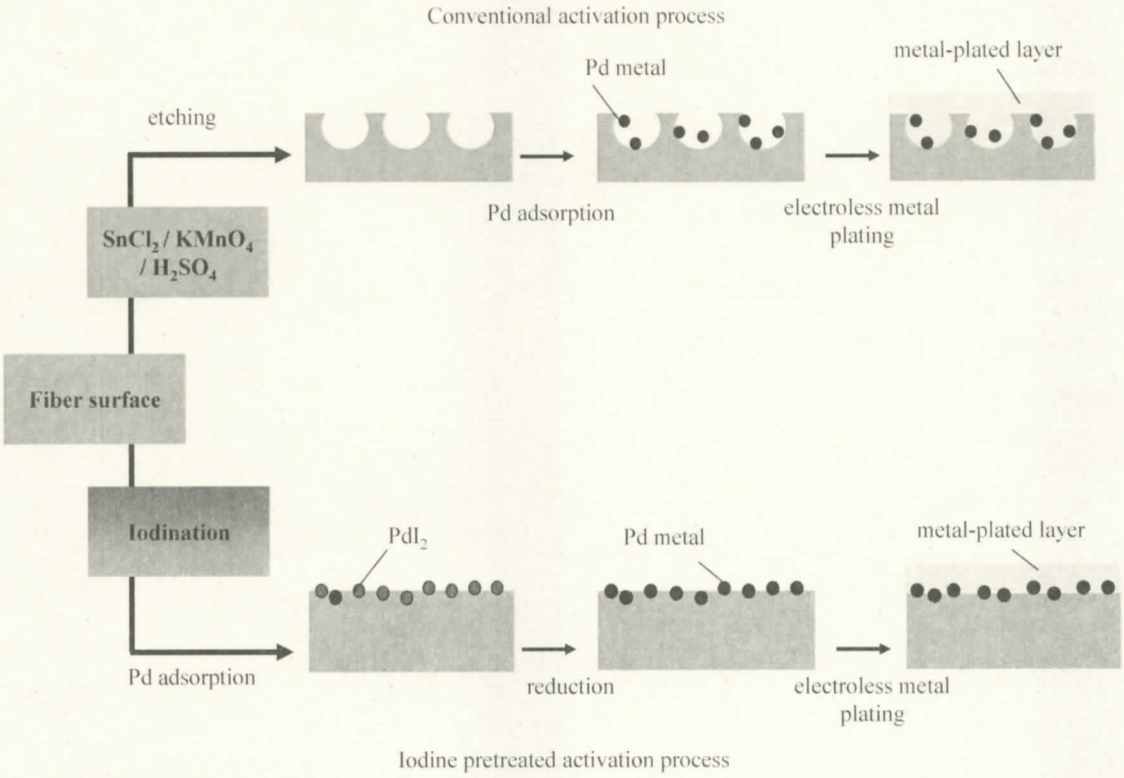

Fig. 1.3 Schematic illustration of iodine pretreated electroless metallization over conventional process.

$$2I_3^- + 3PdCl_2 + 4e^- \rightarrow 3PdI_2 + 6Cl^- \quad \text{..... (i)}$$

$$PdI_2 + 2e^- \rightarrow Pd^{2+} + 2I^- \quad \text{..... (ii)}$$

$$Cu^{2+} + 2HCOH + 4OH^- \rightarrow Cu + 2HCOO^- + 2H_2O + H_2 \quad \text{.....(iii)}$$

$$2HCOH + 4OH^- \rightarrow 2HCOO^- + 2H2O + 2e^- \quad \text{.....(iv)}$$

$$Cu^{2+} + H_2 \rightarrow 2H_2 + Cu \quad \text{.....(v)}$$

Fig. 1.3 and the above reactions scheme illustrate the proposed functionalization technique of iodine pretreatment and Pd activation using electroless Cu plating process over conventional metallization process on HPFs. The pretreatment process consists of iodine sorption and formation of metal iodide near the fiber surface by the reactions between polyiodide ions and metal ions as shown in eqs. (i)–(ii). Afterwards, the electroless Cu plating was conducted at high temperature by catalytic action of the reduced metal Pd particles as shown in eqs. (iii)–(v). This method brings about high adhesive force between fiber and metal plating layer.

1.4 Organization of the thesis

This thesis consists of the following six chapters.

Chapter 1 focuses on iodine and a brief summary of the functionalization process as general introduction. Also, methodologies of fabrication of carbon nanofiber and hollow carbon fibers from the polymeric and the functionalization of high performance fibers using iodine treatment have been discussed, and the structure of the thesis is illustrated.

Chapter 2 deals with the manufacture of neat PVA nanofibers by electrospinning and the fabrication of carbon fibers from electrospun nanofibers using iodine pretreatment. Electrospun PVA nanofibers were treated with iodine vapor and subsequently carbonized at different temperatures, and then structural changes of the derived carbon fibers were investigated. The optimization of the pretreatment process was performed to form carbon nanofibers with improved graphite structure. The influence of metal nanoparticle on the fabrication of carbon fiber and the properties was also investigated by addition of a metal salt, nickel (II) acetate tetrahydrate, to the PVA spinning solution. Incorporation of metal nanoparticles influences the diameter of electrospun fiber and developed the structure and the yield of derived carbon fiber.

Chapter 3 focuses on the fabrication of carbon hollow fibers from the solid PVA fibers with selective iodine pretreatment followed by stabilization and carbonization. Iodination converted the chemical structure of PVA to polyene form due to dehydration reaction, and stabilization of heat treatment at 200 °C in air provided infusibilization of iodinated PVA fibers. These processes extremely enhanced the carbon yield and enabled to obtain carbon fiber. By selective iodination and subsequent stabilization of the fiber surface, hollow carbon fibers were made during the heat treatment temperature of carbonization. Further, the influence of high heat treatment temperature of carbonization on resultant hollow carbon structure has been briefly investigated. Additional attempt has been carried out to improve the functionality of the resultant carbon fiber.

Chapter 4 describes the utilization of iodine for metallization of the HPFs via electroless plating process. First, iodine components were doped into PBO and PPTA fibers using aqueous or vapor media and subsequently immersed in a metal salt solution to form metal iodide particles on the fiber surface. After reduction of metal iodide to metal Cu, Ni and Ag particle, electroless plating was carried out. Here, the metal particles functioned as an

autocatalyst and as anchor during plating process. The optimization of the pretreatment process and electroless plating conditions has been performed to form a uniformly plated fiber that corresponds to high durable and strong adhesive plated layer.

Chapter 5 evaluates the performance of the metal plated high performance fibers. The durability of the plated layer with fiber surface was investigated in terms of ultrasonic peeling, tape peel-off and corrosion resistance. The mechanical, electrical and magnetic properties of the plated super fibers were investigated to assess the functions of the plated HPFs. Furthermore, the metallized fibers were exposed to a xenon lamp for different periods to examine the light shielding effect of the coated metal layer.

Finally, the conclusions of the present work are given in Chapter 6.

1.5 References

[1] United States Geological Survey Mineral Resources Program, http://www.indexmundi.com/en/commodities/minerals/iodine/iodine_t5.html (last accessed on June 20, 2011)

[2] Iodine: Global industry markets & outlooks, Roskill Information services limited, UK, (2010).

[3] Iodine: A Global Strategic Business Report, Global Industry Analysts, Inc, USA, (2011).

[4] http://www.gasukai.co.jp/english/iodine/index.html (last accessed May 16, 2011)

[5] Chiang CK, Fincher CR, Park YW, Heeger AJ, Shirakawa H, Louis EJ, McDiarmid AG, Electrical conductivity in doped polyacetylene, Phys Rev Lett, 39, 1098 (1977).

[6] Tiller JC, Hexyl-PVP special coating kills germs, researcher says, (2001) http://www.mindfully.org/Plastic/Hexyl-PVP-Kills-Germs.htm.(last accessed June 1, 2011)

[7] Science & Technology concentrates—Catalyst for resolving racemic amines: Chem Eng News, 79(3), 39 (2001).

[8] McCoy M, Tall (oil) tale of pine chemicals, Chem Eng News, 78(13), 14–15 (2000).

[9] Stinson S, One pot, four components, one asymmetric C-C bond, two chiral centers, Chem Eng News, 78(20), 50 (2000).

[10] http://minerals.usgs.gov/minerals/pubs/commodity/iodine/770400.pdf, Phyllis AL, Iodine (URL last accessed June 14, 2011).

[11] Takaya M, Surface treatment of aluminum alloys using iodine, Proceedings of Symposium on Iodine Utilization, 3d, Kanto Natural Gas Development Co. Ltd, Chiba, Japan, 25 (2000).

[12] Itaya K, Structures and properties of iodine adlayers on single crystal electrodes, Proceedings of Symposium on Iodine Utilization, 3d, Kanto Natural Gas Development Co. Ltd, Chiba, Japan, 93 (2000).

[14] Shindo A, Sawada Y, Orientation structure in traverse sections of carbon fibers from dehydrated polyvinyl alcohol, Carbon, 18, 419–425 (1980).

[15] Fujimori Y, Gotoh Y, Tamaki N, Ohkoshi Y, Nagura M, Introduction of copper iodide fineparticles into poly(acrylic acid) matrix via a complex of polymer-polyiodide ion, J Mater Chem, 15(45), 4816–4822 (2005).

[16] Fujimori Y, Gotoh Y, Kawaguchi A, Ohkoshi Y, Nagura M, Conductivity and structure of a polyamide/silver iodide nanocomposite, J Appl Polym Sci, 108(5), 2814–2824 (2008).

[17] Ahmed JU, Narusawa T, Gotoh Y, Enhancing mechanical properties of gel-spun polyvinyl alcohol fibers by iodine doping, Polym Eng Sci, 51(4), 647–653 (2011).

[18] Khan MMR, Gotoh Y, Morikawa H, Miura M, Structural and physical properties of Antheraea pernyi silk fibroin fiber treated with I_2-KI aqueous solution, Fiber Polym, 7(4), 333–338 (2006).

[19] Khan MMR, Gotoh Y, Morikawa H, Miura M, Nagura M, Influence of an iodine treatment on the structure and physical properties of *Bombyx mori* silk fibroin fiber, J Polym Sci Polym Phys B, 44(23), 3418–3426 (2006).

[20] Khan MMR, Gotoh Y, Morikawa H, Miura M, Fujimoi Y, Nagura M, Carbon fiber from natural biopolymer Bombyx mori silk fibroin with iodine treatment, Carbon, 45(5), 1035–1042 (2007).

[21] Fatema UK, Ahmed JU, Uemura K, Gotoh Y, Fabrication of carbon fibers from electrospun poly(vinyl alcohol) nanofibers, Tex Res J, 81(7), 659–672 (2011).

[22] Fatema UK, Tomizawa C, Harada M, Gotoh Y, Iodine-aided fabrication of hollow carbon fibers from solid poly(vinyl alcohol) fibers, Carbon, 49(6), 2158–2161 (2011).

[23] Tetsumoto T, Gotoh Y, Fabrication of silver plated nylon 6 nanofibers using iodine, Sen'i Gakkaishi, 66(9), 222–227 (2010).

[24] Laxminarayan K, Jalilo N, Functional nanotube-based textiles: Pathway to next generation fabrics with enhanced sensing capabilities, Tex Res J, 75, 670–680(2005).

[25] Carfagna C, Persico P, Functional textiles based on polymer composites, Macromol Symp, 245–246, 355–362 (2006).

[26] Zhang J, Development of new functional textile for military, Cotton Tex Technol, 1, (2002).

[27] Wei Q, Surface modification of textiles, Woodhead Pub Ltd, UK, (2009).

[28] Ooil WJ, Lup S, Datta S, Surface modification of textile fibers and cords by plasma polymerization, Plasmas Polym, 4(1), 33–55 (1999).

[29] Setton R, Bernier P, Lefrant S, Carbon molecules and materials, Taylor and Francis Pub Ltd, London, UK, p6–9 (2002).

[30] Wang H, Zhang L, Gavalas GR, Preparation of supported carbon membranes from furfuryl alcohol by vapor deposition polymerization, J Memb Sci, 177, 25–31(2000).

[31] Li D, Xia Y, Electrospinning of nanofibers: Reinventing the wheel?, Adv Mater, 16, 1151–1170 (2004).

[32] Koski A, Yim K, Shivkumar S, Effect of molecular weight on fibrous PVA produced by electrospinning, Mater Lett, 58, 493–497 (2004).

[33] Park JY, Lee IH, Bea GN, Optimization of electrospinning conditions for preparation of nanofibers from polyvinylacetate (PVAc) in ethanol solvent, J Indus Eng Chem, 14, 707–713 (2008).

[34] Ding B, Kimura E, Sato T, Fujita S, Shiratori S, Fabrication of blend biodegradable nanofibrous nonwoven mats via multi-jet electrospinning, Polymer, 45, 1895–1902 (2004).

[35] Yamashita Y, Electrospinning–The latest in nanotechnology: The creative challenge of nanofibers, SLS, Japan, p145–190 (2007).

[36] Endo M, Kim YA, Nishimura K, Fujino T, Miyashita K, Recent development of carbon materials for Li ion batteries, Carbon, 38(2), 183–197 (2000).

[37] Kaempgen M, Duesberg GS, Roth S, Transparent carbon nanotube coatings, Appl Surf Sci, 252, 425–429 (2005).

[38] Watson KA, Ghose S, Delozier DM, Smith JG, Connell JW, Polymer, 46, 2076–2085 (2005).

[39] Burchell TD, Carbon materials for advanced technologies, Pergamon, Oxford, UK (1999).

[40] Peng H, Chen D, Huang JY, Chikkannanavar SB, Hänisch J, Jain M et al. Strong and ductile colossal carbon tubes with walls of rectangular macropores, Phys Rev Lett, 101, 145501–4 (2008).

[41] Koresh J, Soffer A, Sep Sci Technol, 18, 723 (1983).

[42] Saufi SM, Ismail AF, Development of polyacrylonitrile (PAN) based carbon hollow fiber membrane, Membrane Sci Technol, 4, 844–853 (2002).

[43] Xie W, Cheng HF, Chu ZY et al. Preparation and microwave absorbing properties of hollow carbon fibers. J Cent South Univ Technol, 14(s2), 112–115 (2007).

[44] Favvas EP, Kouvelos EP, Romans GE, Pilatos GI, Mitropoulos AC, Kanellopoulos NK, Characterization of highly selective microporous carbon hollow membranes prepared from a commercial co-polyimide precursor, J Porus Mater, 15, 625–633 (2008).

[45] Favvas EP, Kapantaidakis GC, Nolan JW, Mitropoulos AC, Kanellopoulos NK, Preparation, characterization and gas permeation properties of carbon hollow fiber membranes based on Matrimid® 5218 precursor, J Mater Proc Technol, 186, 102–110 (2007).

[46] Bhardwaj V, Macintosh A, Sharpe ID, Gordeyev SA, Shilton SJ, Polysulfone hollow fiber gas separation membranes filled with submicron particles, Adv Memb Technol, 984, 318–328 (2003).

[47] Zhu G, Chung TS, Loh KC, Activated carbon-filled cellulose acetate hollow-fiber membrane for cell immobilization and phenol degradation, J Appl Polym Sci, 76(5), 695–707 (2000).

[48] Teresa AC, Antonio BF, Carbon molecular sieve gas separation membranes based on poly(vinylidene chloride-co-vinyl chloride), Carbon, 38, 1067–1073 (2000).

[49] Song C, Wang T, Jiang H, Wang X, Cao Y, Qiu J, Gas separation performance of C/CMS membranes derived from poly(furfuryl alcohol) (PFA) with different chemical structure, J Membrane Sci, 362, 22–27 (2010).

[50] Barbosa-Coutinho E, Salim VMM, Borges CP, Preparation of carbon hollow membrane by pyrolysis of polyetherimide, Carbon, 41, 1707–1714 (2003).

[51] Shi Z, Zhang T, Xu L, Feng Y, A template method for the synthesis of hollow carbon fibers, Microporous Mesoporous Mater, 116, 698–700 (2008).

[52] Ohta Y, Kajiwara K, in: Houck MM (Ed), High performance fibers: structure, characteristics and identification, Identification of textile fibers, Woodhead Pub Ltd, Cambridge, UK, p88–110 (2009).

[53] Hearly JWS, High performance fiber, Woodhead Pub Ltd, UK, (2001).

[54] Chae GH, Kumar S, Rigid rod polymeric structure, J Appl Poly Sci, 100, 791–802 (2006).

[55] Yang HH, Kevlar Aramid fiber, Wiley and Sons, USA, (1993).

[56] Forster AL, Pintus P, Messin GHR, Rilley MA, Petit S, Rossiter W, Chin J, Rice KD, Hydrolytic stability of polybenzobisoxazole and polyterephthalamide body armor, Polym Degrad Stab, (2010), doi:10.1016/polymdegradstab.2010.10.004.

[57] Zhang H, Zhang J, Chen J, Hao X, Wang S, Feng X, Gua Y, Effects of solar irradiation on the tensile properties and structure of PPTA fiber, Polym Degrad Stab, 91, 2761–2767 (2006).

[58] Mallory GO, Hajdu JB, Electroless plating-Fundamentals and applications, William Andrew Pub/Noyes, New York, USA, (1990).

[59] Ohno I, Electroplating chemistry of electroless plating, Mater Sci Eng A, 146, 39–49 (1991).

[60] Dini JW, Electrodeposition: The material science of coatings and substrates, Noyes Pub, USA, (1993).

[61] Qui T, Chu PK, Self-selective electroless plating: An approach for fabrication of functional 1D nanomaterials, Mater Sci Eng R, 61, 59–77 (2008).

[62] Otani S, Okuda, K, Matsuda HS, Carbon fiber, Vol. 3, Kindai Henshu Ltd., Tokyo, Japan, p231 (1983).

[63] Sashio M, Tanaka M, Thermal reaction of poly(vinyl alcohol)-iodine complex membranes, J Polym Sci Part A: Polym Chem, 23, 905–909 (1985).

[64] Hsu CH, Process for making electroless plated aramid fibrids, US Patent 5,422,142, (1995).

[65] Schwarz A, Hakuzimana J, Kaczynska A, Banaszczyk J, Westbroek P, McAdams E et al., Gold coated para-aramid yarns through electroless deposition, Surf Coat Technol, 204(9–10), 1412–1418 (2010).

[66] Gabara V, Hsu CH, Electroless plated aramid surfaces and a process for making such surfaces, US Patent 5,302,415, (1994).

[67] Burch RR, Gould R, Lee KS, Phillips BR, Electroless plated Aramid surfaces, US Patent 5,370,934 (1994).

[68] Yuen CWM, Jiang SQ, Kan CW, Tung WS, Influence of surface treatment on the electroless nickel plating of textile fabric, Appl Surf Sci, 253 (12), 5250–52557 (2007).

[69] Osaka T, Yoshino M, New formation process of plating thin films on several substrates by means of self-assembled monolayer (SAM) process, Electrochimica Acta, 53, 271–277 (2007).

[70] Martinez M, Hisada K, Tabata I, Hirogaki K, Yonezawa S, Hori T, The effectiveness of thermal treatment for development of conductive metallized aramid fiber using supercritical fluid carbon dioxide: Fiber-metal adhesive strength improvement, J Supercritical Fluids, 56(3), 22–329 (2011).

[71] Zhao X, Hirogaki K, Tabata I, Okubayashi S, Hori T, A new method of producing conductive aramid fibers using supercritical carbon dioxide , Surf Coat Technol, 201(3–4), 628–636 (2006).

[72] Belmas M, Tabata I, Hisada K, Hori T, Supercritical fluid-assisted electroless copper plating of aramid film: The influence of surface treatment, Sen'i Gakkaishi, 66(9), 215–219 (2010).

[73] Yang GH, Lim C, Tan YP, Zhang Y, Kang ET, Neoh KG, Electroless deposition of nickel on fluoropolymers modified by surface graft polymerization, Euro Polym J, 38, 2153–2160 (2002).

[74] Charbonnier M, Romand M, Tin-free electroless metallization of glass substrates using different PACVD surface treatment processes, Surf Coat Technol, 162, 19–30 (2002).

Chapter 2

Fabrication of carbon fibers from electrospun poly(vinyl alcohol) nanofibers using iodine pretreatment

1. Introduction

Research and development of nanofibers has gained much prominence in recent years due to the heightened awareness of their potential applications in many fields including textiles, chemical synthesis, medical, engineering and defense [1,2]. Among several methods for nanofiber production, electrospinning (ES) has been a pioneer technology for the production of ultra-thin membranes consisted of 1D nanostructured fibers from a rich variety of materials, including polymers, composites, and ceramics [3]. Nowadays, research on the production methods and conditions of the ES technique has been reconsidered on account of its simplicity and versatility [4–8]. Electrospun ultrathin fibers possess high porosity and a high surface area to volume ratio, which has contributed to the potential applications of electrospun fibers in carbon and graphitic nanofiber fabrication [9].

Carbon nanofibers derived from ES have further expanded the possible applications of nanofibers. For instance, high performance materials prepared from carbon nanofibers and nanotubes have attracted significant attention, due to their outstanding characteristics of high modulus, high strength, high electrical and thermal conductivity, chemical and bio inertness and unique morphology over conventional fibrous nanomaterials [10,11].

Poly(vinyl alcohol) (PVA) is a semi-crystalline fiber with comparatively high carbon content (ca. 54.5%), and easily splits hydroxyl groups in the polymer chain make PVA favorable for use as a precursor for the production of carbonaceous materials. To date, poly(furfuryl alcohol) [12], poly(vinylidine chloride) [13], polyimide [14], poly(acrylonitrile) (PAN) [15], poly(vinylidine fluoride) [16], poly(vinyl alcohol) [17,18], and phenol resin [19] have been used as starting polymer materials for this purpose. The earliest attempt, and subsequent work, utilized wet spun PVA fiber as a precursor for the fabrication of carbon fiber [20,21]. Recently, electrospun poly(acrylonitrile) (PAN) [1,22], pitch [23] etc. and different polymeric blends [24–27] have been reported as precursor for the fabrication of carbon fiber. In this study, we report the fabrication of carbon fibers from electrospun PVA nanofibers. The decomposition of PVA at temperatures slightly higher than its melting point results in lower carbon yield; therefore, PVA precursors with high thermal stability are essential. Researchers reported that the dehydration of PVA from 100 to 290 °C under tension in a mixed gas atmosphere induces the thermal stability required for carbonization [17,21]. Preoxidation or subsequent dehydration has also been employed

as a PVA stabilization process [20]. In addition, iodine acts as a good stabilizer of PVA [17,28] and promotes dehydrogenative polymerization during carbonization. Iodine treatment has also been successfully employed by our coworkers to produce carbon fiber from natural biopolymers such as silk fibroin [29–32]. The carbon yield does not seem to be influenced by whether the polymer is thermoplastic or thermosetting, linear or cross-linked, but rather by whether it is capable of cyclization, ring fusion or chain coalescence at the onset of carbonization [33,34]. Iodine treatment transforms the single bond in PVA hydrocarbon structure into a double bond polyene-like structure, which makes PVA molecules difficult to melt even at the relatively high temperature of carbonization [34]. In addition, the carbon microstructure formed is changed into stable graphite structure during carbonization [35].

Many researchers have incorporated functional components (e.g., nanoparticles, nanowires, or molecular species) into polymeric nanofibers, via ES interaction or liquid phase attachment or deposition/coating, to obtain a diversified range of composites and well defined functionalities. For example, chromium nitrate ($Cr(NO_3)_3$) [36] and palladium diacetate ($Pd(OOCCH_3)_2$) [4] were added into the spinning solution to produce finer nanofibers from PVA and polylactic acid, respectively. Carbon nanotube reinforced polymeric composites were also prepared using ES [37,38]. Iron salts have also been used for the growth of carbon nanotubes in carbon fiber from electrospun PAN fibers [4] or improved graphitization of PVA films at lower temperature [17]. Our coworkers have also reported that the addition of a small amount of Ni metal catalyst promotes the dehydration reaction of PVA during carbonization [39].

In this chapter, we attempted to prepare carbon fibers from electrospun PVA nanofibers followed by iodine treatment. We also explored the effect of metallic salt (Ni-acetate) addition into the PVA spinning solution. The spinning performance, carbon yield, diameter and morphology of the resultant nanofibers were investigated.

2. Experimental

2.1 Materials

PVA chips, atactic type, (Poval-HC, Kuraray Co. Ltd, Japan) with a degree of polymerization (DP) and saponification of ca. 1500 and 99.9%, respectively, were used. PVA requires additional purification processes to remove residual impurities such as sodium acetate, which promotes thermal decomposition during heat treatment. PVA was purified as follows: the PVA chips were washed with a sufficient amount of distilled water at 60 °C under agitation and the water was exchanged twice at 2 h intervals. The PVA was then stirred for 20 h in water followed by stirring in methanol for 24 h at room temperature. The washed PVA chips were filtered using a glass vacuum filter, and dried at 60 °C in a vacuum oven for 24 h. Special grade Ni(II) acetate tetrahydrate $(CH_3COO)_2Ni \bullet 4H_2O$) was purchased from Wako Pure Chemical Ind. Ltd., Japan and used as received.

2.2 Preparation of PVA nanofibers

Purified PVA was dissolved in distilled water at 90 °C for ca. 4 h. During electrospinning of PVA-HC, we tried with different concentration of spinning solution ranging from 2 to 10wt% and measured the viscosity of each solution and found critical concentration was around 7wt%. PVA-HC showed capillary instability at concentration below and over 7wt%, which resulted inconsistent electrospinning of nanofibers with more beads. Therefore, we preferred 7wt% PVA concentration to obtain steady spinning and beads-free nanofiber.

In the case of Ni incorporation, different PVA concentrations were again investigated, and continuous spinning with less beads was realized using a 6wt% PVA solution containing Ni-acetate. Ni-acetate (4 wt% of the PVA solid content) was dissolved in the PVA solution; samples doped with Ni-acetate are denoted as PVA/Ni. Spinning of PVA nanofibers was carried out using a typical ES system as schematically shown in Fig. 2.1. The system consists of mainly three major components: a high voltage direct current (DC) power supply, a metallic spinneret, and a grounded collector. A high voltage is applied between the spinneret and collector, consequently an electrically charged stream of polymer solution is generated, and the polymeric nanofibers are formed on the collector by

vaporization of solvent. PVA nanofibers are collected as web of fibers deposited on polyethylene mesh placed on the surface of grounded collector. However, the method of electrospinning we used in this work is for experimental purpose. The bubble electrospinning technique can be used for mass scale production as reported elsewhere [41, 42].

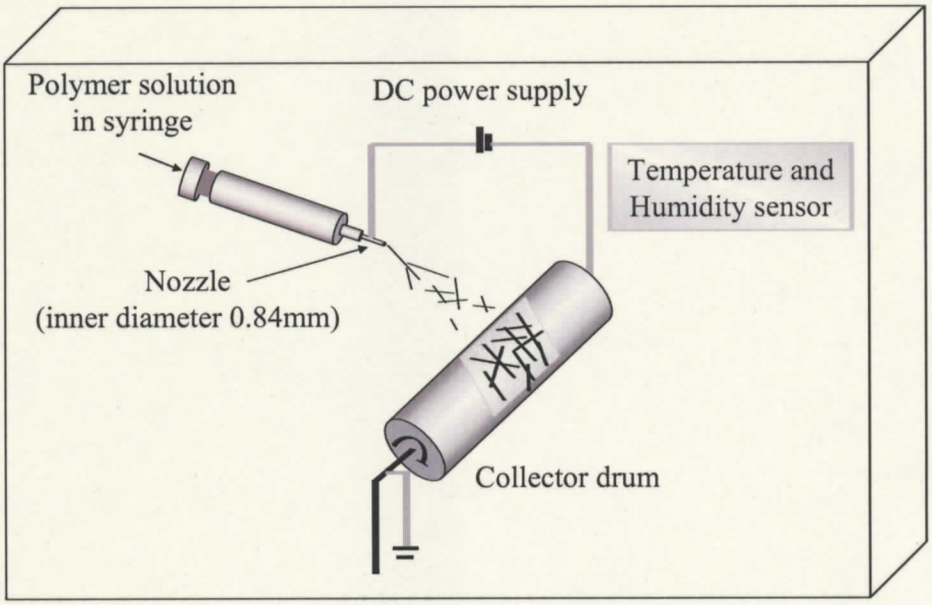

Fig. 2.1 The schematic diagram of experimental setup of electrospinning.

2.3 Iodine treatment

A PVA nanofiber mat was enclosed with a sufficient quantity of solid iodine in a glass bottle. The sealed vessel was placed in an 80 °C oven for different exposure periods during which iodine was vaporized. The color of the PVA sample became dark brown due to complex formation of the PVA with iodine. In the present paper, the iodinated PVA nanofiber will be denoted as I-PVA.

2.4 Carbonization

A ceramic tubular furnace (AMF-9P-Ⅲ THV, Asahi Rika Seisakujo, Japan) was used for the carbonization process. I-PVA nanofiber was heated at 1 °C/min in the furnace under an Ar gas flow.

2.5 Measurements

Thermogravimetric analysis (TGA) was carried out with a Rigaku Thermoplus II TG 8120 under N_2 atmosphere from room temperature to 1000 °C at a heating rate of 10 °C/min.

Scanning electronic microscopy (SEM; Hitachi S-2380N) was conducted after the samples were sputtered with platinum. The diameter of the fibers was analyzed from SEM images using software (Image J; NIH, USA). The experimental results of fiber diameter represent the average of 100–150 individual measurements at different places.

Transmission electronic microscopy (TEM; Jeol JEM-2010) was conducted using an accelerated voltage of 200 kV. Ground samples were dispersed in ethanol and the mixture placed on a copper mesh grid followed by carbon sputtering prior to measurement.

Wide angle X-ray diffraction (WAXD) measurements were performed by the reflection method using a Rigaku Rotorflex RU-200B X-ray generator equipped with a goniometer. The X-ray source was Ni-filtered Cu K_α radiation (λ= 0.15418 nm) generated at 40 kV and 150 mA. Crystallite size was measured using Scherer's equation:

$$D_p = k\lambda/(\beta \cos\theta),$$

where β = Peak full-width at half-maximum (FWHM), θ = Bragg's angle, λ = X-ray wavelength (0.154 nm) and k = Shape factor (for spherical crystals with cubic symmetry, k= 0.94) [43].

Raman spectra were recorded using a Kaiser Hololab 5000 spectrometer, equipped with a MK-II filter probe using an Nd:YAG laser beam of a 532-nm laser with 50-mW power.

3. Results and discussion

3.1 Electrospinning of PVA nanofibers

The morphology and diameter of electrospun fibers are dependent on the number of processing parameters, including the intrinsic properties of the solution (e.g., polymer type, viscosity, electrical conductivity, polarity, surface tension, and impurities) and the operational conditions (e.g., applied electric field and the distance between the spinneret and collector) [3–8,40]. In addition to these variables, the humidity and temperature also play an important role in determining the morphology and diameter of electrospun fibers [44]. In our current work, different spinning conditions were examined and based on the

morphology, fiber diameter and diameter homogeneity the optimum spinning condition was obtained at PVA concentration of 7 wt%, solution extrusion rate of 0.5 ml/h, a 17-cm distance from the nozzle to the collector, an applied voltage 30 kV, a temperature of ca. 20 °C, and relative humidity of 14%. These conditions resulted in the production of nanofibers having a diameter range of 350–700 nm with good reproducibility.

3.2 Effect of iodine treatment on PVA nanofibers

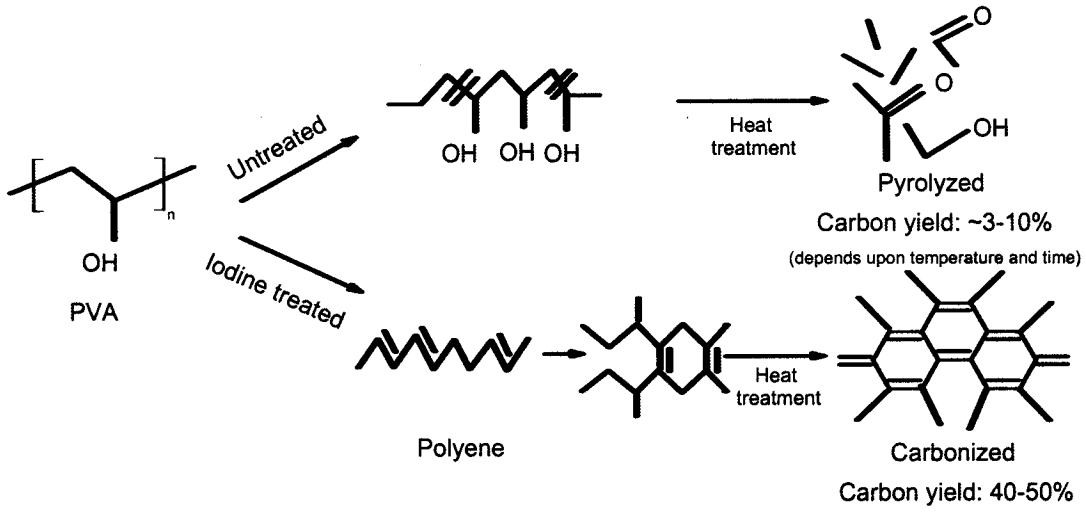

Fig. 2.2 Possible behaviors of untreated and iodinated PVAs during heating.

PVA has relatively high carbon content among vinyl polymers and high molecular orientation in fiber form, but it melts below the carbonization temperature and is thermally decomposed into volatile low molecular weight molecules, which results in an unsustainable form of fiber and considerably low carbon yield [34]. Therefore, it is almost impossible to produce carbon fiber from PVA without pretreatment or additives. Some researchers have reported that the dehydration of PVA induced by iodine treatment enhances the thermal stability of PVA during carbonization [17,45,46]. Possibly, cross linking among PVA chains occur during thermostabilization process and form a water insoluble polyene-type structures, which convert into cyclic polyaromatic structures during carbonization can withstand high temperature of carbonization. These processes extremely enhanced the carbon yield and enabled to obtain intact carbon fiber. The dehydration of

PVA by iodine treatment followed by carbonization can be considered to take place by the reaction scheme illustrated in Fig. 2.2.

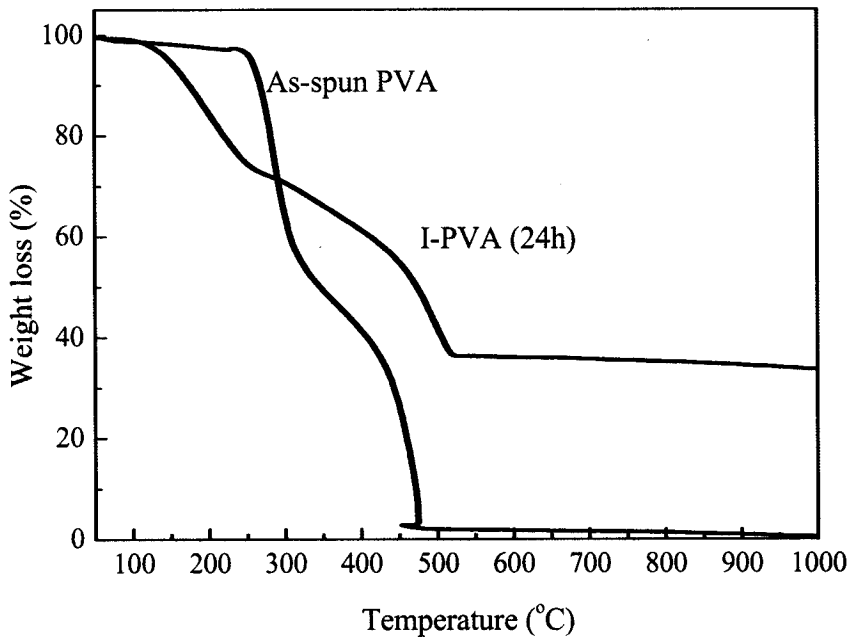

Fig. 2.3 TGA thermograph of PVA as-spun nanofiber and I-PVA nanofiber subjected to 24 h iodination.

As shown in Fig. 2.3, the TGA curves of untreated PVA fiber and I-PVA (24 h) were taken to study the degradation behavior of PVA polymer after iodination. Apart from the weight loss due to content water at the initial stage, the weight loss after iodination was significantly different. Untreated fiber has no weight loss up to 250 °C and drastic weight loss was marked with a sharp declining of the curve at 300 °C that ended at around 460 °C, retaining only ≈2% of its weight. In contrast, the initial degradation of I-PVA fiber started at around 120 °C and then further decomposition was completed at nearly 520 °C, retaining ≈38% of its weight. In the TG curve of I-PVA, initial decomposition is likely to occur due to the evaporation of excess iodine together with desorbed water of PVA precursor, and the later decomposition phase of I-PVA is associated with the evaporation of iodine along with the oxidation of precursor fiber. Considering weight loss during heating, iodination has evidently improved the thermal stability of precursor fiber. Possibly, crosslinking among

PVA chains occur during thermostabilization process that can withstand a high temperature process as illustrated in Fig. 2.2.

3.2.1 Morphological aspect

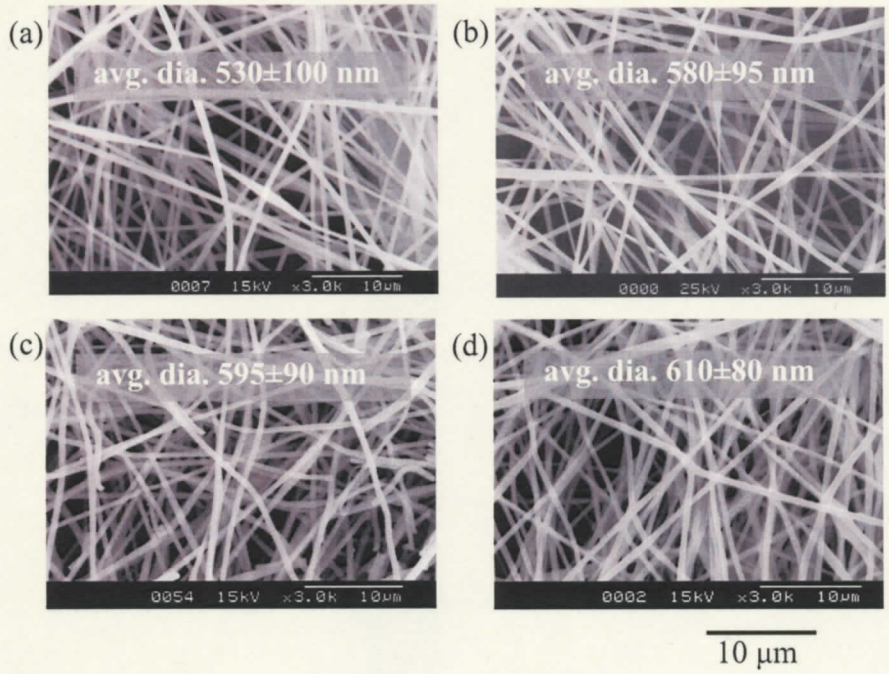

Fig. 2.4 SEM images of PVA nanofibers subjected to different iodination periods of (a) 0 (no iodination), (b) 3, (c) 12, and (d) 24 h.

The morphological changes of nanofibers after iodine treatment were examined. Fig. 2.4 shows the SEM images of PVA and I-PVA nanofibers prepared with different iodination periods of 3, 12, and 24 h with respective average diameter. The morphology of the iodinated nanofibers varies slightly compared to the original fiber, as in Fig. 2.2(a), with minuscule swelling of the PVA nanofiber due to absorption of iodine molecules. Even for an iodination time of 24 h, iodine has no significant effect on the nanofiber morphology. But the diameter of nanofibers exhibits a modest increase in diameter after 3 h iodination. However, further increase in the iodination period to 12 and 24 h results in little change to the nanofiber diameter. It appears that the PVA nanofibers initially absorb iodine over a 3 h iodination period and become saturated, and hence significant change in diameter is not observed with further iodination.

Fig. 2.5 shows SEM images of the carbonized samples obtained from differently iodinated PVA nanofibers with carbonization performed at 1200 °C. The reason for the carbonization temperature of 1200 °C is explained later. The neat PVA fiber melts completely during the carbonization process and becomes a solid film with cracks. The nanofibers iodinated for 3 h also show the melting phenomenon during the carbonization process. Such melting behavior may be attributed to the shorter iodination period of 3 h, which appears to result in insufficient thermal stability of the PVA nanofibers due to improper dehydration during heat treatment. In contrast, the nanofibers iodinated for much longer periods of 12 and 24 h retained their original fibrous structures without melting during carbonization. This reveals that the transformation of PVA into a stable cyclic aromatic structure by intermolecular crosslinking prior to carbonization is a prerequisite to retain the fiber structure. In this regard, longer iodination periods of 12 and 24 h, as evidenced by the Raman spectra in Fig. 2.7, are found to be very favorable for the stabilization of PVA nanofibers prior to carbonization.

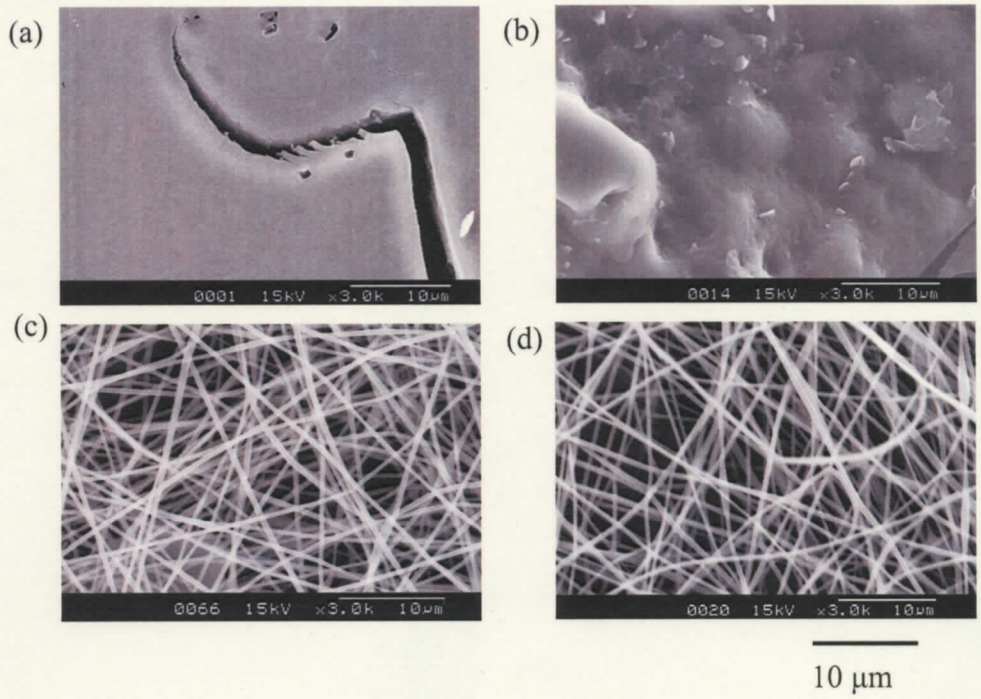

Fig. 2.5 SEM images of carbonized PVA nanofibers subjected to different iodination periods of (a) 0, (b) 3, (c) 12, and (d) 24 h and then carbonized at 1200 °C.

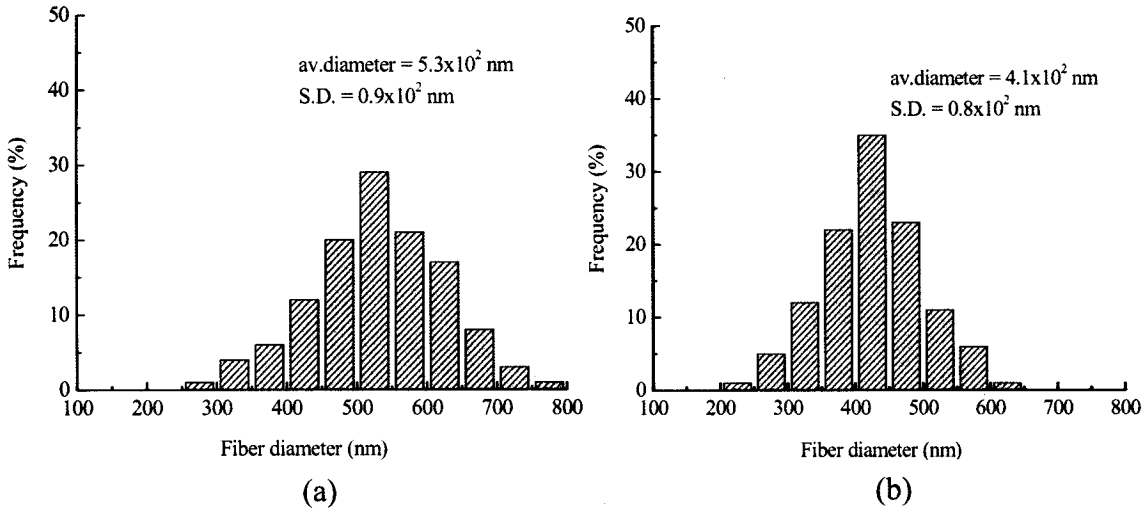

Fig. 2.6 Diameter distribution of (a) as-spun PVA and (b) carbonized PVA nanofibers subjected to 24 h iodination and carbonized at 1200 °C.

Fig. 2.6 shows the diameter histograms of as-spun precursor nanofiber and the carbon fiber obtained from precursor nanofiber with a 24 h iodination period. After carbonization, the average diameter becomes thinner than those of the iodinated PVA precursor fiber. The dehydration and subsequent carbonization of iodinated PVA nanofibers may lead to a finer structure by diameter contraction. Thus, the iodine treatment has appeared to be a decisive step for carbonization in the context of the fiber diameter.

3.2.2 Structural aspect

Raman spectroscopy is an effective way to investigate the structure of an iodinated material. Raman spectra of PVA nanofibers and I-PVA nanofibers with different iodination periods are shown in Fig. 2.7. The spectrum of the as-spun PVA shows most pronounced scattering peaks at around 2912 cm^{-1}, which are assigned to the stretching vibrations of CH_2 and CH, and other peaks at ca. 1440 cm^{-1} assigned to the stretching vibrations of CH and OH in the PVA molecules [47]. For the fiber iodinated for 3 h, two major scattering peaks are observed at ca. 1120 and 1500 cm^{-1}, which are respectively assigned to the single and double bonds of the polyene structure [48]. This implied that PVA molecules were successfully dehydrated and changed into a polyene-like structure. The fibers iodinated for 12 and 24 h have almost the same Raman pattern. The scattering band appearing at ca. 1590

cm^{-1} indicates a polycyclic aromatic structure formed by intermolecular crosslinking of the polyenes [49].

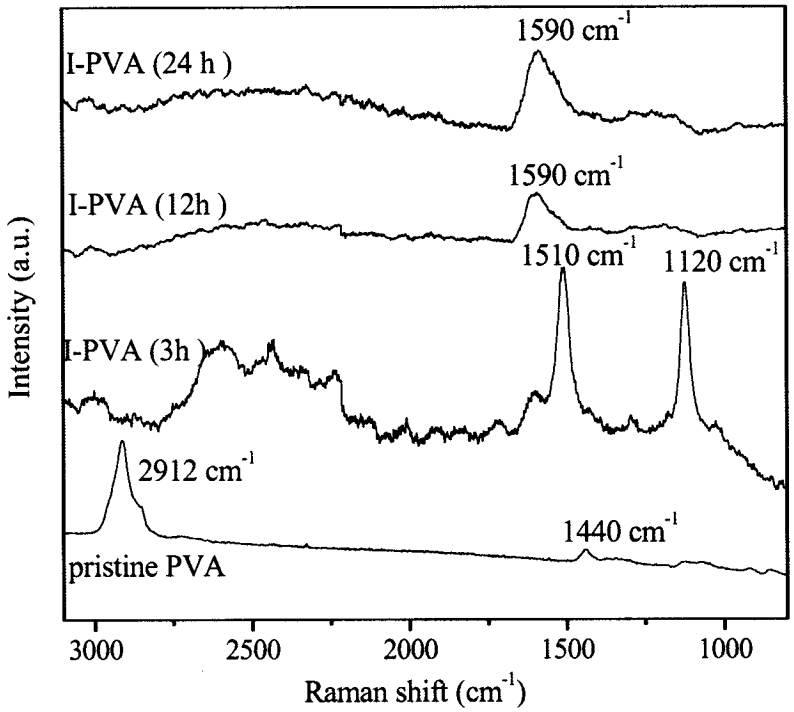

Fig. 2.7 Raman spectra of I-PVA nanofibers subjected to different iodination periods.

An important aspect in carbon fiber production is the yield of residual carbon from a polymeric precursor, because lower yield generally results in higher production costs. The carbon yield obtained for different iodination periods is presented in Table 3.1. As speculated, the carbon yield was significantly improved from 2 to 16% with 3 h iodine treatment. An increase in the iodination period to 12 h further increases the carbon yield to 21%. The reason for the higher yield of carbon fibers from an iodinated PVA sample can be attributed to the increased intramolecular cross-linking of the polyene molecules followed by the formation of polycyclic structures resulting from iodination [50]. This may inhibit the generation of volatile components during heating and lead to higher carbon yield. The carbon yield remains constant, even after an increase of the iodination period up to 24 h, which may be due to saturation of the PVA molecules with iodine, as observed for the Raman spectra of the 12 h and 24 h iodinated nanofibers shown in Fig. 2.7. Therefore,

iodine treatment is proven to be an effective means to enhance the carbonization efficiency of PVA nanofibers.

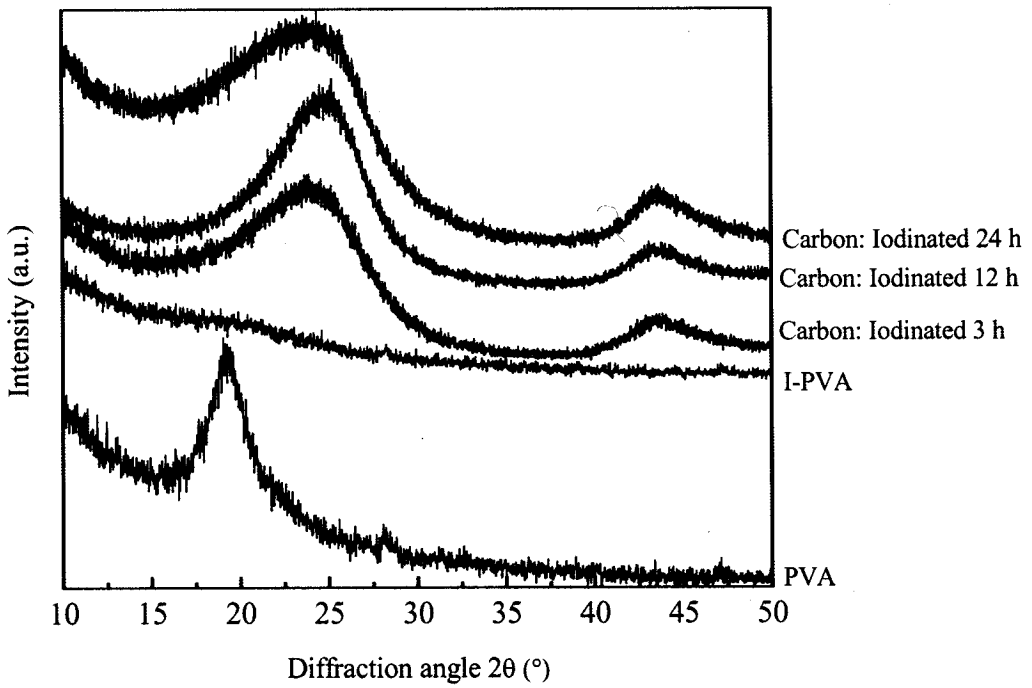

Fig. 2.8 WAXD profiles of PVA, I-PVA (24 h) and carbonized PVA nanofibers subjected to different iodination periods and carbonized at 1200 °C.

Table 3.1

Carbon yield of carbonized PVA nanofibers subjected to different iodination periods and carbonized at 1200 °C.

Iodination period (h)	0	3	12	24
Carbon yield (wt%) ± S.D.	2 ± 2	16 ± 3	21 ± 2	21 ± 2

WAXD measurements were performed to examine the structure of the carbonized PVA nanofibers. Fig. 2.8 shows that the precursor PVA nanofiber exhibits a typical semi-crystalline structure with a peak in the range of 2θ = 17–21°. Upon iodination, the crystal structure of the fibers completely disappears. The carbon fibers prepared with different iodination periods show two broad peaks at around 2θ = 18–28° and 43–45°, which correspond to the (002) and (10) diffractions of disordered micrographite stacking,

respectively [51,52]. An electron diffraction pattern of carbonized fiber with 24 h iodination and carbonized at 1200 °C has been investigated to know the molecular orientation of derived fiber (not shown in this paper) which indicates the carbonized fiber is isotropic and possesses randomly oriented crystals. Thus, it can be said that iodine treatment has an influence on the PVA molecules to produce a disordered graphite-like structure.

Bin et al. reported that a PVA composite film attained the maximum uptake of iodine at 24 h doping and then the uptake decreased with further increase of the iodination time [17]. Similarly, our co-workers also recently found that an iodination period of 24 h was optimum for stabilization of PVA for carbonization [39]. Therefore, in the present work, an iodination period of 24 h was also considered to be optimum to obtain intact carbon nanofibers, in terms of structural morphology and carbon yield.

3.3 Effect of carbonization temperature on fiber structure

3.3.1 Morphological aspect

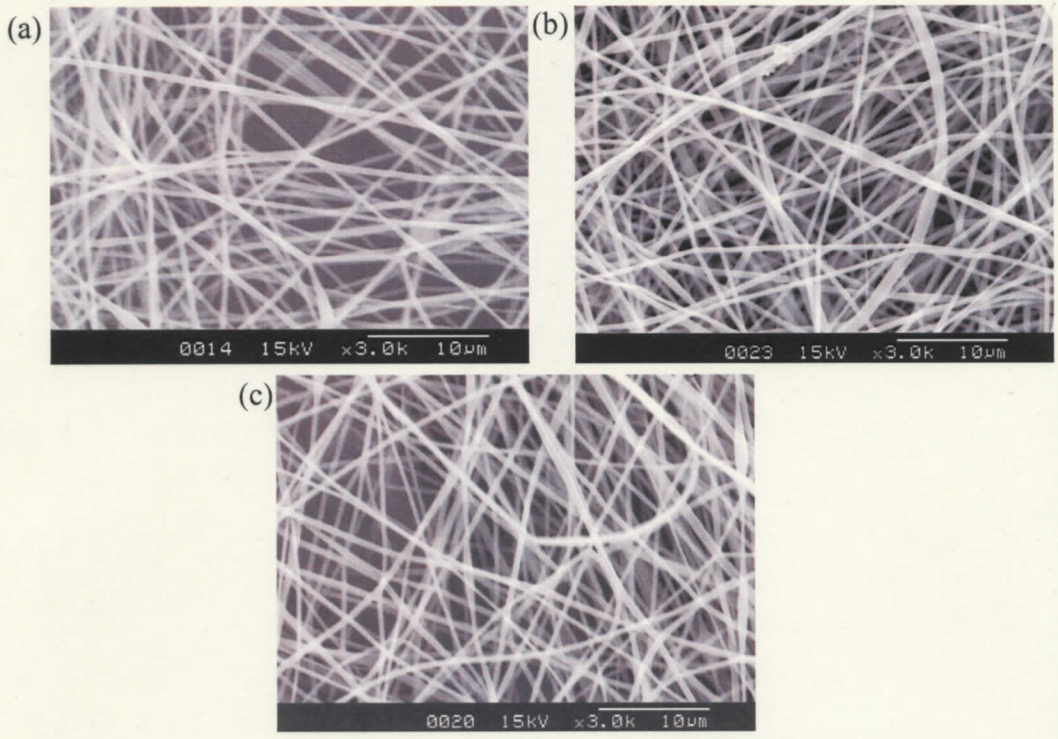

Fig. 2.9 SEM images of carbonized PVA nanofibers subjected to 24 h iodination and carbonized at (a) 800 °C, (b) 1000 °C, and (c) 1200 °C.

The morphologies of 24 h iodinated carbon fibers carbonized at different iodination temperatures of 800, 1000 and 1200 °C were examined using SEM and the results are shown in Fig. 2.9. Irrespective of the carbonization temperature, the fibrous appearance of the PVA nanofiber webs remains intact and is similar to the PVA nanofiber precursor. No significant difference in appearance was observed with variation of the carbonization temperature.

3.3.2 Structural aspect

Raman spectra of these carbonized fibers were measured and are shown in Fig. 2.10. The peak profiles of the as-spun PVA precursor nanofibers and I-PVA nanofibers were previously discussed (Fig. 2.7). For carbonized fibers obtained at different temperatures two new peaks appeared at ca. 1340 and 1590 cm^{-1}, which correspond to the D (characteristics of a disordered sp^2 phase) and G bands (characteristic of the in-plane stretching vibration mode E_{2g} of well crystallized graphite), respectively [53]. The peak positions remain the same with an increase of the carbonization temperature; however, when closely examined, the intensity of the G band appears sharpest for the 1200 °C carbonized sample. This indicates that the graphite structure is better developed at a carbonization temperature of 1200 °C, compared to the carbon fibers carbonized at 800 and 1000 °C.

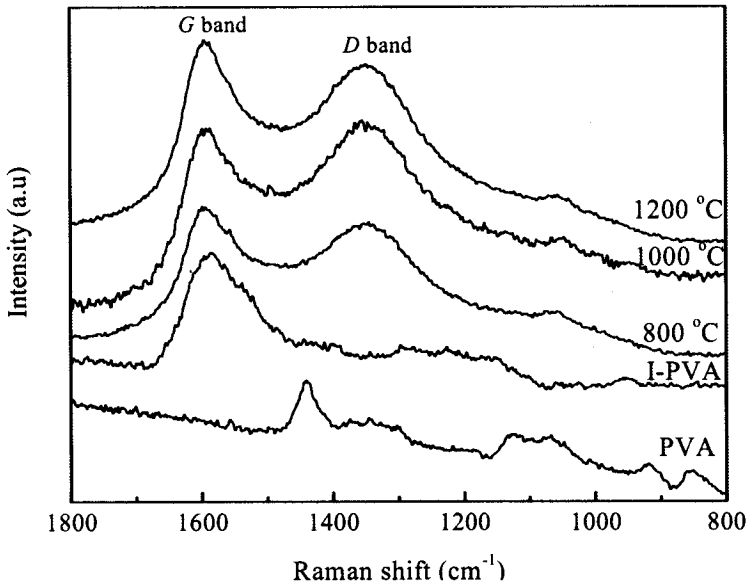

Fig. 2.10 Raman spectra of PVA and carbonized PVA nanofibers subjected to 24 h iodination and different carbonization temperatures.

Fig. 2.11 shows WAXD profiles of the carbon fibers derived from different carbonization temperatures. Similar to Fig. 2.9, each pattern has two peaks in the range of $2\theta = 18 - 28°$ and $43 - 45°$, which indicates the respective diffractions of the (002) and (10) graphite planes. The shape of the first peak becomes sharper and moves towards lower angles for the fibers obtained at a carbonization temperature of 1200 °C. This may imply an improvement in ordered graphitic crystal growth for this fiber. However, the carbon yield for each carbonization condition was measured and was around 21%. Considering the overall morphology and structural analysis, the carbonization temperature of 1200 °C was found optimum in this study.

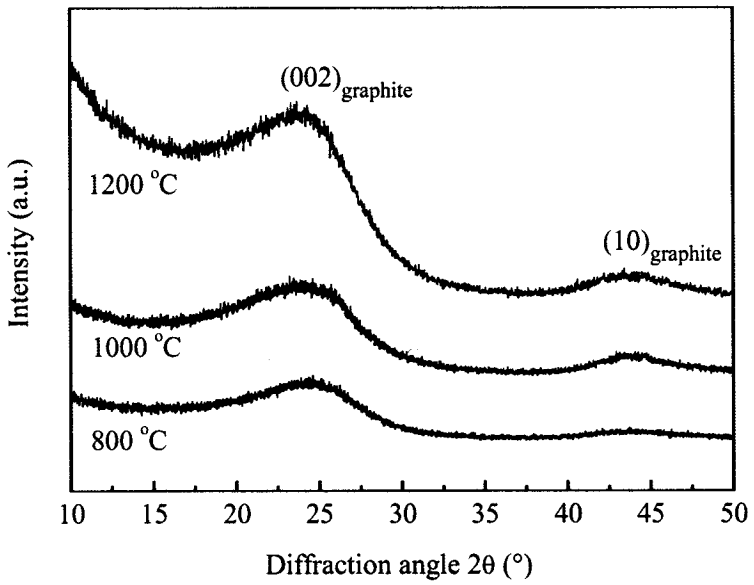

Fig. 2.11 WAXD profiles of carbonized PVA nanofibers subjected to 24 h iodination at different carbonization temperatures.

3.4 Effect of Ni particles addition to the spinning solution on carbonized PVA nanofibers

The addition of metal ions influences the thermal decomposition and carbonization behavior of vinyl polymers [36, 54, 55]. We recently reported a significant enhancement of carbon yield (ca. 48%) and acceleration of graphite formation after the addition of Ni-acetate to PVA fiber [39]. The nucleation and growth process of graphene layers in carbon nanotubes are also influenced by Ni nanoparticles [56]. Therefore, we have investigated the

influence of Ni ion addition on PVA nanofibers to achieve carbon nanofibers with good yield and morphology.

The addition of metal particles to a spinning solution usually changes its properties, such as conductivity and viscosity. Therefore, the electrical conductivity of the spinning solution was measured after the incorporation of Ni-acetate. The electrical conductivity of neat PVA solution was 2.5 mS/m, whereas that of the spinning solution with Ni-acetate was 186.7 mS/m. The addition of an electrolyte increases the elasticity of the spinning solution, which tends to yield fibers with smaller diameters [11]. In contrast, highly conductive solutions exhibit less spinnability [12] and also lead to more bead formation during ES [3,5]. In the present study, 7 wt% PVA solution with Ni-acetate (4 wt% of the PVA solid content) gave unstable spinning performance when using the same process parameters as those for neat PVA electrospinning. In order to obtain stable spinning with less bead formation, different PVA concentrations were investigated, and a 6 wt% PVA solution containing Ni-acetate was found appropriate.

3.4.1 Morphological aspect

Fig. 2.12 shows SEM images of different PVA/Ni nanofibers. The as-spun PVA/Ni nanofibers are visibly smooth with no entanglement and have an average diameter of 4.4×10^2 nm. After 24 h iodination, the PVA/Ni nanofibers became swollen and obvious. The PVA/Ni nanofibers carbonized at 1200 °C appear to be intact. Fig. 2.13 shows a histogram of the fiber diameter for as-spun PVA/Ni nanofibers and carbonized PVA/Ni nanofibers. The diameter distribution pattern of carbonized PVA/Ni nanofibers also resembles to normal distribution pattern with an average fiber diameter of 2.9×10^2 nm that is much finer than the that of precursor one.

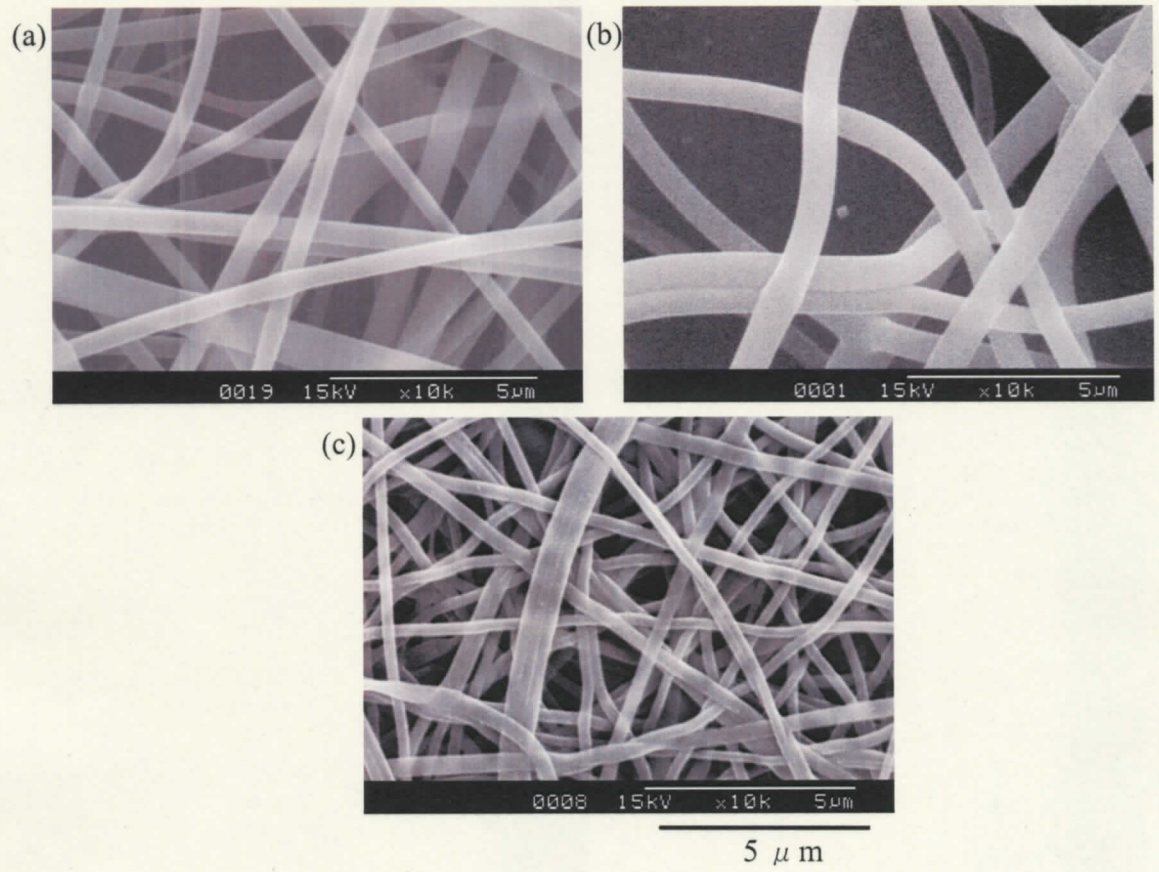

Fig. 2.12 SEM images of (a) as-spun PVA/Ni, (b) 24 h iodinated PVA/Ni, and (c) PVA/Ni nanofibers carbonized at 1200 °C.

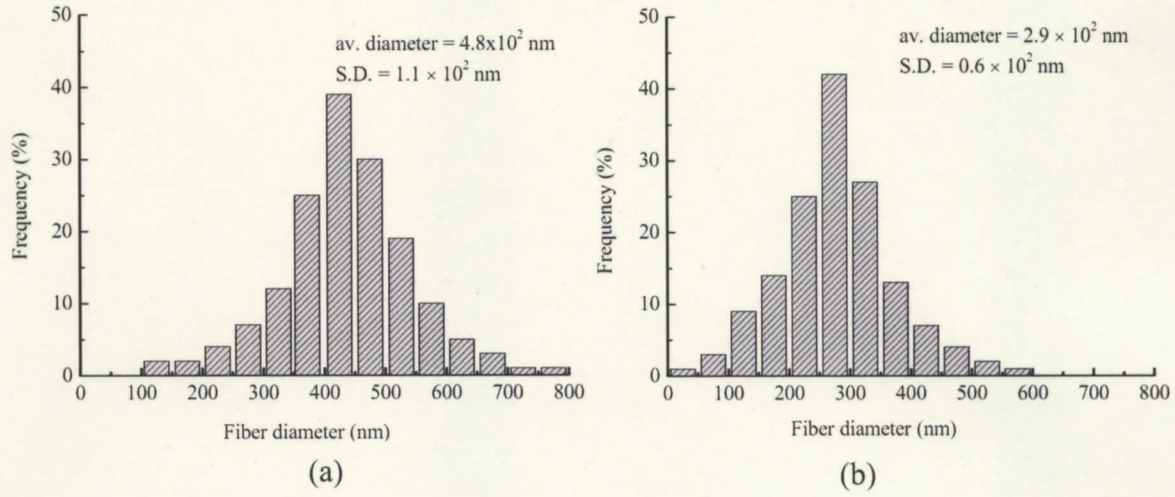

Fig. 2.13 Diameter distribution of (a) as-spun PVA/Ni, and (b) carbonized PVA/Ni nanofibers

3.4.2 Structural aspect

Fig. 2.14 shows Raman spectra of the as-spun PVA/Ni nanofibers, iodinated PVA/Ni nanofibers (24 h iodination) and carbon fibers carbonized at 1200 °C. Addition of Ni-acetate to the spinning solution does not result in such a distinctive structural change of the Raman spectrum. Iodinated PVA/Ni shows a relative sharp peak at ca. 1590 cm^{-1}, which indicates the formation of polycyclic aromatic structures by intermolecular crosslinking of polyenes in the PVA nanofibers. After carbonization of PVA/Ni nanofibers the presence of a sharp G band at ca. 1590 cm^{-1} and the D band at ca. 1350 cm^{-1} confirms the formation of the carbon structure.

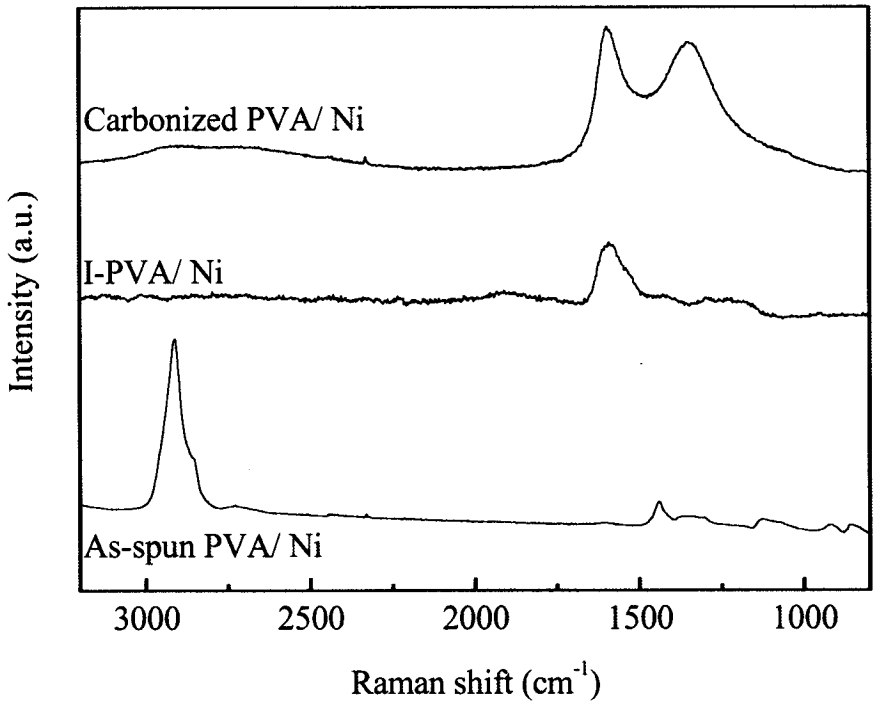

Fig. 2.14 Raman spectra of as-spun PVA/Ni, iodinated PVA/Ni and carbonized PVA/Ni nanofibers.

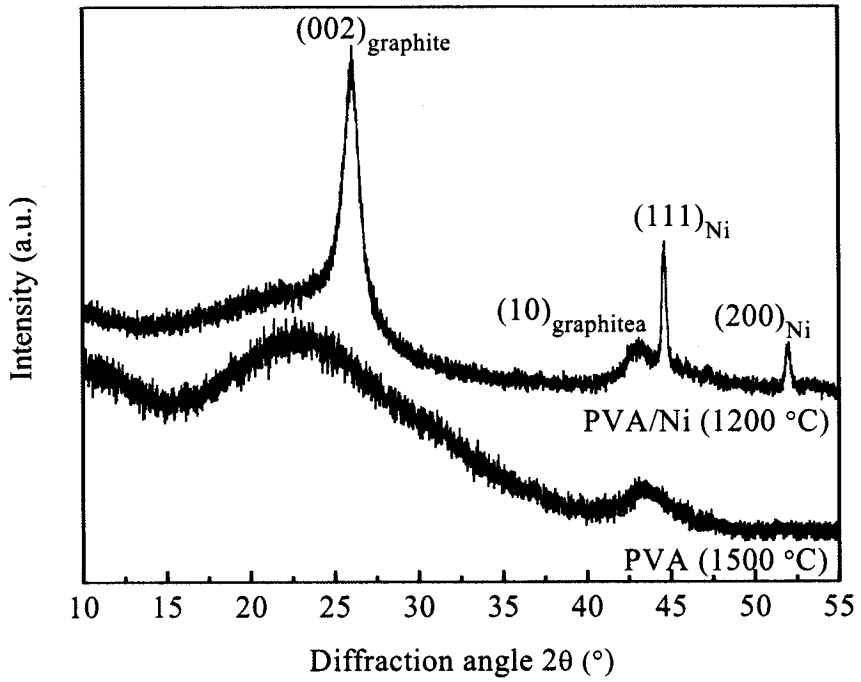

Fig. 2.15 WAXD profiles of carbon fibers from (a) neat PVA nanofibers carbonized at 1500 °C, and (b) PVA/Ni nanofibers carbonized at 1200 °C.

Fig. 2.15 shows WAXD profiles of carbon fibers derived from PVA/Ni nanofibers carbonized at 1200 °C and neat PVA nanofibers carbonized at 1500 °C. Pure PVA nanofibers carbonized at 1500 °C have a broad (002) peak and a small (10) peak of the graphene layer, which confirms their disordered graphite structure. The peaks of the PVA/Ni derived carbon fiber at ca. $2\theta = 26°$ and ca. $2\theta = 43°$, assigned to the (002) and (10) diffractions, respectively, became significantly sharper, which signifies the formation of a very highly ordered graphite-like structure. In contrast, the carbon fibers derived from neat PVA nanofibers at the same carbonization temperature of 1200 °C (in Fig. 2.11) showed a disordered graphite structure. Therefore, the presence of Ni metal particles induced the formation of a graphite-like structure at a lower carbonization temperature of 1200 °C. However, the sharp peaks at $2\theta = 44.6°$ and $2\theta = 52°$ in PVA/Ni derived carbon fiber indicated the (111) and (200) reflection of Ni metal respectively, no other peaks of Ni-oxide or Ni-iodide crystallite was observed [57]. In addition, the reduction growth of Ni nanoparticle was resulted from interaction of Ni^{2+} and reducing agent C, where C might

contribute from either the ligand ($CH_3COO–$) or the PVA polymer which was not investigated in this study. The crystallite size (D_p) of Ni-nanoparticle was measured from the WAXD data using Scherrer formula, where diffraction curves were fitted by Gaussian function. The crystallite sizes of Ni nanoparticle were measured using Scherrer equation and found to be 29.62 nm for Ni (111) and 26.4 nm for Ni (200) which are comparable with the Ni nanoparticle sizes observed in the following TEM image (avg. size: 30–40 nm).

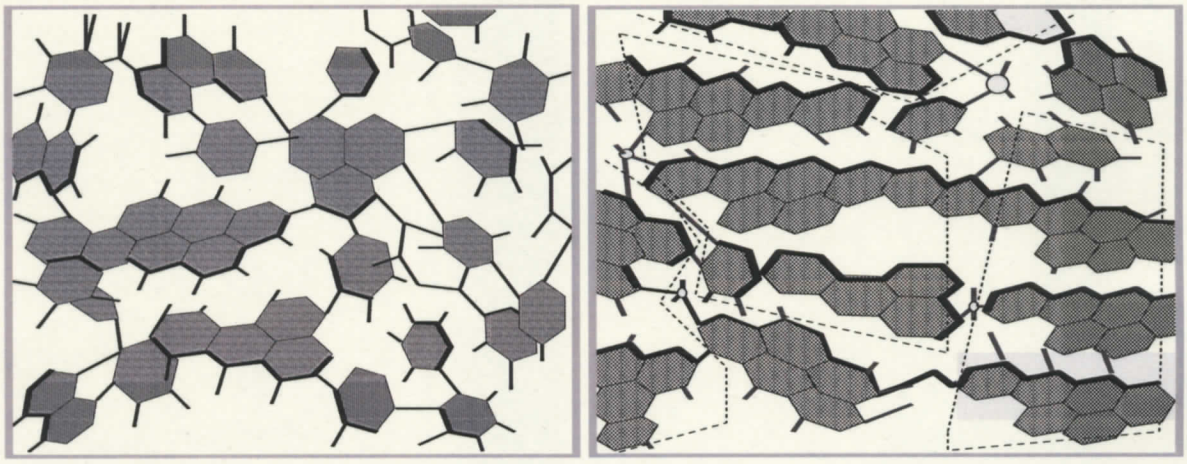

(a) (b)

Fig. 2.16 Possible structural models of carbon fibers derived from (a) neat PVA, (b) PVA/Ni (adapted from ref. 53). The dotted lines in Figure 16(b) indicate the ordered stacking of carbon structure.

Fig. 2.16 describes the possible structural models of our carbon fibers derived from neat PVA and PVA/Ni [52]. It shows that the carbon fiber with Ni particle has more ordered structure and longer graphene layer than neat one, which is further supported by the TEM images of carbon fibers derived from PVA/Ni nanofibers shown in Fig. 2.17. In TEM images other than Ni nanoparticles, the curvy layer-like structure confirms the presence of a graphene layer [46]. So the carbon fibers are believed to show an ordered structure in a very short range and show disordered structure in the long range. The interlayer spacing in a graphite sheet is known to be approximately 0.33 nm [33], and in this case, the spacing was ascertained to be ca. 0.35 nm. These results reveal the formation of a turbostratic graphite-like structure in the PVA/Ni nanofibers carbonized at a low carbonization temperature of 1200 °C.

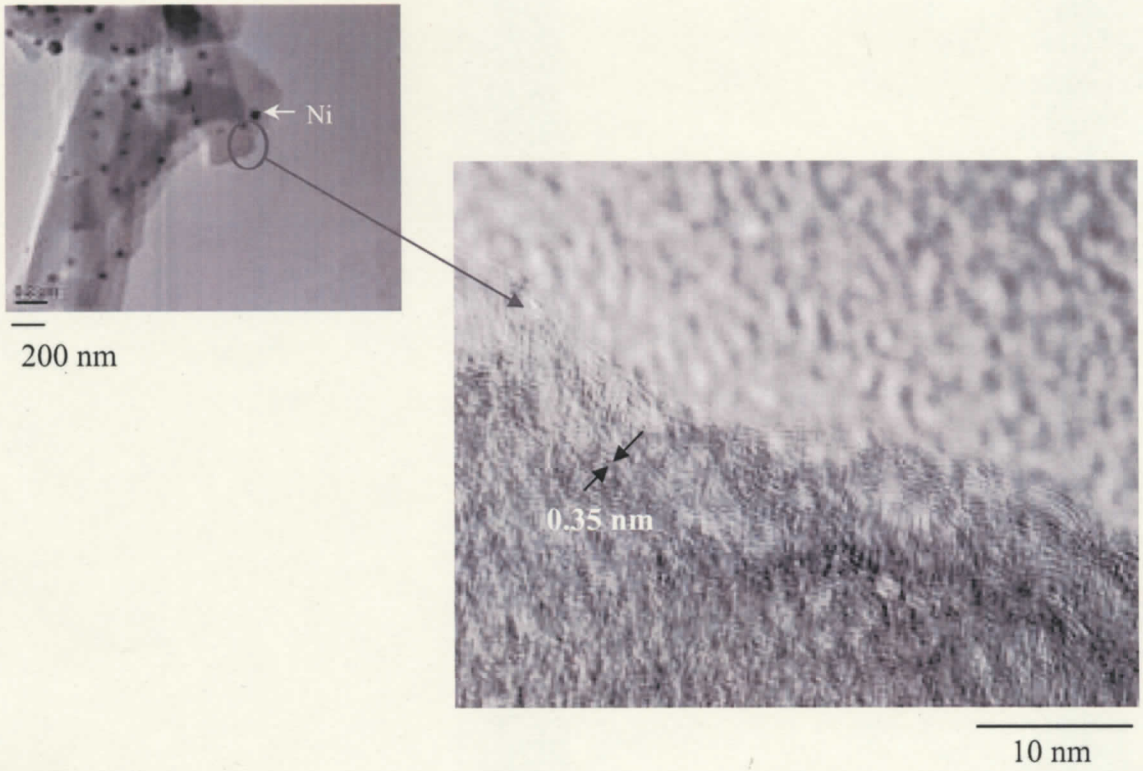

Fig. 2.17 TEM images of PVA/Ni nanofibers carbonized at 1200 °C.

In addition, the carbon yield was noticeably increased from 21 to 34% after Ni addition. It is feasible that Ni stabilizes intramolecular volatile components during heating, which leads to higher carbon yield. Thus, it can be said that Ni improves the carbonization efficiency of the PVA polymeric precursor as a source of carbon material. Furthermore, the derived carbon fiber expectantly possessed splendid magnetic property due to the presence of Ni nanoparticles [57].

4. Conclusions

A simple and effective method was developed to fabricate carbon fibers from precursor PVA nanofibers prepared by ES followed by iodine treatment. Iodine causes structural changes of the PVA nanofibers and imparts thermal stability to endure the carbonization process, which results in improved carbon yield. In this study, 24 h iodination time and carbonization at 1200 °C for 24 h were found to be favorable to obtain good carbon fibers in terms of the structural parameters and carbon yield.

Furthermore, Ni metal nanoparticles were successfully incorporated into the PVA nanofibers using a spinning solution doped with Ni-acetate, which increases the conductivity of the spinning solution. Constant spinning was possible with incorporated Ni when using a lower polymer concentration than that used for pure PVA nanofibers. Moreover, the carbon fiber derived from a PVA/Ni nanofiber precursor resulted in smaller fiber diameter and higher carbon yield. The results also revealed that Ni significantly accelerates the formation of the ordered graphite structure, even at a lower carbonization temperature of 1200 °C.

5. References

[1] Ohkawa K, Hayashi S, Nishida A, Yamamoto H, Preparation of pre-cellulose nanofiber via electrospinning, Tex Res J, 79, 1396–1401 (2009).

[2] Wilson M, Kannangara K, Smith G, Simmons M, Raguse B, Nanotechnology: Basic science and emerging technologies, Chapman and Hall/CRC, Chapter 5, p84 (2002).

[3] Ramakrishna S, Fujihara K, Toe WE, Lim TC, Ma M, An introduction to electrospinning and nanofiber, World Sci Pub. Co. Ltd., p17–26 (2005).

[4] Li D, Xia Y, Electrospinning of nanofibers: Reinventing the wheel?, Adv Mater, 16, 1151–1170 (2004).

[5] Koski A, Yim K, Shivkumar S, Effect of molecular weight on fibrous PVA produced by electrospinning, Mater Lett, 58, 493–497 (2004).

[6] Park JY, Lee IH, Bea GN, Optimization of electrospinning conditions for preparation of nanofibers from polyvinylacetate (PVAc) in ethanol solvent, J Indus Eng Chem, 14, 707–713 (2008).

[7] Ding B, Kimura E, Sato T, Fujita S, Shiratori S, Fabrication of blend biodegradable nanofibrous nonwoven mats via multi-jet electrospinning, Polymer, 45, 1895–1902 (2004).

[8] Yamashita Y, Electrospinning-The latest in nanotechnology: the creative challenge of nanofibers, SLS, Japan, p145–190 (2007).

[9] Liu W, Adanur S, Properties of electrospun polyacrylonitrile membranes and chemically-activated carbon nanofibers, Tex Res J, 80, 124–134 (2010).

[10] Yasuda E, Inagaki M, Kaneko K, Endo M, Ota A, Tanabe Y, Carbon Alloys-Novel concept to develop carbon science and technology, Elsevier Science Ltd., Oxford, UK, p3–11 (2003).

[11] Setton R, Bernier P, Lefrant S, Carbon molecules and materials, Taylor and Francis Pub. Ltd., London, UK, p6–9 (2002).

[12] Wang H, Zhang L, Gavalas GR, Preparation of supported carbon membranes from furfuryl alcohol by vapor deposition polymerization, J Membr Sci, 177, 25–31 (2000).

[13] Kitagawa H, Kobayashi S, Preparation of activated carbon fiber from polyvinylidene chloride waste, Nippon kagakkai Yokoshu, 79, 114 (2001).

[14] Bürger A, Fitzer E, Heym M, Terwiesch B, Polyimides as precursor for artificial carbon, Carbon, 13, 149–157 (1975).

[15] Fitzer E, PAN-based carbon fibers-present state and trend of the technology from the viewpoint of possibilities and limits to influence and to control the fiber properties by the process parameters, Carbon, 27, 621–645 (1989).

[16] Yamasthita J, Shiyo M, Kikutani T, Hashimoto T, Activated carbon fibers and films derived from pol(vinylidene fluoride), Carbon, 39, 207–214 (2001).

[17] Bin Y, Chen Q, Nakamura Y, Tsuda K, Matsuo M, Preparation and characterization of carbon films prepared from poly(vinyl alcohol) containing metal oxide and nanofibers with iodine pretreatment, Carbon , 45, 1330–1339 (2007).

[18] Shindo A, Sawada Y, Orientation structure in traverse sections of carbon fibers from dehydrated polyvinyl alcohol, Carbon, 18, 419–425 (1980).

[19] Oya A, Yoshida A, Abe Y, Iizuka T, Makiyama N, Antibacterial activated carbon fiber derived from phenolic resin containing silver nitrate, Carbon, 31, 71–73 (1993).

[20] Zhang SJ, Quing H, Feng H, PVA based activated carbon fibers with lotus root like axially porous structure, Carbon, 44, 2059–2068 (2006).

[21] Shindo A, Soma I, Highly crystallite-oriented carbon fibers from polymeric fibers, Appl. Polym. Symp., 9, 305–313 (1969).

[22] Zussman E, Chen X, Ding W, Calabri L, Dikin DA, Quintana JP, Ruoff RS, Mechanical and structural characterization of electrospun PAN-derived carbon nanofibers, Carbon, 43, 2175–2185 (2005).

[23] Park SH, Kim C, Choi YO, Yang KS, Preparation of pitch-based CF/AFC webs by electrospinning, Carbon Lett, 41, 2655–2657 (2005).

[24] Kim C, Cho YJ, Yun WY, Ngoc BTN, Yang KS, Chang DR, Lee JW, Kojima M, Kim YA, Endo M, Fabrications and structural characterization of ultra-fine carbon fibers by electrospinning of polymer blends, Solid State Communication, 142, 20–23 (2007).

[25] Bui NNB, Kim BH, Yang KS, Cruz MED, Ferraris JP, Activated carbon fibers from electrospinning of polyacrylonitrile/pitch blends, Carbon, 47, 2538–2539 (2009).

[26] Yang KS, Edie DD, Lim DD, Kim YM, Choi YO, Preparation of carbon fiber web from electrospinning of PMDA-ODA poly(amic acid) solution, Carbon, 41, 2039–2046 (2003).

[27] Zussman E, Yarin AL, Bazilevsky AV, Avrahami R, Feldman M, Electrospun Polyacrylonitrile/Polymethyl methacrylate)-derived turbostratic carbon micro-/nanotubes, Adv Mater, 18, 348–353 (2006).

[28] Yamasthita J, Soneda Y, Kodama M, Hootari H, Shiyo M, Stabilization of poly(vinyl chloride) using iodine vapor for preparing carbon aerogel, J Mater Sci, 39, 1463–1466 (2004).

[29] Khan MMR, Gotoh Y, Morikawa H, Miura M, Fujimori Y, Nagura M, Carbon fiber from natural biopolymer Bombyx mori silk fibroin with iodine treatment, Carbon, 45, 1035–1042 (2007).

[30] Khan MMR, Gotoh Y, Miura M, Morikawa H, Nagura M., Influence of an iodine treatment on the structure and physical properties of Bombyx mori silk fibroin fiber, J Polym Sci Part B: Polym Phys, 44, 3418–3426 (2006).

[31] Khan MMR, Gotoh Y, Miura M, Morikawa H, Influence of iodine treatment on the carbonization behavior of Antheraea pernyi silk fibroin fiber, J Appl Polym Sci, 110, 1358–1365 (2008).

[32] Khan MMR, Gotoh Y, Morikawa H, Miura M, Graphitization behavior of iodine-treated Bombyx mori silk fibroin fiber, J Mater Sci, 44, 4235–4240 (2009).

[33] Jenkins GM, Kawamura K, Polymeric Carbons: Carbon fiber, glass and char, Cambridge university press, UK, pp11–44, 52–80,151 (1976).

[34] Donnet J, Wang TK, Rebouillat S, Peng JCM., Carbon fibers, Vol. 3, Marcel Dekker, Inc., New York, USA, (1998).

[35] Otani S, Okuda, K, Matsuda HS, Carbon fiber, Vol. 3, Kindai Henshu Ltd., Tokyo, Japan, p231 (1983).

[36] Tomash AV, Polevov VN, Mamagulashvili VG, Chernyaeva GA, Shepelev AD, Fabrication of sorption-filtering nonwoven material from ultrafine polyvinyl alcohol carbonized fibers by electrospinning, Fibre Chem, 37, 187–191 (2005).

[37] Wan YQ, He JH, Yu JY, Carbon nanotube-reinforced polyacrylonitrile nanofibers by vibration-electrospinning, Polym Intl, 56, 1367–1370 (2007).

[38] Yan ZY, Chen SY, Ying H, Wang HP, Xue Y, Fabrication of bacterial cellulose/multi-walled carbon nanotubes composite membrane , Nonlin Sci Lett D, 1, 113–117 (2010).

[39] Harada M, Gotoh Y, Nagura M, Ohkoshi Y, Carbonization behavior of iodinated polyviny alcohol containing metal acetate salt, Fiber Preprint , 62, 71–71 (2007).

[40] Wang HS, Fu GD, Li XS, Functional polymeric nanofibers from Electrospinning, Recent Patent on Nanotechnology, 3, 21–31 (2009).

[41] Liu Y, He JH, Bubble electrospinning for mass production of nanofibers, Int J Nonlin Sci Num, 8, 393–396 (2007).

[42] Liu Y, Dong L, Fan J, Kang WM, Xu L, A mathematical model for bubble electrospinning, Nonlin Sci Lett A, 1(3), 239–242 (2010).

[43] Patterson AL, The scherrer formula for X-ray particle size determination, Phys Rev, 56, 978–982 (1939).

[44] Tripatanasuwan S, Zhong Z, Reneker DH, Effect of evaporation and solidification of the charged jet in electrospinning of poly(ethylene oxide) aqueous solution, Polymer, 48, 5742–5746 (2007).

[45] Yamashita, J, Method of manufacturing carbon material from polyvinyl alcohol, Japanese Patent, Japanese Patent 3723844, (2005).

[46] Sashio M, Tanaka M, Thermal reaction of poly(vinyl alcohol)-iodine complex membranes, J Polym Sci Part A: Polym Chem, 23, 905–909 (1985).

[47] Badr YA, El-Kader KMA, Khafagy RM, Raman spectroscopic study of CdS/PVA composite films, J Appl Polym Sci, 92, 1984–1992 (2004).

[48] Goto A, Kyotani M, Tsugawa K, Piao G, Akagi K, Yamaguchi C, Matsui H, Koga Y, Nanostructures of pyrolytic carbon from polyacetylene thin film, Carbon, 41, 131–138 (2003).

[49] Rumelfanger R, Asher SA, Perry MB, UV resonance Raman characterization of polycyclic aromatic hydrocarbons in coal liquid distillates, Appl Spectrosc, 42, 267–272 (1988).

[50] Yang H, Horii F, Investigation of the structure of poly(vinyl alcohol)-iodine complex hydrogel prepared from the concentrated polymer solutions, Polymer, 49, 785–791 (2008).

[51] Short MA, Walker Jr. PL, Measurement of interlayer spacings and crystal sizes in turbo-static carbons, Carbon, 1, (1963) 3–10.

[52] Otani S, Okuda K, Matsuda HS, Carbon fiber, Vol 1, Kindai Henshu Ltd., Tokyo, Japan, p8–9 (1986).

[53] Uglov VV, Kuleshov AK, Samtsov MP, Astashinsakaya MV, Raman light scattering in hydrogenated metal-carbon composite films, J Appl Spectrosc, 73, 388–393 (2006).

[54] Inagaki M, Fujita K, Takeuichi Y, Oshida O, Iwata H, Konno H, Formation of graphite crystals at 1000–1200 °C from mixtures of vinyl polymers with metal oxides, Carbon, 39, 921–929 (2001).

[55] Inagaki M, Okada Y, Miura H, Konno H, Preparation of carbon-coated transition metal particles from mixtures of metal oxide and polyvinylchloride, Carbon, 37, 329–334 (1990).

[56] Shin YH, Hong S, Carbon diffusion around the edge region of nickel nanoparticles, Appl Phys Lett, 92, 043103–1–043103–3 (2008).

[57] Barakat NAM, Kim B, Kim HY, Production of smooth and pure nickel metal nanofibers by the electrospinning technique: Nanofiber possess splendid magnetic properties, J Phys Chem C, 113, 531–536 (2009).

Chapter 3

Iodine-aided fabrication of hollow carbon fibers from solid poly(vinyl alcohol) fibers

1. Introduction

The previous chapter deals the fabrication of carbon fibers from electrospun poly(vinyl alcohol) (PVA) nanofibers using iodine pretreatment. In this chapter, we will explore the idea of selective and controlled iodination technique for the fabrication of hollow carbon fiber from solid PVA fiber.

Research on carbon-based materials in recent years has led to the discovery of several new forms of carbon structures, such as fullerenes, carbon nanotubes, carbon nanofoams and colossal carbon tubes with unique properties and applications [1–4]. Because of their hollow structure, hollow carbon fibers (H-CFs) possess a high specific surface area, and are extremely light weight, with a low density and high-pressure resistance, in addition to the excellent properties of the carbon fiber. H-CFs have shown their potential in applications such as membrane-based gas separation technology, filtration, catalysis, electrodialysis, and energy storage [5,6]. H-CFs have also found important applications in lithium ion batteries owing to their high conductivity and reversible capacity [7–8], and in radars owing to their hollow structure and microwave absorption properties [9–11]. The excellent mass-transfer properties conferred by the hollow fiber configuration led to numerous commercial applications in various fields, such as medicine (blood fractionation), water reclamation (purification and desalination), azeotropic mixture separation, the biochemical industry (bioseparation and bioreactors), and hydrocarbon separation [12–14]. More generally, H-CFs, with their unique and useful characteristics of high heat resistance and chemical resistance, will compete with polymeric and other inorganic hollow structures and pave the way to highly promising new applications.

H-CFs have typically been prepared from various hollow polymeric precursors based on polyacrylonitrile, polyimide, polysulfone, cellulose acetate, polyvinylidene chloride, polyfurfuryl alcohol, and polyetherimide [15–21]. The spinning process usually employed to fabricate precursor fibers involves wet, melt, dry, or dry/wet extrusion of the precursor followed by a thermal treatment to stabilize the fibers and carbonize them to ultimately afford carbon fibers. Recently, electrospun fibers were used for the fabrication of nano H-CFs [23–24], and also a template method was reported for the synthesis of polypropylene-based H-CFs [25]. These processes require multiple preparation steps, and are therefore costly. However, to authors' knowledge, there has been no report regarding the fabrication

of hollow carbon structures from solid polymeric fibers. In this chapter of thesis, we focus on the fabrication of H-CF from commercially available PVA fiber using iodine pretreatment followed by stabilization and subsequent carbonization processes at 800 °C [26]. Iodination converted the chemical structure of PVA to the polyene form through a dehydration reaction, and stabilization of heat treatment at 200 °C in air ensured insolubilization of the iodinated PVA fibers. These processes greatly enhanced the carbon yield and resulted in intact carbon fibers [27,28]. The selective iodination and subsequent stabilization of the fibers close to the fiber surface yielded H-CFs after carbonization at 800 °C. Afterwards, we increase the heating temperature of carbonization of PVA fibers from 800 to 3000 °C, and evaluate the influence of carbonization conditions on hollow morphology and structure of resulted H-CFs.

The final structure of carbon materials and their ultimate properties are largely governed by the carbonization process, as reported in a number of studies [29–38]. Wei Xie et al. investigated the effect of carbonization time on polyacrylonitrile-based hollow fibers (PAN-H-CFs), and succeeded in increasing the degree of graphitization, electrical volume and permittivity at high temperatures [39]. Tsai HA et al. found that the morphology of heat-treated PAN-H-CF membranes became denser with the improvement of pervaporation performances at high heat treatment temperatures (HTT) [40]. Sun et al. were able to improve the specific surface area and adsorption properties by studying the activation and HTT of carbonization of PAN-H-CFs [41,42]. However, most of this research is limited to PAN-H-CFs, and the use of a high HTT of 3000 °C on PVA-based H-CFs has not been reported elsewhere. As part of an extended study, we investigate the carbonization of PVA fibers at high HTTs of 800 to 3000 °C and discuss the influence of carbonization conditions on the hollow structure formation and the structural development of the resultant H-CFs. Furthermore, the effects of HTT on the hollow characteristics are also considered. Finally, we investigate the bending behavior of the H-CFs obtained, after the incorporation of a polymeric filler inside the core of the H-CFs.

2. Experimental

2.1 Materials

A molecularly oriented solid PVA multifilament with a diameter of ca. 110 μm was used as a precursor fiber. Special-grade iodine (I_2), ammonium iodide (NH_4I), and methyl methacrylate monomer (MMA) were purchased from Wako Pure Chemicals Co. Ltd., and benzoyl peroxide (BPO) from Nacalai Tesque Inc., and used as received.

2.2 Pretreatment and carbonization

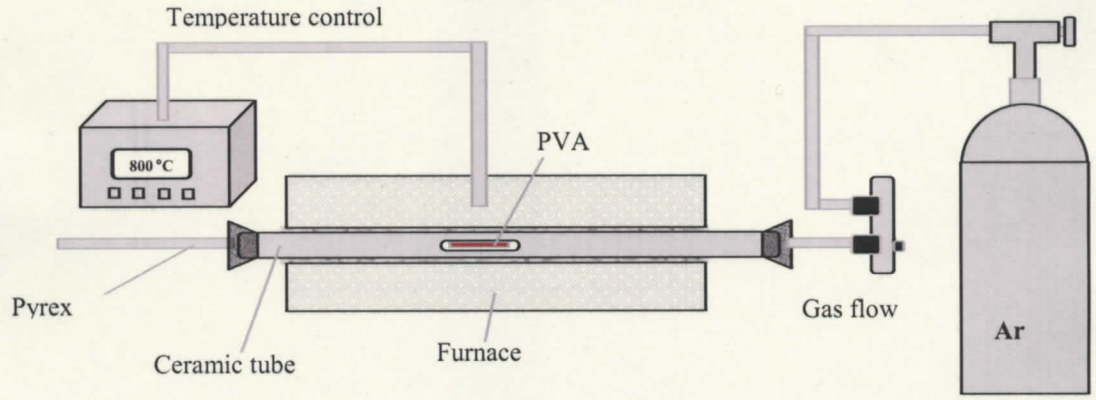

Fig. 3.1 Tubular carbonization system for PVA based H-CFs fabrication.

The pretreatment of PVA filament was performed by iodine doping techniques. First, PVA filament was treated with an aqueous solution of I_2-NH_4I (I_2: 0.05 mol/L, NH_4I: 0.2 mol/L) for 2 h at 90 °C. The color of the precursor became dense brown due to the sorption of iodine components. The iodinated PVA (I-PVA) was stabilized in an air atmosphere at 200 °C for 24 h under a small loading (ca. 2 kPa) to inhibit marked shrinkage. Then, the stabilized PVA (S-PVA) was carbonized at 800 °C in an alumina tubular furnace under an Ar flow at a heating rate of 1 °C/min. Afterwards, carbonization at HTTs of 800, 1500, 2000, 2500, and 3000 °C, using the heating rates 2, 5, and 10 °C/min were investigated. Notably, for high HTTs of carbonization from 2000 to 3000 °C, the H-CFs were first carbonized at 1500 °C and at a heating rate of 2 °C/min, and then heated further in the high temperature furnace. The heating rate was optimized for structural quality of the H-CFs, as

explained in the Results and discussion section. The ceramic tubular carbonization furnace was constructed as shown in Fig. 3.1.

2.3 Stuffing of polymer into H-CFs

Bulk radical polymerization was conducted to fill polymethyl methacrylate (PMMA) in the core of the H-CFs. Polymerization of the monomer MMA was initiated by benzoyl peroxide (BPO) at a monomer-to-BPO weight ratio of 1 to 0.045. The H-CFs were immersed in the monomer solution and placed under vacuum for 10 min. Thus, the cores of the H-CF were filled with monomer solution. Then, the polymerization to PMMA was conducted at a high HTT of 70 °C for 15 min, followed by another 15 min at 90 °C after proper sealing of both ends of the H-CFs with epoxy.

2.4 Measurements

X-ray measurements were carried out using a Rigaku Rotorflex RU-200B X-ray generator. The X-ray source was Ni-filtered Cu-K_α radiation (λ = 0.15418 nm) generated at 40 kV and 150 mA. X-ray photographs were captured with a Fuji film imaging plate, and the wide angle X-ray diffraction (WAXD) was measured with a goniometer. The X-ray parameters were measured on the ground samples mixed with high-purity silicon powder as an inner standard, according to conventional procedure. A correction was made for peak broadening due to the equipment by using the silicon standard. The Bragg's diffraction law was used to determine the interlayer spacing (d):

$$d = \lambda / 2\sin\theta$$

where d is the interlayer spacing (nm) and θ is the Bragg's angle.

The Scherrer's equation was used to determine the crystallite size (L):

$$L_c(L_a) = k \cdot \lambda / \beta \cdot \cos\theta$$

where L_c is the crystallite height in the direction normal to (002) plane, β is the full-width at half-maximum (FWHM) (radians), k is the Scherrer constant, which for the (002) peak is 0.94, while L_a is the crystalline width in the direction of (100) planes, and the value of k for the (100) peak is 1.84. Another way to obtain the crystalline width (L_a) is to use Knight's empirical formula using the Raman spectra [43].

$$L_a = 4.35\ (I_D/I_G)^{-1}$$

where I_D/I_G is the area ratio of Raman *D* and *G* bands. This method is useful when the (100) peak is not clearly defined in the X-ray diffraction profile, and was used in this study.

The graphitization degree or the probability of nearest neighboring pairs ordering in graphite relation (P_1) is estimated by the following equation [44], although the value should be taken with reservation [45]:

$$d_{002} = 0.335\ P_1 + 0.344\ (1\text{-}P_1)$$

where P_1 is the degree of graphitization and d_{002} is the interlayer spacing of (002) plane.

The orientation factor of the resultant H-CFs crystallite (π) is determined as follows:

$$\pi = (180\text{-}H^\circ)/180$$

where H° is the half-width of the intensity distribution curve along the Debye-Scherrer ring.

Transmission electron microscopy (TEM) observation was conducted at an acceleration voltage of 200 kV using JEOL JEM-2010 instrument.

Raman spectra were recorded using a Kaiser Hololab 5000 spectrometer, equipped with a MK-II filter probe using an Nd:YAG laser beam (λ=532 nm) generated at 50 mW.

The scanning electron microscopy (SEM) observation was performed on a Hitachi S-2380N after sputtering probe with platinum. The fiber diameter and wall thickness of the H-CFs obtained were measured from SEM images using NIH Image J. The carbon yield was determined by measuring the change in weight of the precursor PVA fibers (W_{PVA}) and the resultant H-CFs ($W_{H\text{-}CFs}$) before and after carbonization, and expressed in percentage as follows:

$$\text{Carbon yield (\%)} = (W_{PVA}\text{-}W_{H\text{-}CFs})/W_{PVA} \times 100$$

The electrical conductivity of the resultant H-CFs was evaluated from their volume resistivity as measured by the conventional two-terminal method using a single fiber attached to a silver electrode with silver paste [46].

The single fiber tensile property test was carried out using a Shimadzu EZ-S tensile tester at room temperature using a 50 N load cell and a gauge length of 20 mm. The tensile strength and elongation of the resultant H-CFs at their breaking point were evaluated. For each sample, 5 to 10 specimens were tested. The cross-sectional areas of the H-CF used to calculate the tensile strengths are determined by SEM and calculated as the area between the inner and the outer shells of the H-CF wall.

3. Results and discussion

3.1 Characterization of hollow carbon fiber

PVA has a relatively high carbon content (54.5 wt%) among vinyl polymers and the capability of high molecular orientation by drawing. However, PVA melts above its melting temperature due to its thermoplastic character and is thermally decomposed into volatile low molecular weight molecules, which results in an unsustainable form of fiber and considerably low carbon yield. Researchers have reported that the dehydration of PVA induced by iodine treatment sustains the initial sample shape during carbonization [26,27]. That is, iodine treatment changes the PVA molecule into polyene-type structures. In addition, stabilization process is also important to impart infusiblization to the precursor by oxygenation and cyclization that enable to withstand high temperatures during carbonization process. Effect of oxidization on stabilization of polymeric precursor was reported; infusible part was formed on the surface of polyvinyl chloride pitch filament by ozone treatment and heating above 220 °C [48]. In contrast, the uniodinated part is susceptible to thermal decomposition by high-temperature treatment during carbonization. Considering these results, we attempted to prepare H-CF from a solid PVA precursor by selective iodination and carbonization within the fiber cross-section.

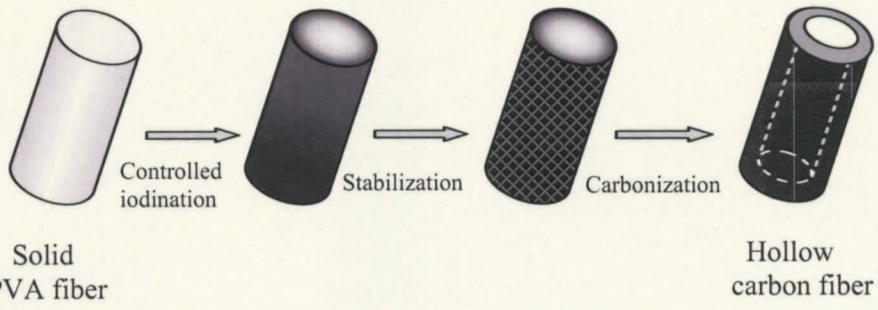

Fig. 3.2 Schematic diagram for the fabrication of hollow carbon fiber from solid PVA fiber using an iodine pretreatment.

First, precursor PVA fiber was treated with iodine solution. The outer iodinated layer of the precursor surface was stabilized by oxidization in air. With high-temperature exposure

during carbonization, the inner non-iodinated part was thermally decomposed to form the hollow structure, as shown schematically in Fig. 3.2.

Thermogravimetric analysis was carried out under an N_2 atmosphere from room temperature to 600 °C at 10 °C/min to clarify the thermal decomposition behavior of the specimens, and the results are shown in Fig. 3.3. For the pristine PVA precursor, there was no significant weight change to near 300 °C, but drastic weight loss was evident from 350 °C, and ended with an almost zero weight residue around 500 °C. On the other hand, the iodinated specimen exhibited considerably different thermogravimetric behavior. For I-PVA, an initial weight decrease occurred between 160 and 230 °C, which is mainly attributed to the vaporization of iodine. A second drastic weight decrease then appeared between 420 – 480 °C due to thermal degradation and reached to 22% of the initial I-PVA weight at 600 °C. The carbon yield obtained for S-PVA at the end of the heating process was 38% of the initial specimen weight. During stabilization, the weight increases by oxygenation of the polymeric chain that would harden the fiber. Moreover, I-PVA was easier to melt and agglomerate at high temperature. These suggest that the stabilization process prevents melting of the fiber surface and facilitates the formation of a hollow structure by carbonization.

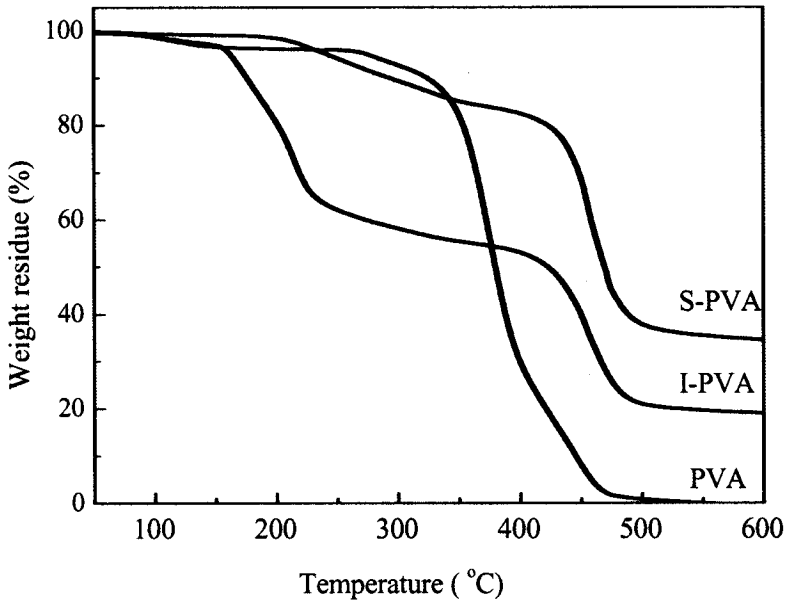

Fig. 3.3 Thermogravimetric curves for the PVA precursors.

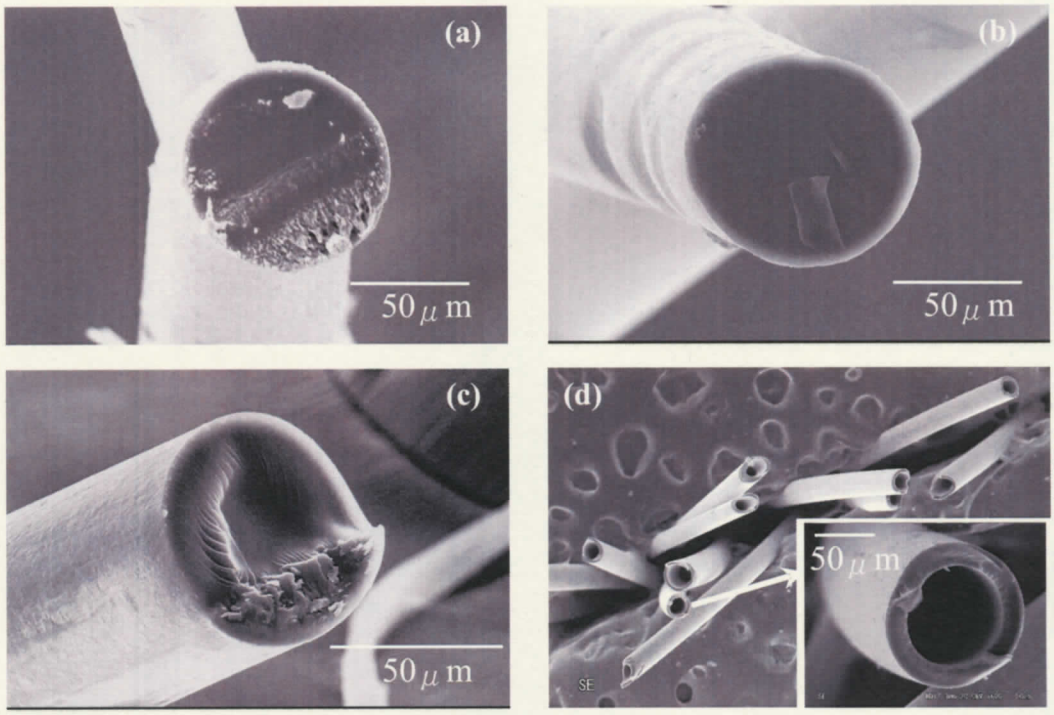

Fig. 3.4 Cross-sectional SEM images of the (a) precursor PVA, (b) I-PVA, (c) S-PVA, and (d) H-CFs.

Cross sections of the precursor PVA fibers and derived H-CFs were investigated under SEM and shown in Fig. 3.4. The precursor fiber in Fig. 3.4(a) has a solid circular cross-section. Although no noticeable structural change was observed in precursor fiber after iodination (in Fig. 3.4(b)), while a biphasic structure was noticed in S-PVA after 24 h stabilization at 200 °C (in Fig. 3.4(c)). Following stabilization process, the center of iodinated precursor became slightly malformed than periphery due to its inadequate iodine adsorption and therefore, lack of stabilization was assumed to be occurred at fiber center. The insufficiently iodinated and less stable fiber center decomposed during high temperature of carbonization process and formed hollow structure within the fiber as evident in Fig. 3.4(d). The fabricated H-CFs, shown in the inset image of Fig. 3.4(d), have hollow core with the wall thickness of ca. 20 μm. The hollow core volume was ca. 40–50%. The extent and nature of the hollow structure and the surface area are largely dependent on the morphology of the precursor fiber and the heat treatment [15,25,26,47]. Therefore, hollow fibers with varying hollow sizes may be fabricated depending on the morphology of

the precursor, the pretreatment conditions (degree of iodination, stabilization time) and the manner of carbonization (heating rate, temperature and time).

Fig. 3.5 presents WAXD profiles of the fibers at each processing stage. For I-PVA, iodine treatment did not apparently alter the PVA crystal form but crystallinity was clearly decreased. Thus, the diffraction peaks are attributed to the PVA crystallites of the uniodinated inner part of the PVA fiber. The crystal structure based on PVA crystallites of the precursor fiber disappeared after the stabilization process. The WAXD profile of H-CF has broad peaks at around 2θ = 18–24 ° and 2θ = 42–45 °, assigned to the (002) and (10) diffractions of graphite, respectively [28,47]. Furthermore, a selected area electron diffraction pattern from TEM images, in Fig. 3.6, shows the presence of a broad (002) arc (in Fig. 3.6(a)) and several diffraction spots (in Fig. 3.6(b)), which indicates that the carbonized fibers possess the preferred orientation in the fiber.

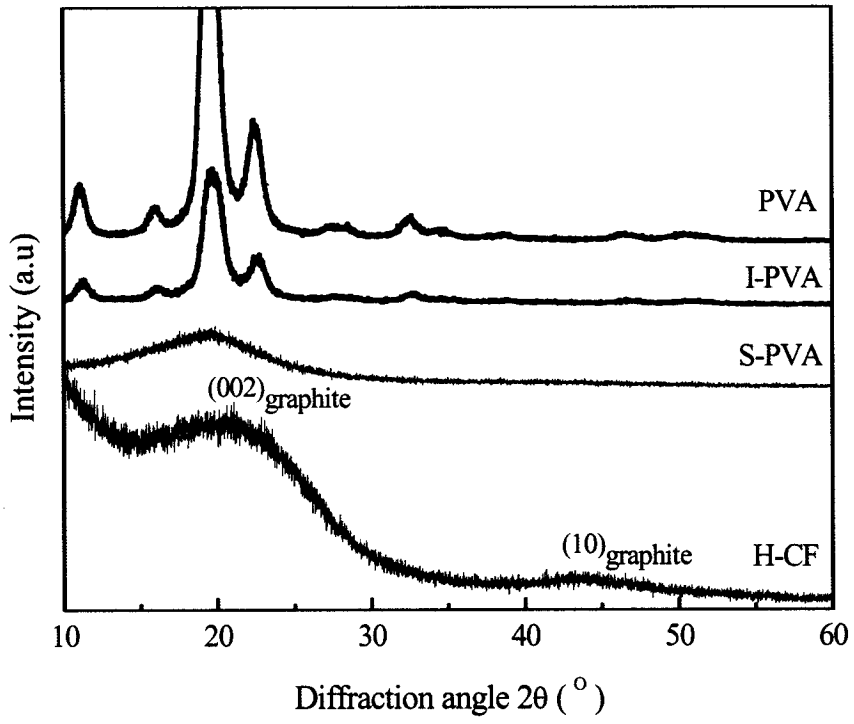

Fig. 3.5 WAXD profiles for PVA fibers at each stage of the process and the resultant H-CFs.

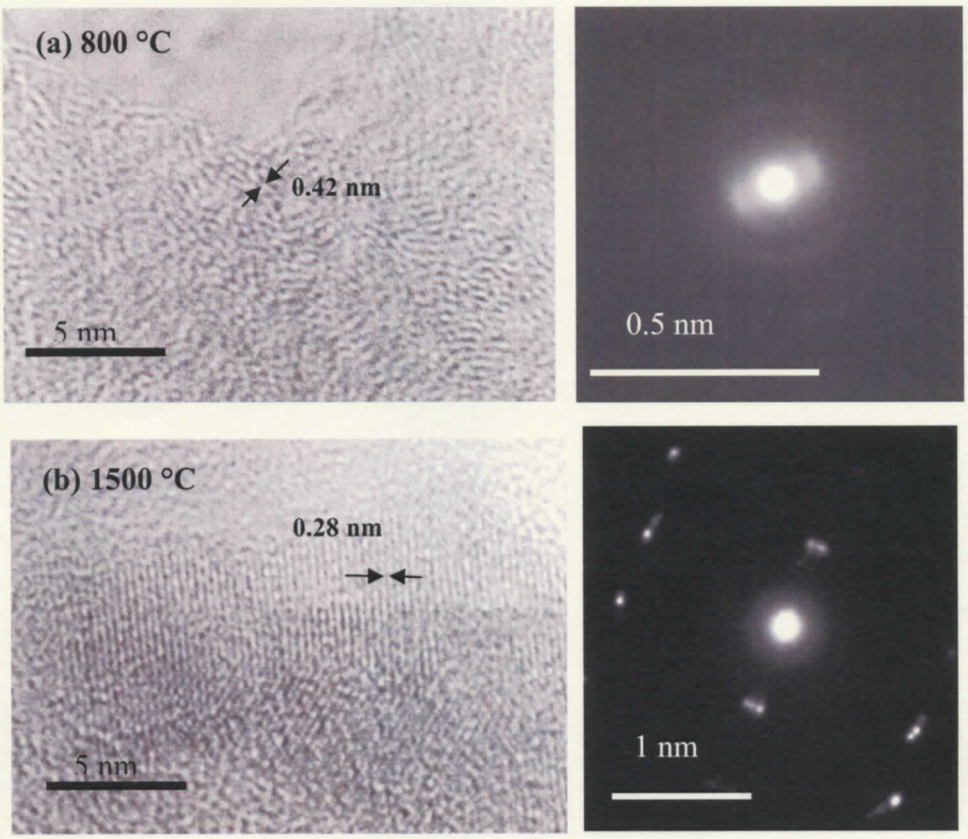

Fig. 3.6 TEM and selected area electron diffraction images of H-CFs subjected to carbonization temperature of (a) 800 °C, and (b) 1500 °C.

The structure of the specimens was further investigated using Raman spectroscopy. The precursor PVA, in Fig. 3.7, gives typical Raman peaks assigned as the stretching of C-C (at 855 and 917 cm^{-1}), C-O and O-H (at 1092 cm^{-1}) and bending of C-H and O-H (at 1360 and 1447 cm^{-1}) [49]. In contrast, the Raman spectrum of I-PVA includes some small peaks that refer to the presence of polyiodide ions (indicated by arrows at 160 (I_3^-), 217 (I_5^-), and 320 (I_3^-) cm^{-1}), and the two strong peaks at around 1120 and 1500 cm^{-1} ascribe the formation of polyene structures generated from the dehydration of PVA [26]. The Fourier transform infrared spectrum of S-PVA also confirmed the transformation of the vinyl alcohol sequence into polyene structure accompanied by a ketone (C-C(=O)-C) structure. The Raman spectrum of H-CF shows two prominent peaks, the D (defect structure of graphite) and G (normal graphite structure) bands, at 1344 and 1586 cm^{-1}, respectively. The intensity ratio of the D to G bands (I_D/I_G) for the derived H-CF was 0.93, which implies low crystallinity.

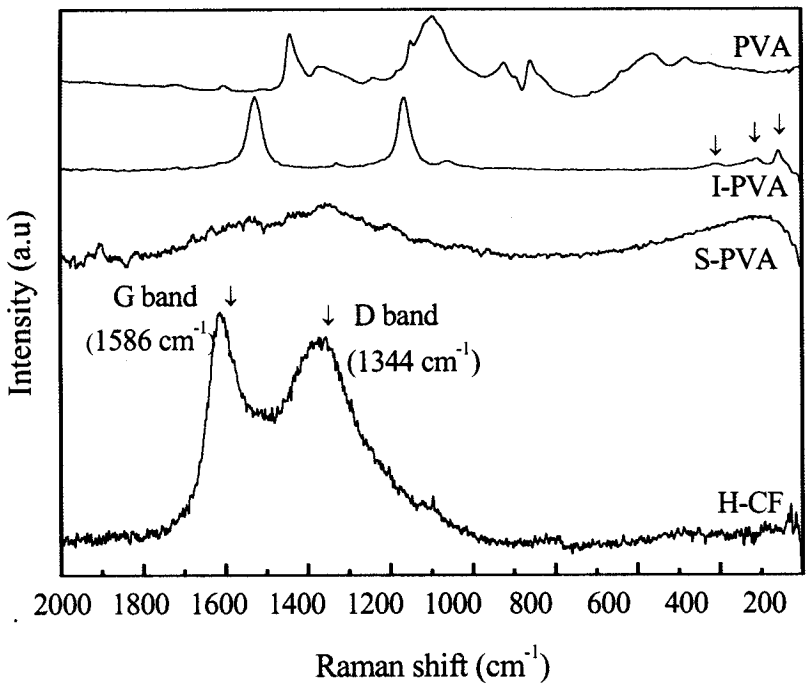

Fig. 3.7 Raman spectra for PVA fibers at each stage of the process and the resultant H-CF.

The WAXD and Raman results signify that PVA-derived H-CF has a turbostratic graphitic structure with a disordered crystal structure. Furthermore, the carbon yield obtained from the total fabrication process was ca. 29% of the pristine precursor PVA weight.

3.2 Effect of heating rate during carbonization

Hereinafter, we fabricated H-CFs from iodine pretreated solid PVA filaments using a carbonization temperature of 800 °C. The current study explores the use of high HTT of carbonization between 800 and 3000 °C, and discusses the influence of carbonization conditions on hollow structure formation and carbon structure development.

First, we focus on the influence of the heating rate up to the HTT. To this end, H-CFs were carbonized at 1500 °C and subjected to different heating rates: 2, 5, and 10 °C/min. SEM, WAXD, and Raman analyses of the resultant H-CFs are presented in Fig. 3.8, Fig.3.9, and Fig. 3.10, respectively. Table 3.1 summarized the WAXD and Raman characteristics of resulted H-CFs.

No significant morphological differences were observed in the hollow structure of the resultant H-CFs due to the different heating rates, as reflected in the cross-sectional SEM images of the resultant H-CFs in Fig. 3.8. The WAXD profiles of the H-CFs subjected to different heating rates exhibited a prominent diffraction peak at around $2\theta = 26°$ for the (002) plane along with a small diffraction peak from the (10) plane at around $2\theta = 41–45°$ in Fig. 3.9 [47]. Two other broadened diffraction peaks from (004) and (110) planes are observed at around $2\theta = 51–55°$ and 77–81°. On the basis of the peak intensity and width of the (002) diffraction, the crystal lattice was most ordered in the case of the heating rate of 2 °C/min, followed by 5 °C/min. However, a further increase in heating rate to 10 °C/min resulted in disorder in the crystal lattice, as indicated by the increase in the (002) peak width. The slower heating rate of 2 °C/min resulted in the minimum *d*-spacing because of crystallite growth, while too rapid a heating rate led to distortion of the crystallite lattice, as evident from Table 3.1 data.

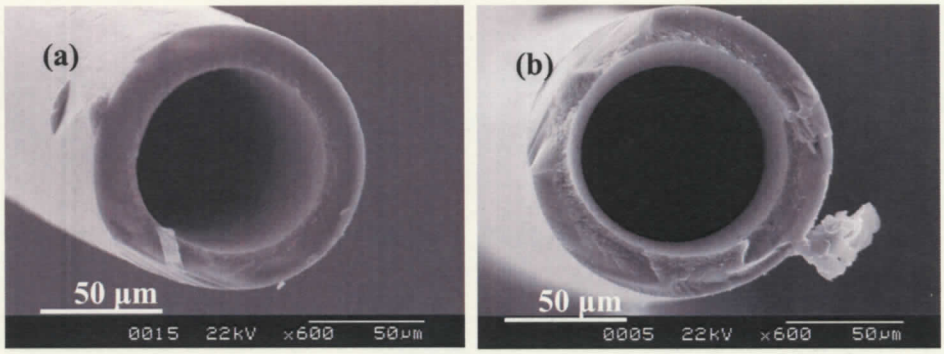

Fig. 3.8 SEM images of H-CFs carbonized at 1500 °C with different heating rates; (a) 2 °C/min and (b) 10 °C/min.

Some criteria for graphitization indices from Raman spectra are: position of G band, width of G band, and the intensity ratio (I_D/I_G) of the D band to G band. In Fig. 3.10, the Raman spectra of H-CFs subjected to different heating rates exhibited disorder-induced D bands and graphite-structure-induced G bands at around 1340 and 1580 cm^{-1}, respectively. Here, the prominent intensity of the D bands in all samples, except the one heated at 2 °C/min, corresponds to the unaligned 2-D graphite structure. Hence, the I_D/I_G ratio is inversely proportional to the degree of graphitization; the I_D/I_G ratio of H-CFs heated at 2 °C/min has the lowest value indicating the least disordered structure with improved

graphitization. Moreover, the slower heating rate of 2 °C/min results in the lowest width of the G band (35 cm^{-1}) at a position of 1574 cm^{-1}, as presented in Table 3.1.

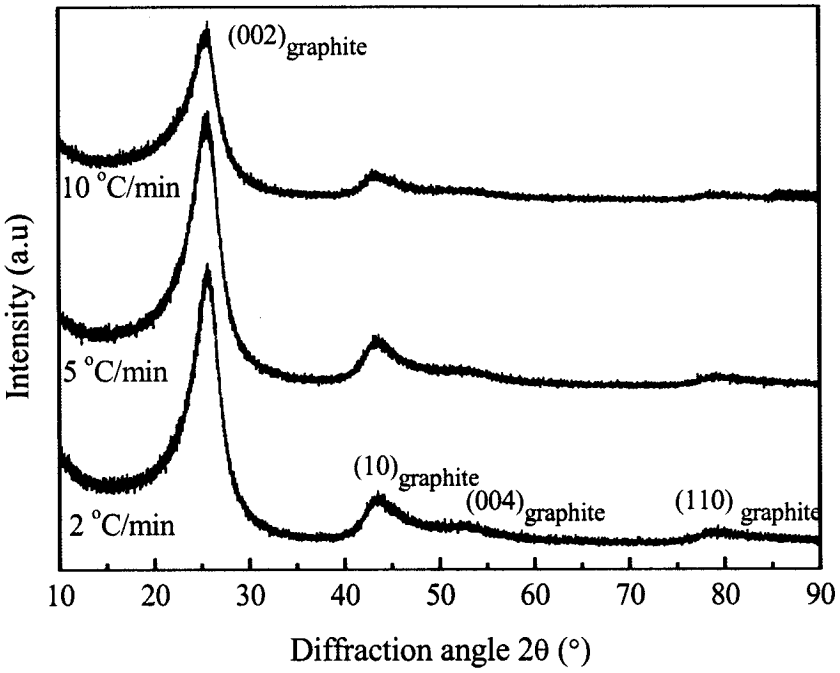

Fig. 3.9 WAXD profiles of H-CFs subjected to different heating rates at 1500 °C.

Table 3.1

WAXD and Raman characteristics of H-CFs subjected to different heating rates at 1500 °C.

Heating rate (°C/mim)	d_{002} (nm)	L_c (nm)	I_D/I_G	G-band position (cm^{-1})	FWHM of G-band (cm^{-1})	G′-band position (cm^{-1})
2	0.344	2.73	0.59	1574	35	2895
5	0.347	2.37	1.06	1591	70	2682
10	0.348	2.37	0.97	1594	72	2684

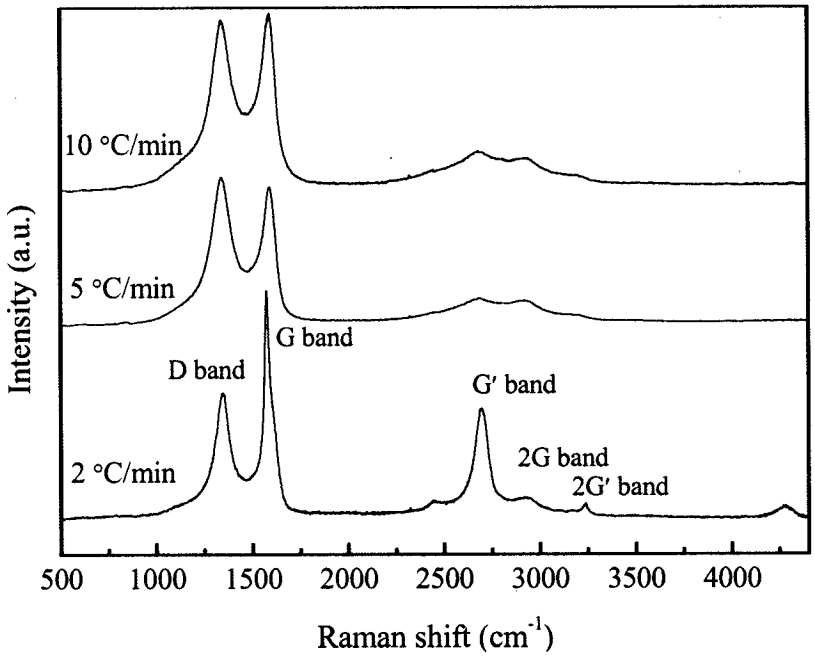

Fig. 3.10 Raman spectra of H-CFs subjected to different heating rates at 1500 °C.

Furthermore, the Raman spectra of H-CFs at 2 °C/min exhibited a sharp G′ band (also called 2D or D* band) at around 2680 cm^{-1}, which corresponds to the overtone of D bands. This band is symmetry-allowed and considered to be the second most prominent feature in the Raman spectrum of completely ordered 3-D graphite. Also, the shape of the G′ bands is sensitive to the stacking order of the graphene sheets along the *c* axis and can be used for probing the electronic structure of carbonaceous materials [50,51]. In Fig. 3.10, the G′ band (as well as the 2G′ band) of slow-heated (2 °C/min) H-CFs is much more intense compared to that of rapidly heated H-CFs (5 and 10 °C/min), indicating the possibility of more ordered graphene stacking. However, the H-CF heated at a rate of 2 °C/min shows the most intense and up-shifted G′ band position (at 2695 cm^{-1}) with the lowest d_{002} value (0.344 nm), Table 3.1, corresponding to an improved alignment of the graphite layer. It may be assumed that the slower heating rate orders the stacking of adjacent layers and improves the crystallite size. However, the resultant H-CFs are turbostratic graphite, whose interplanar spacing (> 0.344 nm) is larger than that for crystalline graphite (0.335 nm). The turbostratic carbon structure of H-CFs prepared at a heating rate of 2 °C/min could be improved to the crystalline structure if the samples could be heated at a high carbonization temperature.

Therefore, we gradually increased the HTT to 3000 °C at a heating rate of 2 °C/min to prepare the H-CFs that were used in subsequent experiments.

3.1 Effect of high HTT during carbonization

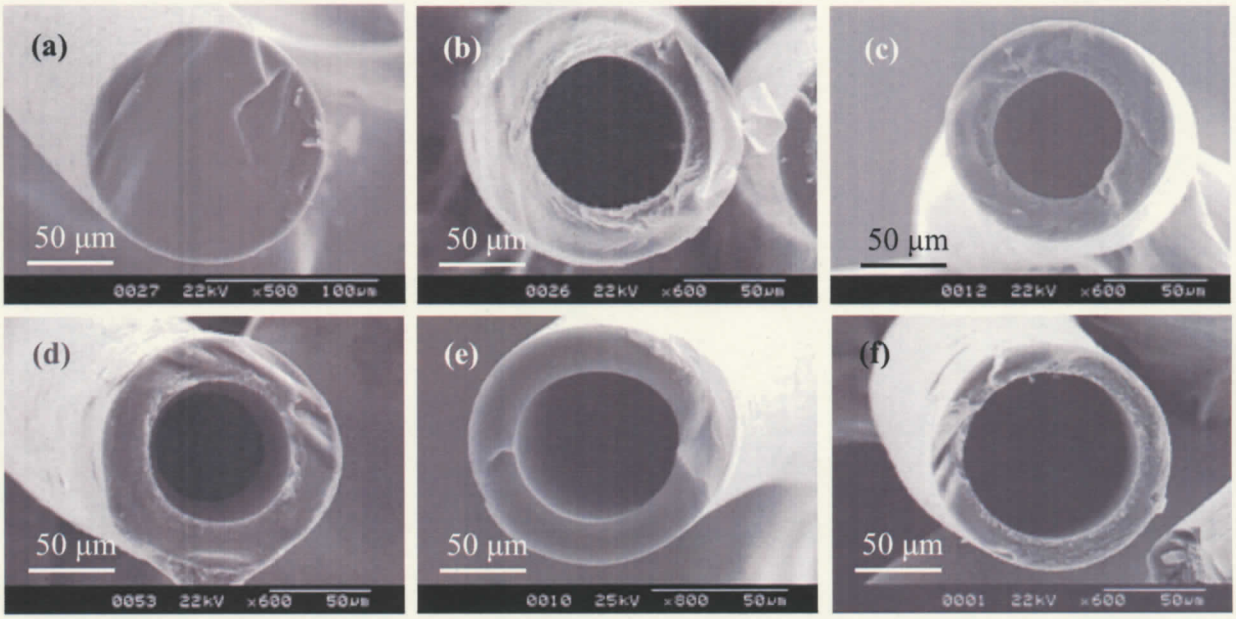

Fig. 3.11 Cross-sectional SEM images of the precursor PVA (a) and resultant H-CFs subjected to a heating rate of 2 °C/min and different HTTs of carbonization: (b) 800, (c) 1500, (d) 2000, (e) 2500, and (f) 3000 °C.

The H-CFs carbonized at 1500 °C using a heating rate of 2 °C/min were further carbonized at high HTTs of 2000, 2500, and 3000 °C. Fig. 3.11 shows the cross-sectional SEM images of the precursor PVA and the resultant H-CFs carbonized at different HTTs. The H-CFs fabricated at different HTTs of carbonization have a well-shaped hollow structure with a homogenous wall thickness. During carbonization, the non-iodinated inner part of the precursor fiber decomposed at high temperature, whereas the outer iodinated and stabilized layer could withstand the high temperature and formed a hollow structure. Thus, the preservation of the hollow structure even at a HTT of 3000 °C demonstrates the effectiveness of the proposed iodine pretreatment method on the thermoplastic PVA polymer. Though the morphological differences between the samples are very small, the data in Table 3.2 reflect a gradual shrinkage of the wall thickness from 26 to 15 μm in

going from a HTT of 800 to 3000 °C. As the wall thickness decreases, the hollow core volume steadily increases. The carbon yields obtained suggest that the decrease in wall thickness was related to the decrease in both *d*-spacing and carbon yield.

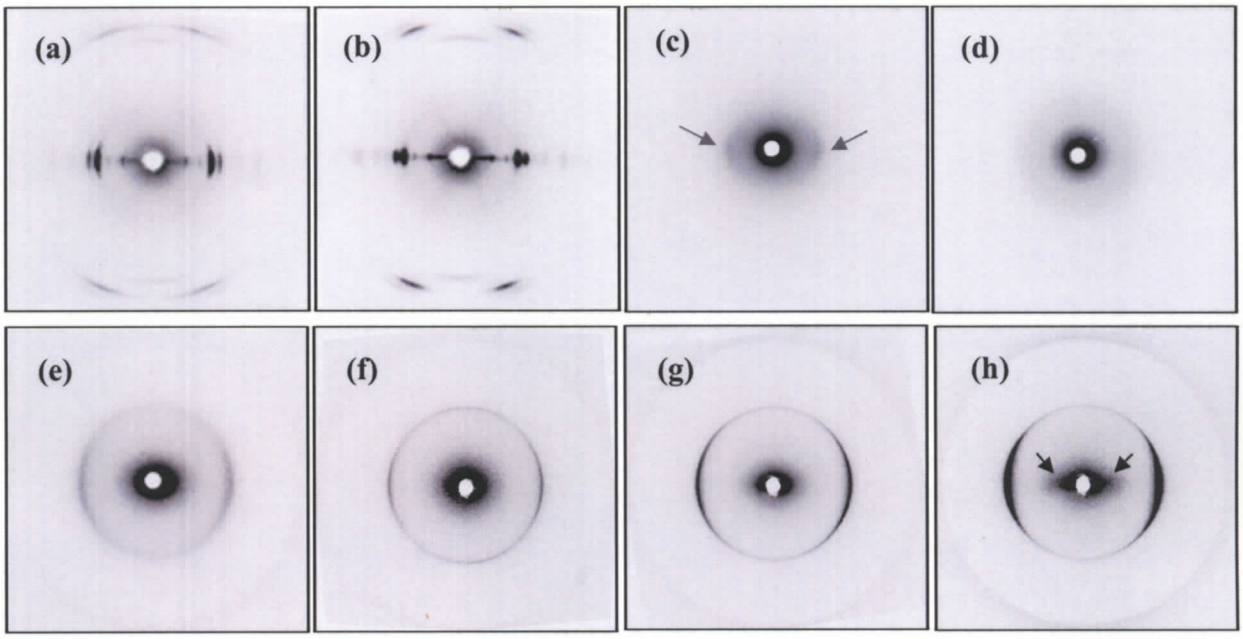

Fig. 3.12 WAXD photographs of (a) precursor PVA, (b) I-PVA, (c) S-PVA and resultant H-CFs subjected to different carbonization temperatures; (d) 800, (e) 1500, (f) 2000, (g) 2500, and (h) 3000 °C.

Fig. 3.12 presents the WAXD photographs of PVA, I-PVA and the H-CFs obtained at different HTTs. The precursor PVA shows a highly oriented crystalline structure along the fiber axis, and iodination did not alter the original molecular orientation of the precursor fibers significantly, as is evident from the I-PVA photograph. However, the weak scattering arc shown in the equatorial direction by arrows (Fig. 3.12(c)) indicates that the crystallinity and molecular orientation decreased markedly upon stabilization. A comparison of the photographs reveals that, the H-CFs fabricated at 800 °C show no distinct crystallinity, but rather a disordered structure with random orientation. The elevation of HTT to 1500 °C results in the appearance of weak Debye-Scherrer arcs in the WAXD photograph, indicating the progressive formation of an ordered structure.

Indeed, the selected area electron diffraction from the TEM image of H-CFs prepared at 800 °C shows no distinct diffraction spots, while that of the H-CFs fabricated at 1500 °C shows obvious diffraction spots reflecting the transformation from a random orientation state to an oriented state. Further increases in HTT gradually enhance the intensity of the Debye-Scherrer arc, which is indicative of an increase in structural order. The H-CFs carbonized at 3000 °C exhibit the most intense Debye-Scherrer arc of the (002) plane, with a pair of strong scattering streaks (shown by arrows in Fig. 3.12(h)) along the equatorial direction. The streaks originate from rod-like entities such as needle-shaped voids or microfibrillar structures. The appearance of streak is related to the development of orientation structure. Thus, the orientation of graphite is enhanced with increasing HTT, although the extent of orientation is not sufficiently high compared to those of commercialized carbon fibers. The orientation factors (π) of H-CF crystallites obtained at different HTTs show that the H-CFs treated at 3000 °C possess the highest crystallinity.

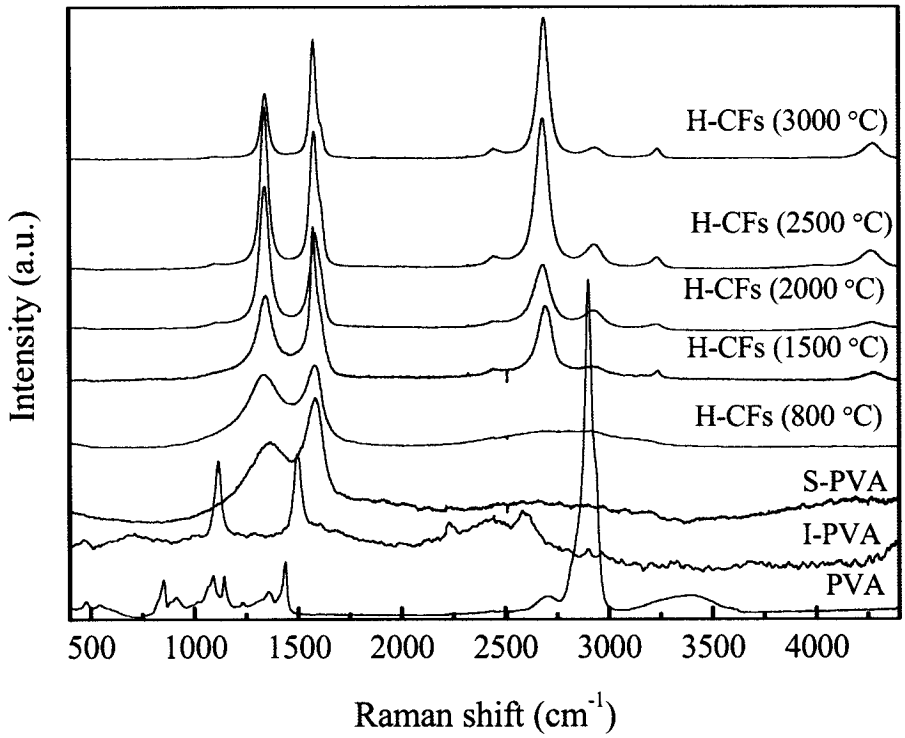

Fig. 3.13 Raman spectra of resultant H-CFs subjected to different carbonization temperatures.

Table 3.2

Properties of H-CFs subjected to different temperatures.

Temperature (°C)	800	1500	2000	2500	3000
Wall thickness (μm)	26	24	23	17	15
Hollow core volume (%)	32	35	35	40	55
Carbon yield (%) ± S.D.	28 ± 2	25 ± 2	22 ± 3	20 ±2	19 ±2

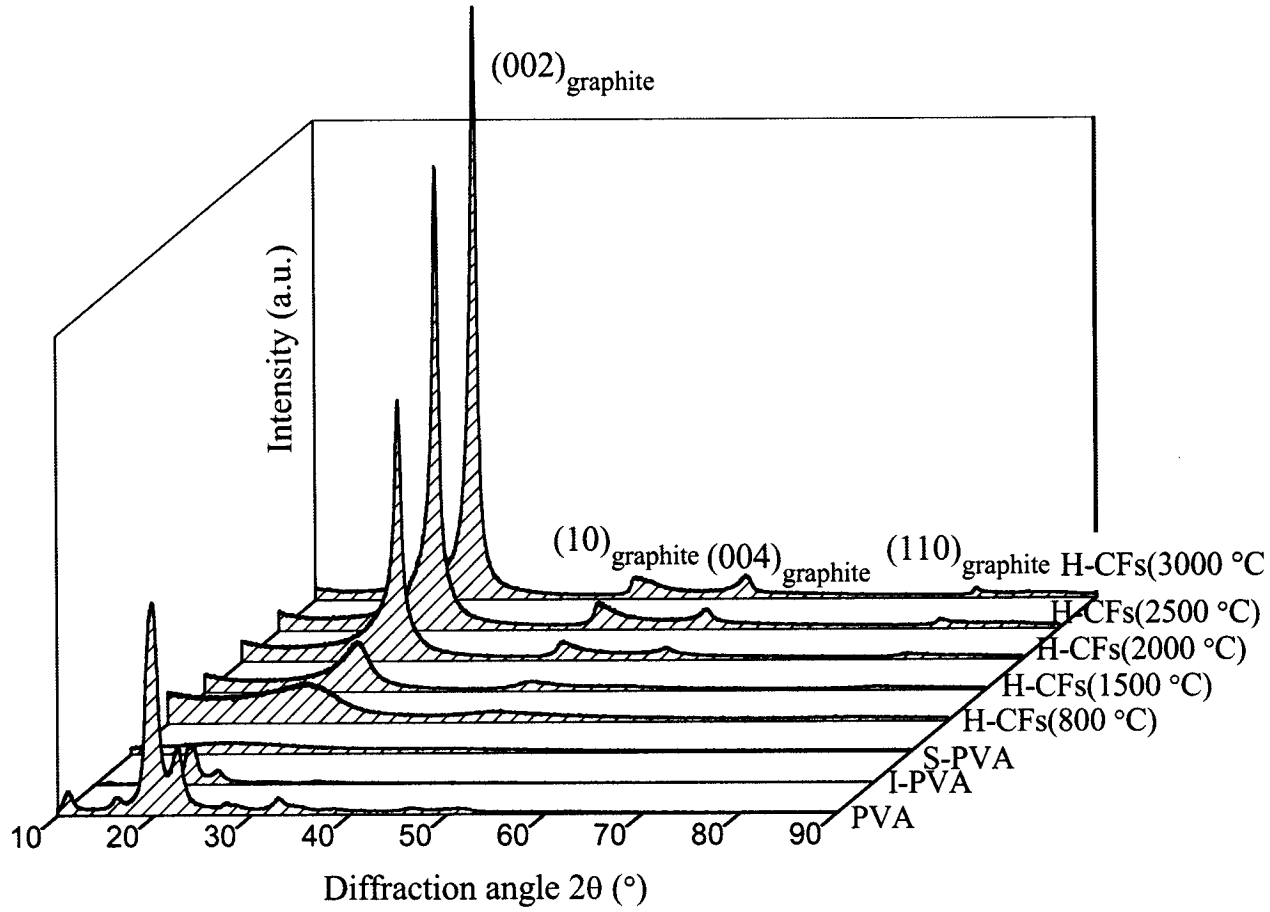

Fig. 3.14 WAXD profiles of precursor PVA at different processing stages and the resultant H-CFs subjected to different carbonization temperatures.

Table 3.3

WAXD and Raman characteristics of H-CFs subjected to different carbonization temperatures.

Temperature (°C)	π	I_D/I_G	d-spacing (nm)	Crystallite size (nm)	
			d_{002}	L_c	L_a
800	randomly oriented	0.93	0.360	2.756	2.134
1500	0.28	0.59	0.346	3.418	3.916
2000	0.35	1.42	0.341	9.943	3.172
2500	0.48	1.16	0.340	11.397	4.205
3000	0.55	0.58	0.338	11.481	7.398

The quality and crystallinity of H-CFs subjected to different HTTs of carbonization were further investigated using Raman spectroscopy, the results of which are shown in Fig. 3.13. The transformation of the PVA structure to a polyene-type structure in I-PVA due to iodination was evident in our previous work [26,28]. In brief, the typical Raman peaks of the PVA fiber disappeared in I-PVA, and two strong peaks appeared at around 1120 and 1500 cm^{-1}, ascribable to the formation of polyene structures generated by the dehydration of PVA. Compared to the XRD results of I-PVA (see Fig. 3.12(b)), the structure and the crystallinity of the precursor PVA was retained almost unaltered in I-PVA. It can be concluded that the Raman spectrum of I-PVA was mainly due to the outer iodinated part, rather than any reflections from the non-iodinated inner core of the fiber. Meanwhile, the XRD spectrum reflects the resultant diffraction pattern of the substrate, and therefore, the WAXD photograph of I-PVA shows an XRD pattern similar to that of the precursor. The difference in the Raman spectra of I-PVA and the precursor PVA also indicates that the iodine treatment has transformed the outer skin of PVA into a thermally stable structure that facilitates the formation of a hollow structure at high HTTs of carbonization. In S-PVA, the characteristic peaks of PVA and I-PVA disappeared, and two new peaks emerged close to the positions of the D and G bands, indicating that the graphite structure had already

started to form. The Raman spectra of the H-CFs carbonized at different HTTs show the D and G bands at around 1340 and 1585 cm^{-1}, respectively. In particular, the G band position is shifted from 1587 to 1577 cm^{-1} as the HTT increases from 800 to 3000 °C. This means that the graphene layers in the H-CFs become more ordered at higher HTTs. Heating of H-CFs above 1500 °C also results in the formation of G′ bands, and the H-CF carbonized at 3000 °C has the strongest G′ band intensity, which suggests it has the most ordered graphitic layer, shown in Table 3.3. Here, the intensity of the G′ band is 1.13 times stronger than that of the G band. Notably, HTTs above 1500 °C lead to a Raman peak at around 4270 cm^{-1}, not evident in H-CFs carbonized at 800 °C. The I_D/I_G ratio of the resultant H-CFs decreased from 0.93 to 0.58 as the HTT increased from 800 to 3000 °C. With its broad (002) diffraction peak, the WAXD profile of the H-CFs heat-treated at 800 °C is indicative of an amorphous structure (see Fig. 3.14). As the HTT increases, the diffraction peak of the (002) plane becomes sharper and shifts towards higher angles, reflecting the progress of graphitization. Also, distinct broad diffractions appear from the (10), (004) and (110) planes of graphite at around $2\theta = 42°$, 53°, and 77°, respectively, when H-CFs are subjected to HTTs above 2000 °C. Remarkably, the (10) peak of H-CFs shows the typical structure of turbostratic carbon. However, the H-CFs carbonized at 3000 °C give the strongest (002) diffraction peak, indicating that the most ordered structure, i.e., the highest crystallinity, occurred at the highest graphitization temperature. The crystallite size and interplanar spacing data (Table 3.3), i.e., the dramatic increase in crystallite size from 2.756 to 11.481 nm and the reduction in the interplanar spacing between graphene layers from 0.360 to 0.338 nm, also reflect that the H-CF structure was significantly improved with increasing HTT up to 3000 °C. The L_c value and the ratio of L_c to L_a are considerably increased when the carbonization temperature reaches 2000 °C, and consequently, the anisotropy of the crystalline structure is well developed, which corresponds to the trend shown in Fig. 3.12. It can be assumed that at high temperatures, the movement of an individual carbon atom or single carbon ring fills a void, improving the order in a crystallite and hence the alignment of the graphite layer [52]. The graphitization induced by heat treatment is the consequence of the associated changes in crystallite size. Thus, the formation of the graphite structure at high HTTs is due to the crystallite growth, accompanied by the transformations of the crystal structure [53]. Fig. 3.15 shows the HTT dependence of volume resistivity of the

resultant H-CFs. The conductivity is the reciprocal of volume resistivity. As shown in Fig.3.15, the electrical conductivity gradually increases with increasing HTT. The volume resistivity of the H-CFs was 3.77×10^{-5} Ω m at a carbonization temperature of 3000 °C. The degree of graphitization increases with increasing carbonization temperature, which influences the crystallinity of H-CFs, and the higher crystallinity leads to the higher electrical conductivity.

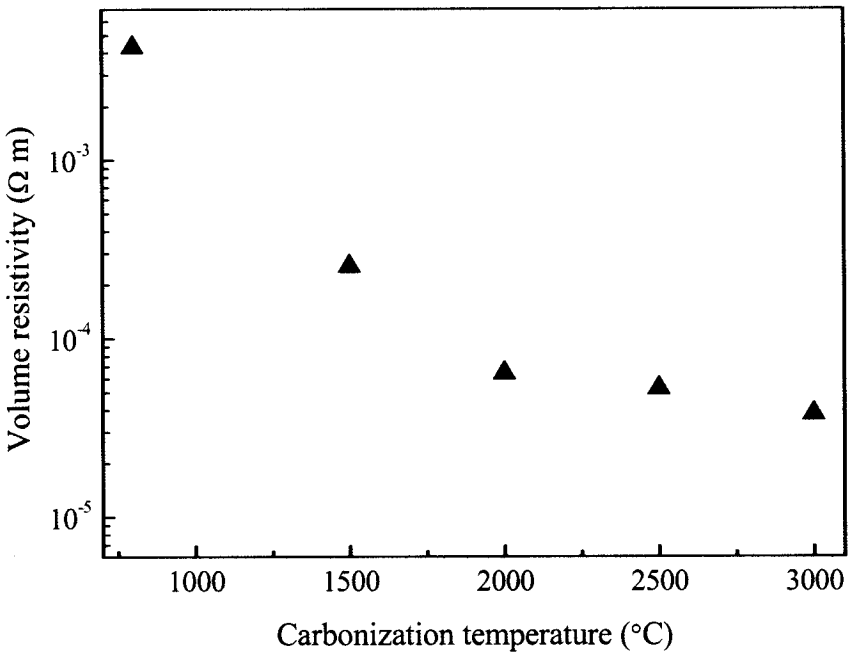

Fig. 3.15 Heating temperature dependence of volume resistivity of resultant H-CFs.

The Raman, WAXD and conductivity results all confirm that the HTT of 3000 °C yielded the most ordered crystal structure, with improved orientation and alignment of the graphene layer. However, the asymmetric shape of the (10) and (110) diffraction planes and the presence of a single Raman G′ band suggests that the layer stacking is still turbostratic.

3.3 Filling of polymer component in the hollow part

We would expect that the H-CFs could be utilized for various kinds of functionalization. As an example, the present study investigates polymer filling.

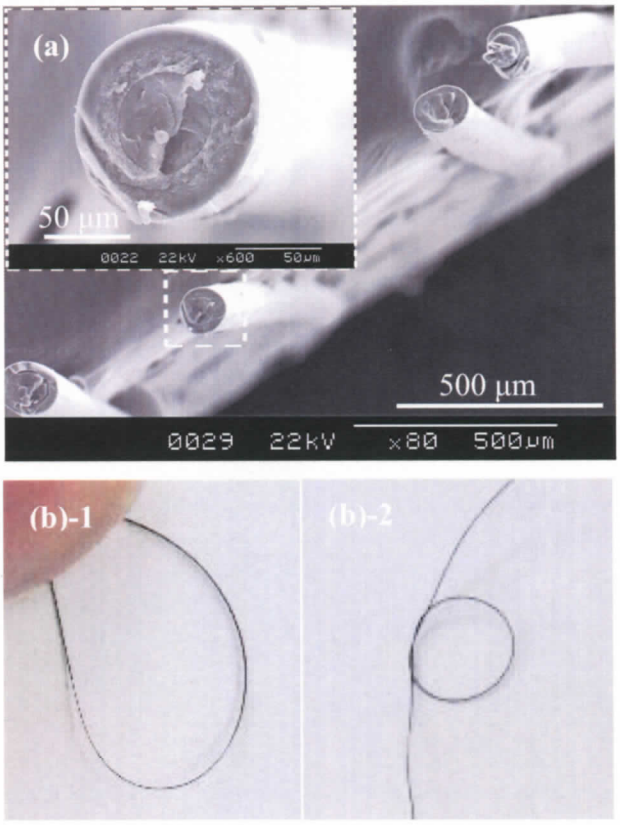

Fig. 3.16 (a) SEM images of H-CFs with PMMA filler, (b) photographs of maximum bendability of H-CFs before failure; (b)-1 pristine H-CF and (b)-2 H-CF with PMMA filler.

Fig. 3.16(a) shows SEM images of H-CFs with PMMA filler in the fiber core, which adhered to the walls and filled the H-CF core completely. As expected, incorporation of the polymeric filler reduces the brittleness of H-CFs: The pristine H-CF could be bent to the maximum position shown in Fig. 3.16(b)-1; further bending while knotting resulted in breakage. In contrast, H-CFs loaded with PMMA could be bent and knotted without breakage, as shown in Fig. 3.16(b)-2. The minimum radii of the loop curvature before breakage were around 3 and 1.5 mm for pristine and PMMA-loaded H-CFs, respectively, which indicates a significant reduction in brittleness. Thus, an improvement in bendability of H-CFs was achieved by incorporating PMMA inside the fiber core.

4. Conclusions

Hollow carbon fibers can be fabricated from solid PVA fibers using a controlled and selective iodine pretreatment followed by stabilization and carbonization at elevated temperature. Our investigation of the use of high HTTs during the fabrication process confirms the favorable effects on the structure and final properties of the resultant carbon fibers. The final carbon structure and the graphitization process are also influenced by the rate of heating during carbonization. Morphological evidence suggests that a heating rate of 2 °C/min was optimal for the proposed fabrication process in terms of the resultant crystal quality and crystallite layer alignment. Moreover, increasing the HTT of carbonization from 800 to 3000 °C improved the order of the crystal structure and molecular orientation of the resultant H-CFs. The highest degree of graphitization and molecular orientation were obtained for the sample heated at 3000 °C and at an interlayer spacing of 0.338 nm and crystallite size of 11.48 nm, which indicate the formation of an oriented and ordered graphitic structure in the H-CFs. Our morphological observations reflected that the densification of the fiber wall and decrease in carbon yield were consequences of the high HTT. Raman spectroscopy data also confirmed the improvement of the structure of H-CFs heat-treated at a high HTT of 3000 °C. Heat treatment of the precursor PVA resulted in H-CFs with a turbostratic and improved graphitic structure. Furthermore, incorporation of the PMMA filler improved the bendability of the H-CFs.

5. References

[1] Burchell TD, Carbon materials for advanced technologies, Oxford, Pergamon, UK (1999).

[2] Peng H, Chen D, Huang JY, Chikkannanavar SB, Hänisch J, Jain M et al. Strong and ductile colossal carbon tubes with walls of rectangular macropores, Phys Rev Lett, 101, 145501–145504 (2008).

[3] Saufi SM, Ismail AF, Fabrication of carbon membranes for gas separation–a review, Carbon, 42, 241–259 (2004).

[4] Robert LN, Timothy DB, Hollow carbon fibers, US Patent, 5,338,605 (1994).

[5] Koresh J, Soffer A, Molecular sieve carbon selective membrane, Part 1: Presentation of a new device for mixture separation, Sep Sci Technol, 18, 723–734 (1983).

[6] Ismail AF, David LIB, A review on the latest development of carbon membranes for gas separation, J Membr Sci, 193, 1–18 (2001).

[7] Adelhelm P, Hu YS, Antonietti M, Maierd J, Smarsly BM, Hollow Fe-containing carbon fibers with tubular tertiary structure: preparation and Li-storage properties, J Mat Chem, 19, 1616–1620 (2009).

[8] Yu Y, Gu L, Wang C, Dhanabalan A, Aken PA, Maier J, Encapsulation of Sn@carbon nanoparticles in bamboo-like hollow carbon nanofibers as an anode material in Lithium-based batteries, Angew Chem Int Ed, 48, 6485–6489 (2009).

[9] Xie W, Cheng HF, Chu ZY, Zhou YJ, Liu HT, Chen ZH, Effect of FSS on microwave absorbing properties of hollow-porous carbon fiber composites, Mater Design, 30, 1201–1204 (2009).

[10] Xie W, Cheng HF, Chu ZY, Preparation and microwave absorbing properties of hollow carbon fibers, J Cent South Univ Technol, 14(s2), 112–115 (2007).

[11] Yanan S, Jose KA, Neo CP, Experimental investigations of microwave absorber with FSS embedded in carbon fiber composites, Microwave Opt Technol Lett, 32(4), 245–9 (2002).

[12] Donnet J, Wang TK, Rebouillat S, Peng JCM, Carbon fibers, vol. 3. Marcel Dekker Inc., New York, USA (1998).

[13] Lan YJ, Tai SC, Raj R, Dual-layer hollow carbon fiber membranes for gas separation consisting of carbon and mixed matrix layers, Carbon, 45, 166–72 (2007).

[14] Yang MC, Chou MT, Effect of post-drawing on the mechanical and mass transfer properties of polyacrylonitrile hollow fiber membranes, J Membr Sci, 116, 279–91 (1996).

[15] Saufi SM, Ismail AF, Development of polyacrylonitrile (PAN) based carbon hollow fiber membrane, Membr Sci Technol, 4, 844–853 (2002).

[16] Favvas EP, Kouvelos EP, Romans GE, Pilatos GI, Mitropoulos AC, Kanellopoulos NK, Characterization of highly selective microporous carbon hollow membranes prepared from a commercial co-polyimide precursor, J Porus Mater, 15, 625–633 (2008).

[17] Favvas EP, Kapantaidakis GC, Nolan JW, Mitropoulos AC, Kanellopoulos NK, Preparation, characterization and gas permeation properties of carbon hollow fiber membranes based on Matrimid® 5218 precursor, J Mater Proc Technol, 186, 102–110 (2007).

[18] Bhardwaj V, Macintosh A, Sharpe ID, Gordeyev SA, Shilton SJ, Polysulfone hollow fiber gas separation membranes filled with submicron particles, Adv Membr Technol, 984, 318–328 (2003).

[19] Zhu G, Chung TS, Loh KC, Activated carbon-filled cellulose acetate hollow-fiber membrane for cell immobilization and phenol degradation, J Appl Polym Sci, 76(5), 695–707 (2000).

[20] Teresa AC, Antonio BF, Carbon molecular sieve gas separation membranes based on poly(vinylidene chloride-co-vinyl chloride), Carbon, 38, 1067–1073 (2000).

[21] Song C, Wang T, Jiang H, Wang X, Cao Y, Qiu J, Gas separation performance of C/CMS membranes derived from poly(furfuryl alcohol) (PFA) with different chemical structure, J Membr Sci 362, 22–27 (2010).

[22] Barbosa-Coutinho E, Salim VMM, Borges CP, Preparation of carbon hollow membrane by pyrolysis of polyetherimide, Carbon, 41, 1707–1714 (2003).

[23] Cheng Y, Zhang J, Zhang Y, Chen X, Wang Y, Ma H et al., Preparation of hollow carbon and silicon carbide fibers with different cross-sections by using electrospun fibers as templates, Eur J Inorg Chem, 4248–4254 (2009).

[24] Sun L, Cheng H, Chu Z, Zhou Y, Fabrication of PAN-based hollow carbon fibers by coaxial electrospinning and two post-treatments, Acta Polymerica Sinia, 1, 61–65 (2009).

[25] Shi Z, Zhang T, Xu L, Feng Y, A template method for the synthesis of hollow carbon fibers, Micropor Mesopor Mater, 116, 698–700 (2008).

[26] Fatema UK, Tomizawa C, Harada M, Gotoh Y, Iodine-aided fabrication of hollow carbon fibers from solid poly(vinyl alcohol) fibers, Carbon, 49(6), 2158–2161 (2011).

[27] Yamashita J, Method of manufacturing carbon material from polyvinyl alcohol, JP Patent 28407 (2003).

[28] Fatema UK, Ahmed JU, Uemura K, Gotoh Y, Fabrication of carbon fibers from electrospun poly(vinyl alcohol) nanofibers, Tex Res J, 81(7), 659–672 (2011).

[29] Han GC, Marilyn LM, Asif R, Stabilization and carbonization of gel spun polyacrylonitrile/single wall carbon nanotube composite fibers, Polymer, 48, 3781–3789 (2007).

[30] Zhang Q, Yang DJ, Wang SG, Yoon SF, Ahn J, Influences of temperature on the Raman spectra of single-walled carbon nanotubes, Smart Mater Struct, 15, (2006) S1–S4 doi:10.1088/0964-1726/15/1/001.

[31] Li WZ, Wen JG, Ren ZF, Effect of temperature on growth and structure of carbon nanotubes by chemical vapor deposition, Appl Phys A, 74, 397–402 (2002).

[32] He M, Rikkinen E, Zhu Z, Tian Y, Anisimov AS, Jiang H et al., Temperature dependent Raman spectra of carbon nanobuds, J Phys Chem C, 114, 13540–13545 (2010).

[33] Khan MMR, Gotoh Y, Morikawa H, Miura M, Graphitization behavior of iodine-treated Bombyx mori silk fibroin fiber, J Mater Sci, 44, 4235–4240 (2009).

[34] Chaishi S, Murakami Y, Miyauchi Y, Maruyaman S, Temperature measurements of single-walled carbon nanotubes by Raman scattering, Thermal Sci Eng 7(4), (1999) 10–11.

[35] Kokaji K, Oya A, Maruyama K, Carbonization and graphitization behavior of decacyclene, Carbon, 35(2), 253–221 (1997).

[36] Shinn-Shyong T, Pan JH, Oxidative stabilization of petroleum pitch at high pressure and its effects on the microstructure and carbon yield after carbonization/graphitization, Mater Chem Phys, 74, 214–221 (2002).

[37] Linda V, Boris L, Inbal D, Processing and characterization of extruded drawn MWNT-PAN composite filaments, Compos Part A Appl Sci Manuf, 38, 1354–1362 (2007).

[38] Tin PS, Xiao YC, Chung TS, Polyimide-carbonized membranes for gas separation: structural, composition and morphological control of precursors, Sep Purif Rev, 35, 285–318 (2006).

[39] Wei X, Cheng HF, Chu ZY, Chen ZH, Effect of carbonization time on the structure and electromagnetic parameters of porous-hollow carbon fibers, Ceram Inter, 35, 2705–2710 (2009).

[40] Tsai HA, Ciou YS, Lee KR, Yu DG, Lai JY, Heat-treatment effect on the morphology and pervaporation performance of asymmetric PAN hollow fiber membrane, J Membr Sci, 255, 33–47 (2005).

[41] Sun J, Wu G, Wang Q, Effects of carbonization temperature on the properties and structure of PAN-based activated carbon hollow fiber, J Appl Polym Sci, 97, 2155–2160 (2005).

[42] Sun J, Wang Q, Effects of activation temperature on the properties and structure of PAN-based activated carbon hollow fiber, J Appl Polym Sci, 100, 3778–3783 (2006).

[43] Tai FC, Wei C, Chang SH, Chen WS, Raman and X-ray diffraction analysis on unburned carbon powder refined from fly ash, J Raman Spectrosc, 41(3), 933–937 (2010).

[44] Okino F, Kawasaki S, Touhara H, Lin H, Kimura M, Shirai H, Carbonization and graphitization of polyamidine films, Synth Met, 125, 197–200 (2002).

[45] Iwashita N, Inagaki M, Relations between structural parameters obtained by X-ray powder diffraction of various carbon materials, Carbon, 31, 1107–1113 (1993).

[46] Line up catalogue, Resistivity meter series, Mitsubishi Chemicals Group, 2007, p3–4. http://www.dins.jp/dins_e/1prdcts/pdf/Cat%200704-LP2000US_em.pdf (last accessed March 12, 2011)

[47] Otani S, Okuda K, Matsuda S, Carbon fiber, vol. 1, Kindai Henshu Ltd., Tokyo, Japan, p. 8–9 (1986).

[48] Otani S, Mechanism of the carbonization of MP carbon fiber at the low temperature range, Carbon, 5, 219–225 (1967).

[49] Martinelli A, Matic A, Börjesson L, Navarra MA, Fernicola A, Panero S et al., Structural analysis of PVA-based proton conducting membranes, Solid State Ionics, 177, 2431–2435 (2006).

[50] Barros EB, Demir NS, Filho AGS, Filho JM, Jorio A, Dresselhaus G et al., Raman spectroscopy of graphitic foams, Phys Rev B, 71, 165422 (2005).

[51] Pimento MA, Dresselhaus G, Dresselhaus MS, Cancado LG, Jorio A, Saito R, Studying disorder in graphite based systems by Raman spectroscopy, Phys Chem Chem Phys, 9, 1276–1291 (2007).

[52] Smisek M, Cerny S, Active carbon-manufacture, properties and applications, Elsevier Pub Co Ltd, New York, USA, p.53 (1970).

[53] Belenkov EA, Formation of graphite structure in carbon crystallites, Inorganic Mater, 37(9), 928–934 (2001).

Chapter 4

Metallization of high performance fibers utilizing iodine pretreatment

1. Introduction

In previous chapter, we utilized iodine for the fabrication of high performance carbon fiber from polymeric precursor fiber. In this chapter, we focus on the functionalization of some high performance fibers through metallization using iodine pretreatment.

High performance fibers of poly(*p*-phenylene benzobisoxazole) (PBO) and poly(*p*-phenylene terephthalamide) (PPTA) are important engineering fibers and considered as super fibers because of their rigid-rod chain structure and outstanding physical properties such as high modulus, strength, chemical and heat resistance etc. Therefore, these fibers have been widely used in the composites, defense, industrial, military, automotive, and aerospace fields etc. [1–6].

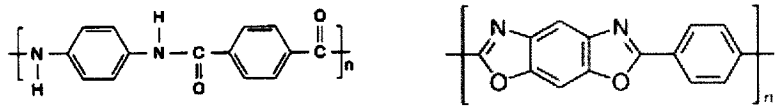

PPTA (Kevlar) **PBO (Zylon)**

Fig. 4.1 Structure of the used high performance fibers

However, the PBO fiber is sensitive to sunlight, UV and fluorescent lamps. Moreover, the deterioration of strength accelerates in extremely humid atmospheres, even at temperatures less than 100 °C [7]. The reason for its mechanical loss has been reported as follows: the opening of benzoxazoles and oxazole rings in the PBO molecules is the main part of hydrolysis [8] and complete hydrolysis by moisture results in chain scission on the fiber skin and subsequent reduction in molar mass [9–10]. Furthermore, the hydrolytic degradation in PBO accelerates in the presence of impurities such as phosphoric acid that used during its production process [11–12]. Besides, PPTA fiber is also sensitive to lights and can absorb the light of 300 to 450 nm wavelength and UV component due to its special physical and chemical structures [13], which deteriorate the useful mechanical properties and structures of fiber. Similar to PBO, light and UV radiation deteriorates more severely on the PPTA surface or skin layer and the crystalline defect or amorphous areas of the fiber by chain scission and causes mechanical loss [14,15]. Therefore, PBO and PPTA fibers require protection from both light sources and moisture for outdoor applications and storage

at high temperatures and high humidity environment for extended periods.

Metallization of fiber maintains the mechanical properties of materials in the presence of light, rust, and corrosion. In addition, new functionalities and surface properties can also be tailored, thus further enhancing their applicability in industrial and technical fields. For metallization of these high performance fibers (HPFs), electroless metal plating was preferred because of the simplicity of the process. Electroless plating refers to the autocatalytic or chemical reduction of metal ions and subsequent plating onto substrates in aqueous media, which is applied to non-conductive polymeric materials [16–19]. This process is a common industrial practice for the surface coating of materials. A variety of metals such as Au, Cu, Ag, Co, Pt, Pd, Ni, Pb, and Sn are used for coating fibers. Cu is an excellent conductor for both heat and electricity making it popular for many engineering applications. In addition, considering its decorative value, malleability, ductility, diffusion barrier properties and good corrosion resistance and high chemical reactivity, Cu coating is designated as an economical coating method. Besides, electroless plating of Ni has the significant merit of lower cost, fast deposition, and formation of good plated layer at lower temperature. Ag plating is also an engineering coating due to its superior conductivity and corrosion resistance, which allows for its extensive use in electrical components.

PPTA and PBO fiber possess a chemically inert surface, which leads to poor interfacial adhesion between the fiber and the plated layer even if electroless plating is conducted. Therefore, a catalyst fixation process that imparts strong interfacial adhesion is necessary. Conventional catalyzation fixation process requires surface etching and use of strong chemical which deteriorates the strength of fiber [20–23]. Recently, researchers approach several new methods of surface catalyzation [24–30]. In this thesis, we propose a new catalyzation process to improve interfacial adhesion between fiber and plated surface without deterioration of the mechanical properties of plated fiber. Previously, our group introduced a successful method of imparting of metal iodides into a polymer matrix via iodine pretreatment for various polymers for preparation of organic/inorganic composites [31], and metal iodides formed in and on a polymer matrix can be reduced to metal nanoparticles that can serve as catalysts for electroless plating. This method brings in high adhesive forces between the fiber and the metal plating layer. However, studies have been limited to polymers having high affinity for iodine, while PPTA and PBO have high

crystallinity, hydrophobicity, and low affinity for iodine, which makes it difficult to insert iodine.

In this study, we performed electroless plating on the PPTA and PBO fibers via the aforementioned iodine pretreatment process. Since Pd and Ag are most widely used catalyst nuclei used for electroless plating process [32–34], we studied both catalyzation processes. The PPTA and PBO fibers were doped with iodine using iodine aqueous or vapor treatment, and subsequently converted to metal iodides (silver iodide AgI or palladium iodide PdI_2). The resulted metal iodides were reduced to the respective metals (Ag or Pd) and then electroless plating was conducted by catalytic action. We performed electroless plating using Cu, Ni and Ag on high performance PBO and PPTA fibers.

2. Experimental

2.1 Materials

Multifilament of Kevlar® K-29 (DuPont-Toray Co. Ltd., Japan) and Zylon® AS (Toyobo Co. Ltd., Japan) was used. The diameter of each filament was 15 and 12 μm, respectively.

Special grade chemicals of iodine (I_2), sodium dodecyl sulfate (SDS), palladium(II) chloride ($PdCl_2$), hydrochloric acid (HCl), 36% formalin, sodium tetrahydroborate ($NaBH_4$), potassium iodide (KI), silver nitrate ($AgNO_3$) were purchased from Wako Pure Chemicals Industries Ltd. (Japan) and used as-received. For Cu plating, the plating reagents Thru-cup PSY-1A ($CuSO_4$-based aqueous solution) and Thru-cup PSY-1B (NaOH-based aqueous solution) were purchased from C. Uyemura & Co. Ltd. (Japan). Ni plating reagents nickel (II) acetate tetrahydrate ($Ni(CH_3COO)_2{\cdot}4H_2O$), citric acid anhydrous ($C_6H_9O_7$), sodium phosphinate monohydrate ($NaH_2PO_2{\cdot}H_2O$), dimethyl amine-borane (DMAB) ($(CH_3)_2NH \cdot BH_3$) and 28% ammonia solution (NH_3); and Ag plating reagents glucose (Dextrose, anhydrous ($C_6H_{12}O_6$)) and sodium hydroxide (NaOH) were also purchased from Wako Pure Chemicals Industries Ltd. (Japan).

2.2 Sample preparation

2.2.1 Pretreatment

The surface activation of PPTA fiber was initiated by an iodine doping technique for electroless plating, as illustrated schematically in Fig. 4.2. First, multifilament of HPFs

wound to a Teflon frame was enclosed with iodine in a glass vessel and placed in an oven where iodine was vaporized for 6 h at 100 °C. The original golden color of the PBO and the yellow color of the PPTA fibers both became dark brown due to the sorption of iodine, which was later confirmed by Raman spectroscopy. The performance and durability of the plated layer is significantly dependent on the adhesion strength of the plated layer to the fiber matrix. Therefore, improvement of the wettability of the hydrophobic PPTA surface is necessary for use in an aqueous electroless plating bath. The iodinated fibers (I-PBO and I-PPTA) were treated with an aqueous solution of 0.05 wt% SDS surfactant for 5 min at room temperature. Then, for Pd catalyzation the fibers were immersed in a solution of 0.03 mol/L $PdCl_2$ and 0.5 mol/L HCl at 80 °C for 1 h. As a result, fine particles of PdI_2 were formed within the fiber (denoted as PdI_2-PBO/PPTA). This formation was attributed to the more readily occurring interaction between soft acid Pd^{2+} ions and soft basic I^- ions (as opposed to Cl^- ions), and easier coordination exchange reactions. The resulting PdI_2 was subsequently reduced to metal Pd by immersing the fiber (denoted as Pd-PBO/PPTA) in 0.25 wt% $NaBH_4$ aqueous solution at room temperature for 30 min.

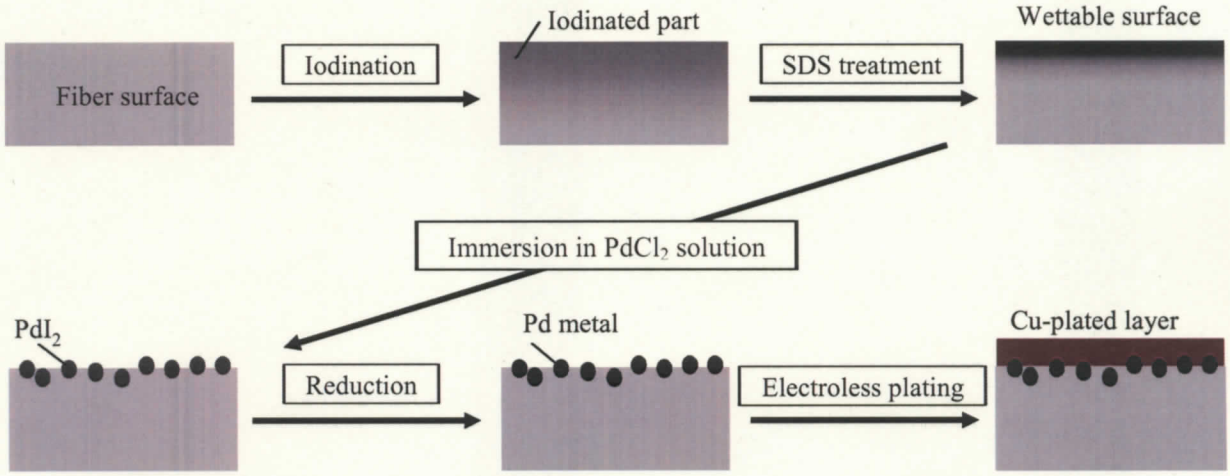

Fig. 4.2 Schematic of electroless Cu plating process on HPF via iodine pretreatment.

For Ag catalyzation, iodine doping on PBO fiber was carried out using iodine vapor method, while PPTA fiber was pretreated by aqueous iodine doping technique. A special

type PPTA filament was used that was partially dehydrated with micropores on the surface. An aqueous iodination process was employed, where initially PPTA was treated in aqueous I_2-KI solution (I_2: 0.1mol/L, KI: 0.4 mol/L) for 4 h at 90 °C. The iodinated fiber (denoted as I-PPTA) was thoroughly rinsed with acetone and deionized water to remove excess iodine. The original yellow color of the PPTA fiber became golden brown due to the sorption of iodine, which was later confirmed by Raman spectroscopy. The performance and durability of the plated layer is significantly dependent on the adhesion strength of the plated layer to the fiber matrix. Therefore, improvement of the wettability of the hydrophobic PPTA surface is necessary for use in an aqueous electroless plating bath. I-PPTA was treated with an aqueous solution of 1 wt% SDS, an anionic surfactant, for 5 min at room temperature. In addition, processing without SDS was conducted to investigate the influence of the surfactant on the adhesion performance of the plated layer. The treated I-PPTA fiber was then immersed in a solution of 0.1 mol/L $AgNO_3$ at 90 °C for 1 h and the color of fiber became light yellow, which is typical of AgI. Thus, fine AgI particles were formed within the fiber (denoted as AgI-PPTA). Formation of the fine AgI particles is attributed to the readily occurring interaction of I^- ions with Ag^+ ions and the ease of such coordination exchange reactions, which resulted in the precipitation of AgI in the fiber matrix. The generated AgI was reduced to metallic Ag by immersion of the AgI-PPTA in 0.50 wt% aqueous $NaBH_4$ solution at ambient temperature for 30 min, and the color of fiber (denoted as Ag-PPTA) became dark grey, which indicates the formation of Ag particles. The Ag particles formed on the fiber surface act as a catalyst for the subsequent electroless plating process.

2.2.2 Electroless plating

Cu plating

Cu plating was carried out in an electroless plating bath containing 1 ml of Thru-cup PSY-1A, 0.4 ml of Thru-cup PSY-1B, 0.2 ml of 36% formalin, and 25 ml of distilled water. The plating temperature and time were maintained at 70 °C and 45 min, respectively. The pH of the plating bath was maintained in between 12.5–13.0 throughout the process.

Ni plating

Ni plating was conducted in an electroless bath composed of 0.2 mol/L Ni-acetate, 0.15 mol/L $NaPH_2O_2$, 0.1 mol/L citric acid, and 0.05 mol/L DMAB. The plating time, pH, and temperature of the plating bath were 30 min, 9.5, and 70 °C, respectively. The pH of the plating bath was adjusted by the addition of aqueous NH_3 solution. These values are based on optimization results for Ni-deposition on a fiber substrate as a function of solution composition, temperature, time, and pH. Unlike the plating bath composition for Pd-catalyzed PPTA fibers, the Ag-catalyzed fiber requires the addition of DMAB as a reducing agent for initiation of the plating reaction [40].

Fig. 4.3 Photographs of pristine and metal plated PBO fibers.

Ag plating

Ag plating was carried out based on a typical silver mirror reaction. The plating solution was prepared as follows: 1 ml of 2.5wt% ammonia solution was dropped into 5 ml of 2.5wt% $AgNO_3$ until Ag_2O precipitation disappeared. Then, the solution of ammine complex of Ag^+ was mixed with 5 ml of 5wt% glucose ($C_6H_{12}O_6$) and 1 drops of NaOH aqueous solution. Then the pretreated fiber was put on the above mixer solution at 60 °C placed on a magnetic stirring bath for 1 h in a polypropylene vessel.

2.3 Measurements

Raman spectroscopy were carried out with Hololab 5000 equipped with an MK-II filter probe (Kaiser Optical Systems, Inc., USA). The light source was an Nd:YAG laser of 532 nm generated at 50 mW.

X-ray measurements were carried out using an X-ray generator Rotorflex RU-200B

(Rigaku, Japan). The X-ray source was Ni-filtered Cu-K_α radiation (λ = 0.15418 nm) generated at 40 kV and 150 mA. X-ray photographs were captured with a Fuji film imaging plate, and the wide angle X-ray diffraction (WAXD) was measured with a goniometer. The degree of catalyzed PBO crystal orientation (π) is determined and expressed as percentage as follows:

$$\pi\,(\%) = (180 - H^\circ)/180 \times 100$$

where H° is the half-width of the intensity distribution curve along the Debye-Scherrer ring.

Transmission electron microscopy (TEM) was performed using an electron microscope JEM-2010 (JEOL, Japan) at an accelerating of 200 kV.

Scanning electron microscopy (SEM) was conducted using an electron microscope S-2380N and S-3000N (Hitachi, Japan) electron microscope attached to energy dispersive X-ray diffraction (EDX) equipment..The diameter of the fibers and thickness of the plated layer were determined from the SEM images with NIH Image J. For observing the fiber cross section, a single fiber was embedded in epoxy resin, cut using a diamond knife, and observed by field emission scanning electron microscopy (FE-SEM) using an electron microscope S-5000 (Hitachi, Japan).

3. Results and discussion

3.1 Characterization of pretreated fibers

Uniform and adequate pretreatment is important in order to ensure uniform and good quality plating layer deposition. Iodination is also an essential requirement in the current study. For Pd catalyst activation and doping of iodine, we performed iodine vapor treatment. Vaporized iodine exhibits the ability to easily penetrate into hydrophobic super fibers, while iodine-potassium iodide aqueous solution was used for PPTA to insert iodine. Fig. 4.4 shows the Raman spectra of the pristine and iodinated super fibers. In contrast to the pristine fiber, some Raman peaks assigned to the polyiodide ions (I_5^-: 162 cm^{-1} and 324 cm^{-1}, I_3^-: 110, 230 cm^{-1} and) were observed in the both iodinated fibers, which indicates that I_2 was absorbed, reduced, and converted to polyiodide ions [35–37]. By this approach, the formed polyiodide components became precursors of metal iodide.

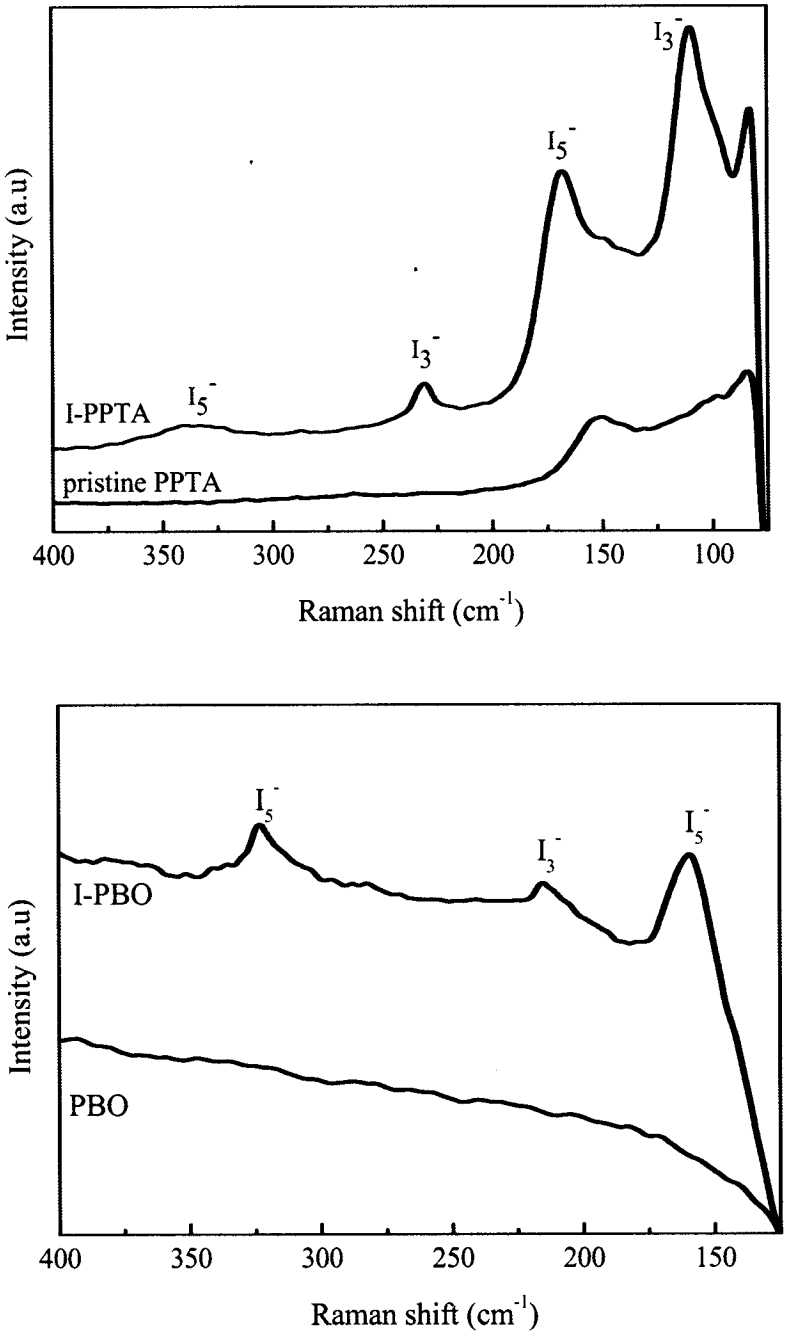

Fig. 4.4 Raman spectra of pristine and iodinated fibers.

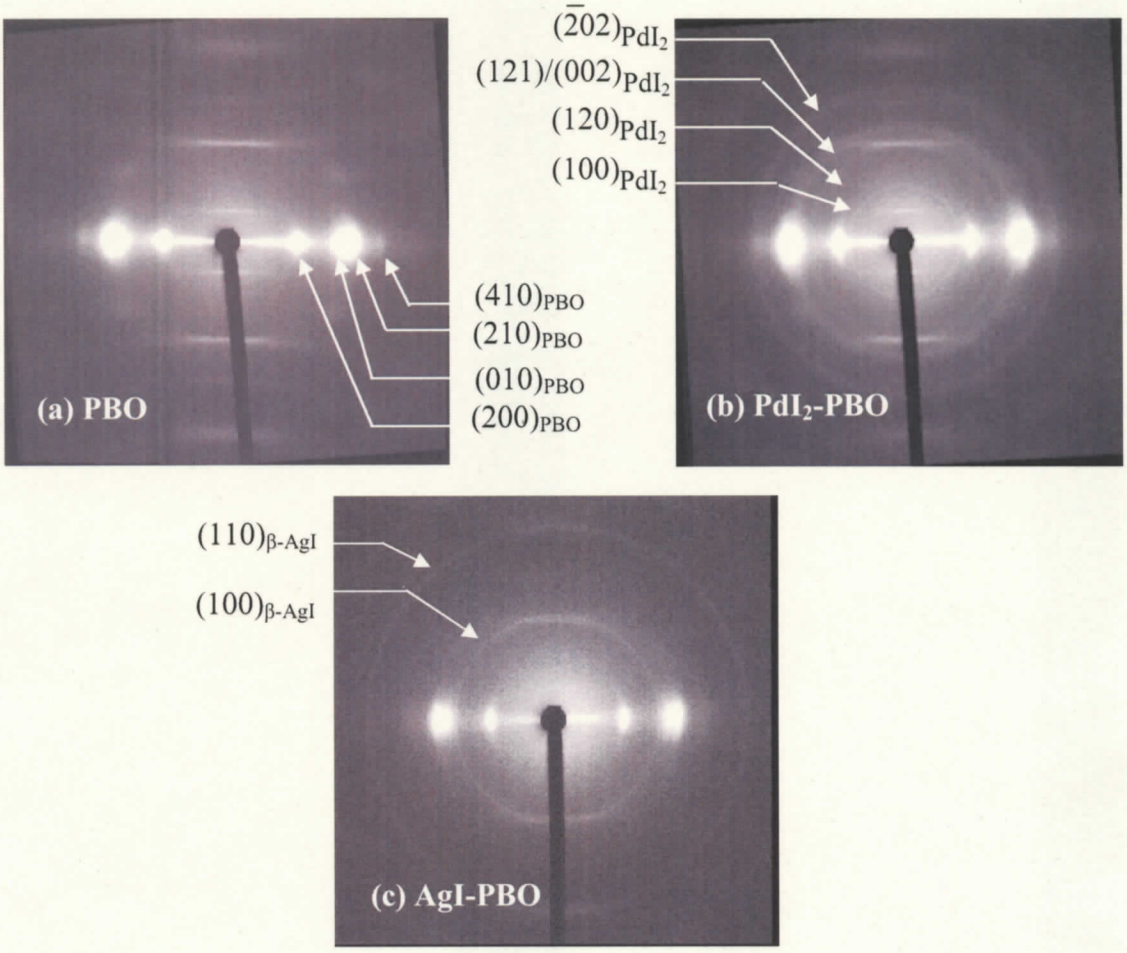

Fig. 4.5 WAXD diffraction photographs of pristine and after metal iodides formation on PBO fiber.

Fig. 4.5 and Fig. 4.6 show the X-ray diffraction photographs of the pristine and PBO and PPTA fibers after metal iodide formation during formation of PdI_2 (photographs b) and AgI (photographs c), respectively. The diffraction photograph of pristine super fibers shows highly oriented crystalline structure of PBO and PPTA fiber in respective images, while some new Debye-Scherrer rings are detected in photo (b) of each fiber. Comparison of the photographs revealed that monoclinic PdI_2 crystal was formed in the PPTA and PBO fibers [38,39]. In addition, the degrees of orientation of the PBO crystallite were calculated as 87% and 85% for PBO and PdI_2–PBO, respectively. This result indicates that iodine treatment did not significantly influence the HPFs crystalline structure. Accordingly, during Ag catalyzation, AgI was formed in fiber that is clearly indicated in respective photographs

(c). The WAXD photographs (c) also detected some new Debye-Scherrer rings of β-AgI in each fibers indicating the formation of β-AgI crystal [41]. Similarly, degree of orientations of PPTA crystallite was calculated as 83% for PPTA and 80% for AgI-PPTA. This result also confirms that the iodine assisted the formation of metal iodide within PBO and PPTA molecules without influence their crystalline structure.

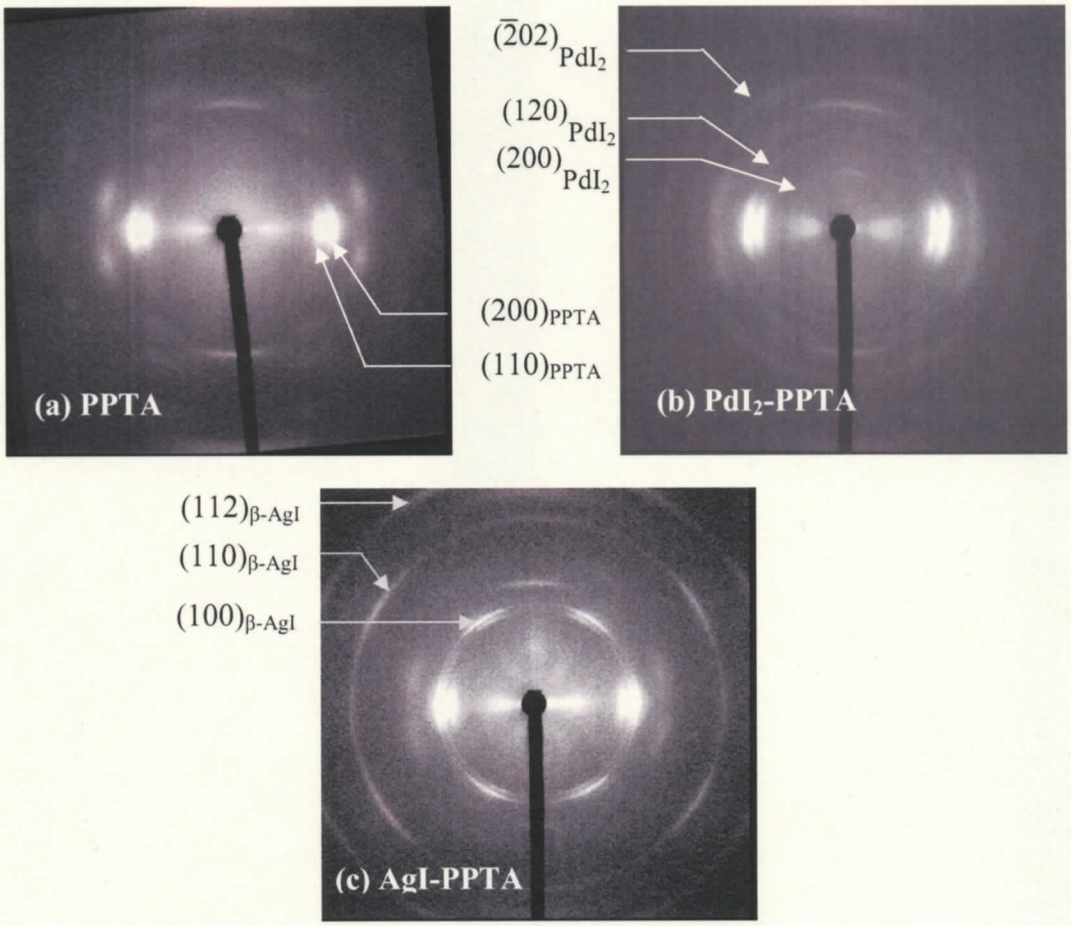

Fig. 4.6 WAXD diffraction photographs of pristine and after metal iodides formation on PPTA fiber.

The nature and distribution of catalyst particles on a fiber surface influence the deposition and quality of the plated layer; and the network created between the fibers and metallic complexes ensure anchoring of the plated layer to the fiber. Therefore, the formation of PdI_2 and AgI on the fiber surfaces was investigated. The TEM images of the longitudinal section of PdI_2-PBO, in Fig. 4.7(a), shows a distinct phase consists of nano-

sized PdI_2 particles exist near the surface, which will later reduced to metal Pd particles and act as catalyst during plating and ensures strong anchoring.

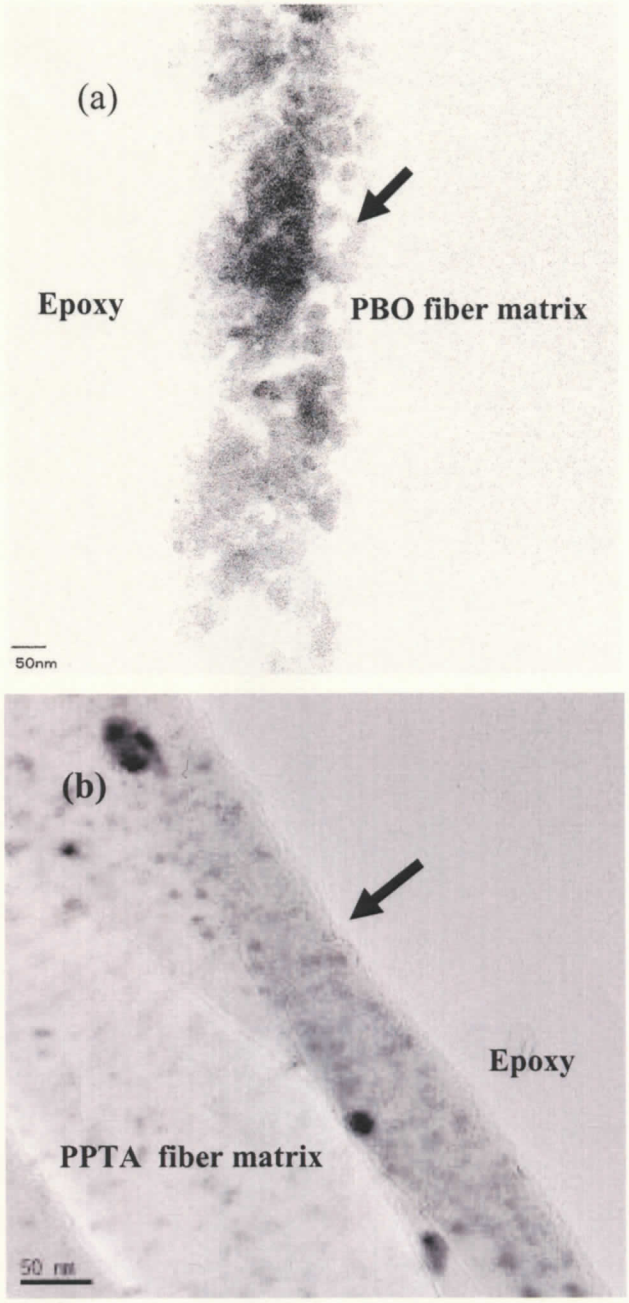

Fig. 4.7 TEM images of (a) longitudinal section of PdI_2-PBO fiber, and (b) cross section of AgI-PPTA fiber.

Similarly, in Fig. 4.7(b) the TEM image of AgI-PPTA fiber shows that many β-AgI particles with sizes in the range of several nanometers to 20 nm were present in the vicinity of the surface forming a distinct phase due to the adequate sorption of iodine component into the PPTA fiber surface due to treatment in aqueous media, and subsequent formation of AgI. However, some aggregations of β-AgI particles were also present. In both cases, metal iodide particles distributed mainly on surface region due to adequate sorption of iodine component to on the fiber surface in both aqueous and vapor phase. However, after the reduction of PdI_2 and AgI particles respective metal particles generated on the fiber surface and electroless plating was carried out successfully, thus indicating that the Pd and Ag particles served as plating catalysts.

3.2 Characterization of metallized super fibers

The electroless plating of Cu, Ni and Ag result uniformly plated fibers with lustrous appearance of respective metals. Plated fiber possesses reasonable flexibility and good hand feel. Fig. 4.3 and Fig. 4.8 show the photographs and SEM images of differently plated super fibers, respectively. The average thickness varied depending on the plate bath concentration, pH, temperature and time. The influences of some plate bath factors are discussed in details in the later part of this chapter.

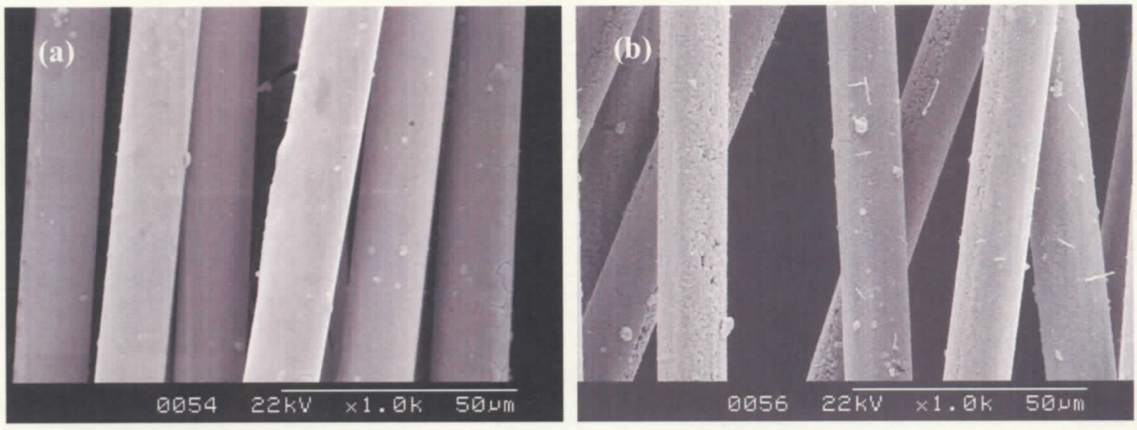

Fig. 4.8 SEM images of Ni plated (a) PPTA and (b) PBO fibers.

Also, Figs. 4.9(a) and (b) show that Cu-plated PBO fibers covered with a uniform metallic layer and possessed bright copper color and flexibility. The thickness of the layer was ca. 500–650 nm. Energy-dispersive X-ray spectroscopy (EDX) analysis confirmed that

the layer coating of the PBO surface was composed of metal copper. Three distinct phases are recognized in the cross-sectional FE-SEM image of the plate frontier of Cu-plated PBO shown in Fig. 4.9(c): the fiber matrix, Cu-plated layer, and the interface. The distinct interfacial zone (PBO/Pd) exhibits good continuity between the fiber and the plated layer, and is considered to be composed of the Pd particles embedded in PBO from the contrasts observed in the FE-SEM image. This well-deposited catalyst layer enhances the adhesion strength and minimizes the surface roughness, thereby improving the smoothness, durability and performance of the plated layers during their application. Inadequate iodination or the absence of SDS treatment led to separation of the Cu-plated layer from the fiber matrix, as discussed later. These results provide evidence that the plated layer and fiber matrix were firmly adhered to each other and the strong cutting force of trimming was limited, which indicates that the PBO/Pd phase strongly anchored the Cu layer to the PPTA.

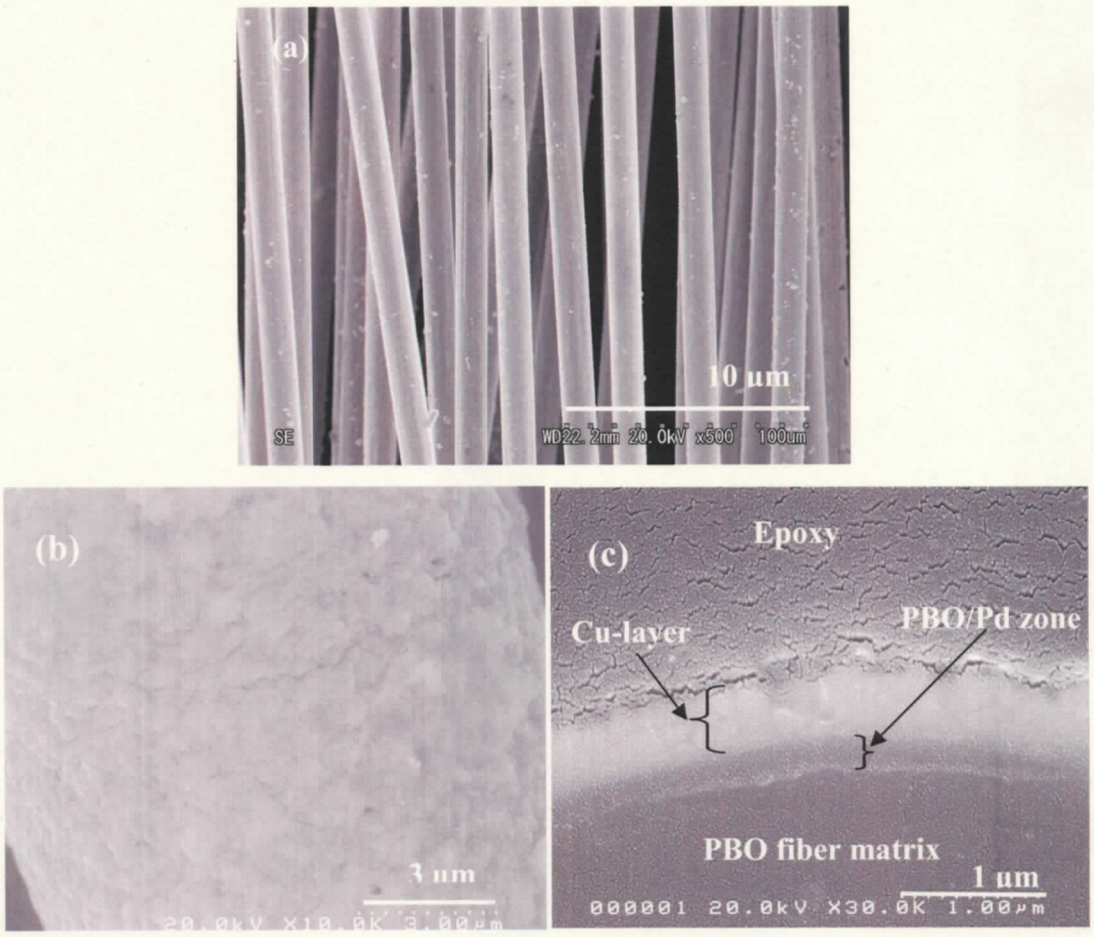

Fig. 4.9 SEM images of Cu-plated PBO fibers: (a) side view and (b) surface, and (c) cross-sectional view.

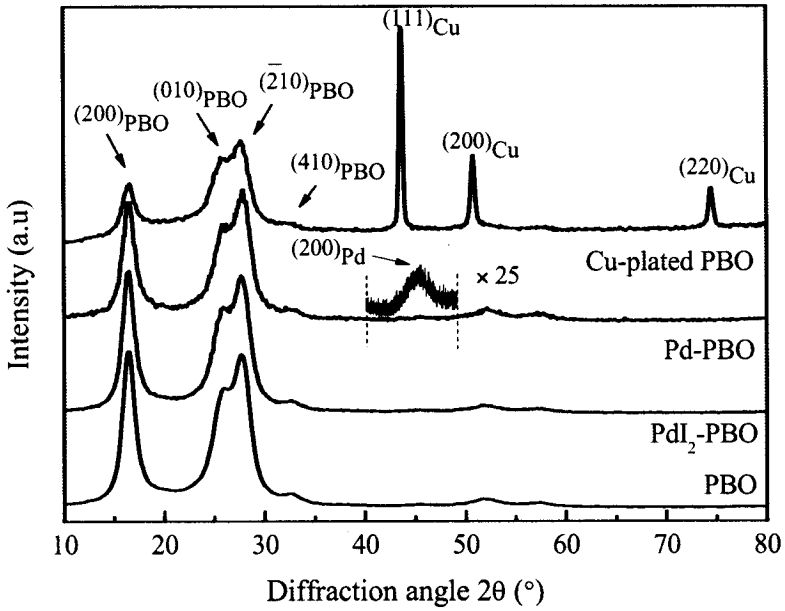

Fig. 4.10 (a) WAXD profiles of Cu-plated PBO fiber at different processing stages using Pd catalyzation process.

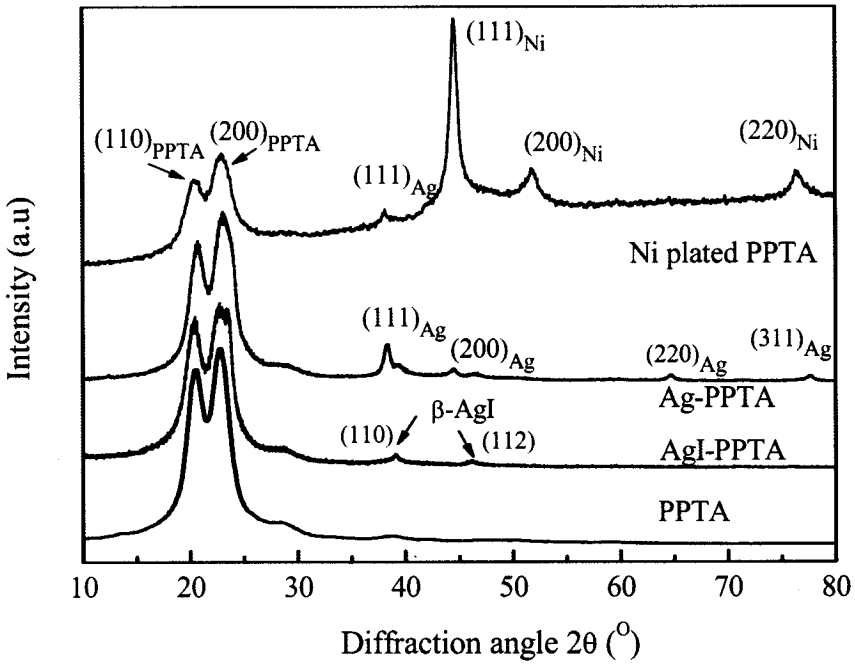

Fig. 4.10 (b) WAXD profiles of Ni plated PPTA fiber at different processing stages using Ag catalyzation process.

The plating condition of super fiber surface was further investigated using WAXD profile. Figs. 4.10(a) and (b) shows the WAXD profiles of differently pretreated and metallized PPTA and PBO fibers at each stage of process.

In Fig. 4.10(a) the WAXD profiles of the pristine fibers show the typical equatorial pattern of HPFs in each respective profile. After PdI_2 generation and subsequent reduction, diffraction peaks with low intensities for PdI_2 and Pd metal were hardly detected because of the hindrance by the intense equatorial peaks of precursor fibers. Therefore, as an evidence of existence of Pd particles in Pd-PBO fiber, the magnified small area of WAXD diffraction profile of at $2\theta = 40-50°$ for Pd-PBO and 35–45° for Pd-PPTA are shown in the figure. The diffraction peak at around $2\theta = 39°$ and $2\theta = 46°$ assigned to the (111) and (200) planes of Pd metal, respectively. This indicates that the Pd particles were surely formed on the fiber surfaces. After electroless plating prominent diffraction peaks from planes of (111), (200) and (220) of Cu metal on metallized PBO and (111), (200) and (221) Ni metal on metallized PPTA surface were appeared at around $2\theta = 44.4$, 51.8 and 76.4°, respectively. This also proved the formation of Pd particles on the surface that served as a catalyst for the plating processes.

Again, Fig. 4.10(b) shows WAXD profiles of PPTA fibers at each stage of the process. The WAXD profile of the pristine fiber shows a typical equatorial pattern of a highly crystalline fiber. The WAXD profile of AgI-PPTA shows some peaks at $2\theta = 23$, 39.1, and 46.2°, which were assigned to the (100), (110), and (112) planes, respectively, of the β-AgI crystal [35,41]. After the reduction of AgI-PPTA to Ag-PPTA, peaks of Ag were confirmed on the corresponding diffraction profile at around $2\theta = 38.3$, 45, 65, and 77°, which represent the (111), (200), (220), and (311) planes of metallic Ag, while the diffraction pattern of the PPTA fiber remained unchanged. Moreover, strong diffraction peaks of Ni were prominent on the PPTA surface after the electroplating process.

3.3 Effect of plating conditions

In electroless deposition, plating bath conditions are really crucial to form a good quality plated layer. The usage of surfactant during pretreatment and plate bath compositions accompanied with plating conditions (e.g., temperature, pH, time) have significant effect onto coating surface structure as well its properties (e.g., hardness, wear and corrosion

resistance, electrical conductivity etc.). In this context, different plating bath conditions such as pH, temperature, time and use of reducing agent in plating bath and surfactant prior to plating onto coating performance was investigated in electroless Ni plating of PPTA fiber.

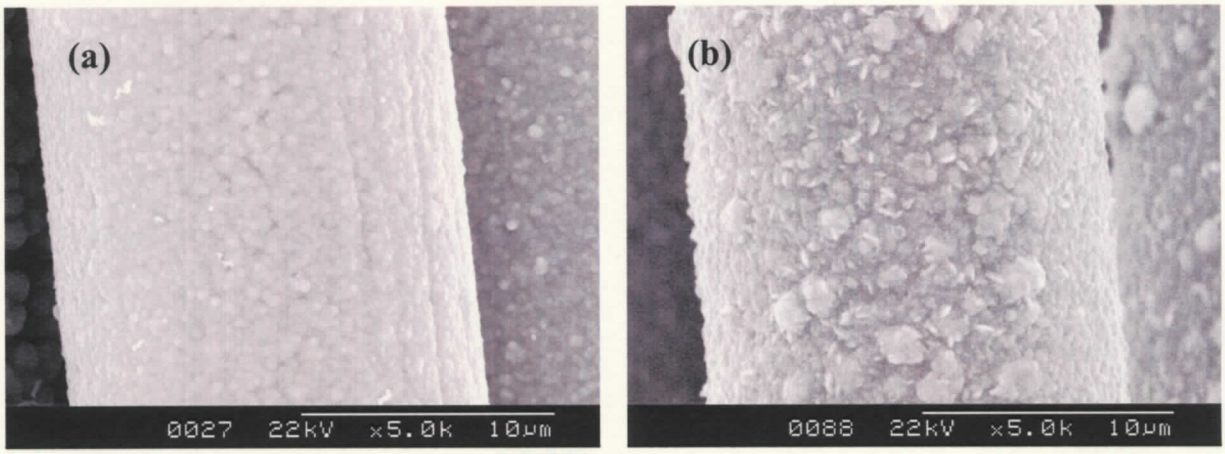

Fig. 4.11 SEM images of Ni layer on PPTA without use of reducing agent DMAB (a) and with DMAB (b) in plating solution of 80 °C, pH 9.5 for 30 min.

Addition of a reducing agent in plate bath influences the deposition quality as apparent in Fig. 4.11. Plate bath containing 0.05 mol/L of DMAB results extraneous outgrowth of plated deposits on layer surface. Here, reducing agent DMAB initiates the plate bath reaction and therefore, bath stability is not good compared with plate bath without it and resulted bridges of Ni particles on layer surface. Thus, plate bath without any reducing agent formed a smooth and clean plated surface on PPTA fiber, as shown in Fig. 4.11(a).

To qualitatively evaluate the effect of plate bath variables on the surface morphology of the Ni-layer deposit, samples were processed in plating solutions having different pH values, ranging from pH= 5.0, 7.5, 8.5 and 9.5, and operating temperatures of 50, 60, 70, 80 and 90 °C for plating time of 15, 30, 40, 50 and 60 min. The SEM image analysis evidenced distinct different surface morphology with the change in operating pH, temperature and time as shown in Figs. 4.12, 4.13 and 4.14. In these figures, the SEM images are correlated to the Ni plating rates achieved at the specific bath temperature, time and pH values.

Significant changes in microstructure were observed after the deposition tests at different plating solution pH values and a constant operating temperature at 80 °C for 30

min. The SEM images of Fig. 4.12 reveal that the Ni surface smoothed with the increasing pH value of the solution. Seemingly, the size of individual Ni particle was largest for the deposit produced at an operating pH value of 5.0 with minimum layer thickness. At the same time, the effect of pH on obtainable Ni layer thickness and porosity is related to its effect on deposit morphology. At pH value of 9.5, the plated layer thickness was most with closely packed fine particles covering the surface evenly. This phenomena leads to the assumption that in presence of OH^- ions the Ni decomplexing is promoted, and deposition towards fiber is accelerated until the charge exchange process stops.

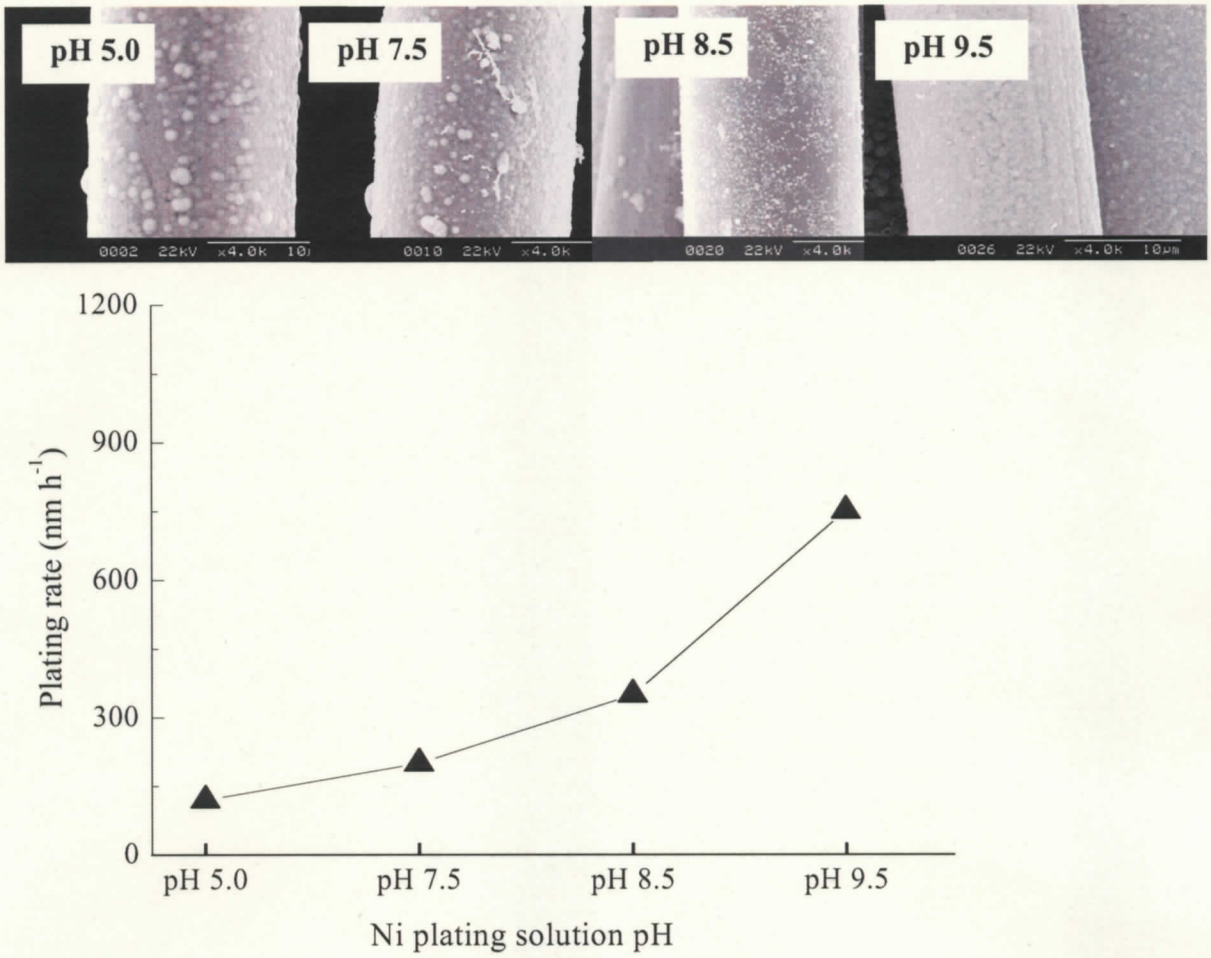

Fig. 4.12 SEM images of surface morphology of the Ni layer on PPTA as a function of pH.

The variation of deposition rate could also be observed when changing the operating temperature of solution from 50 to 90 °C keeping the pH and time constant at 9.5 and 30

min, respectively. It can be seen from Fig. 4.13 7 that at 50 °C the slow plating rate resulted smooth but thin plating layer, while with the increasing temperature the rate of plating was accelerated linearly but the surface roughness was noticeably increased at 60 °C. In contrast, with further increase of temperature the size of Ni particles became more uniform, and the surface roughness was noticeably reduced.

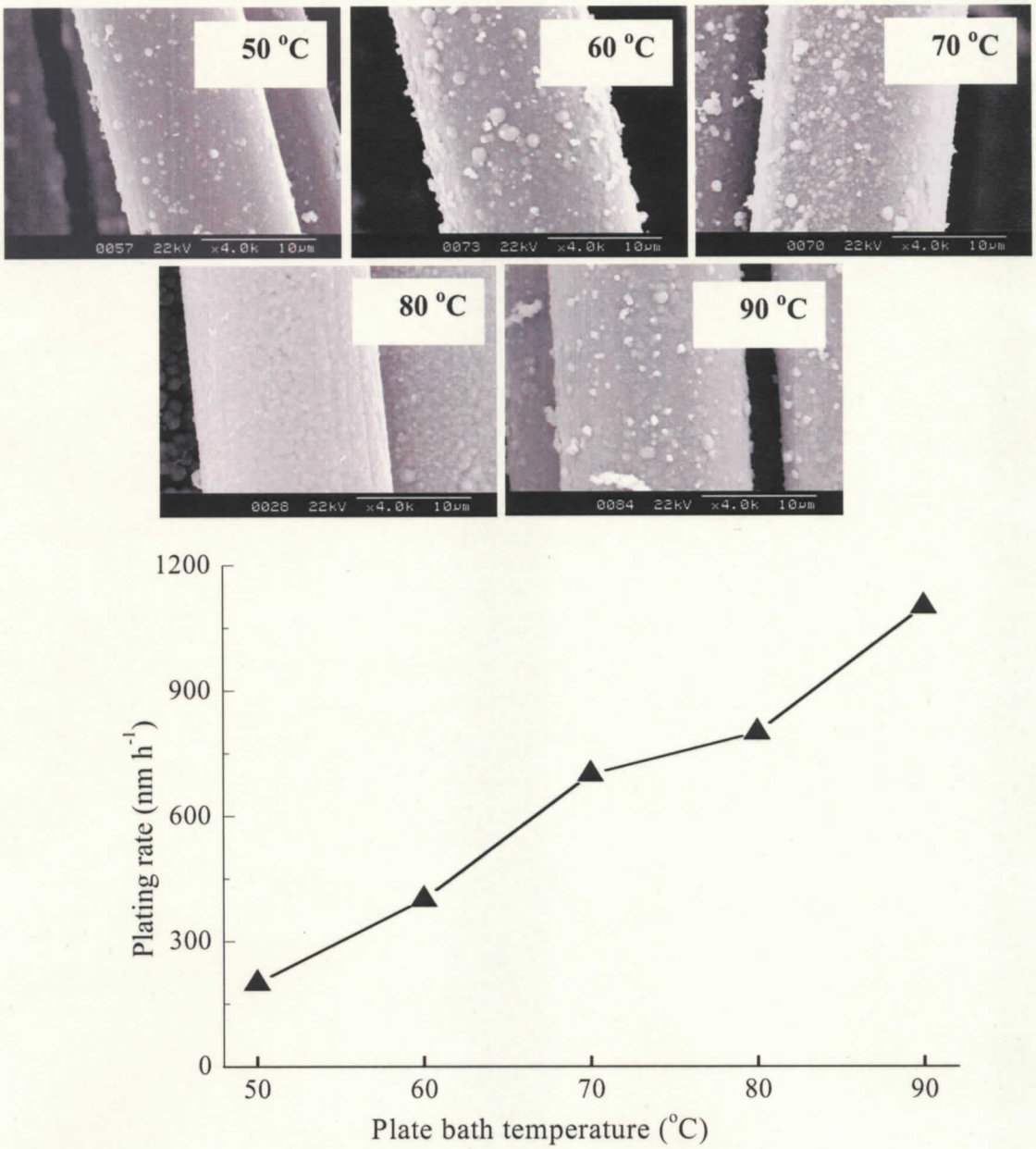

Fig. 4.13 SEM images of surface morphology of the Ni layer on PPTA as a function of temperature.

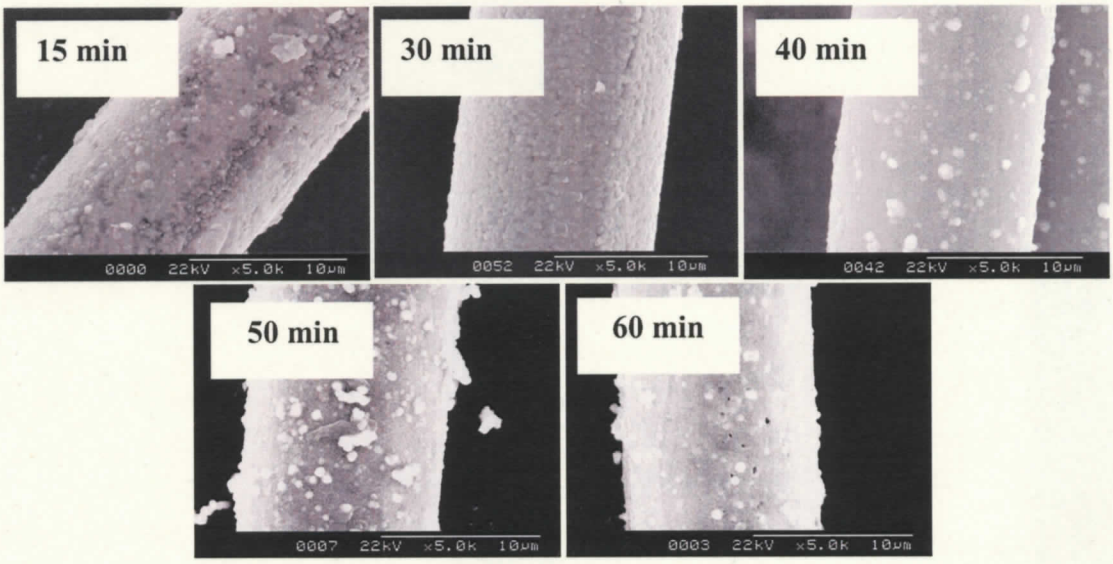

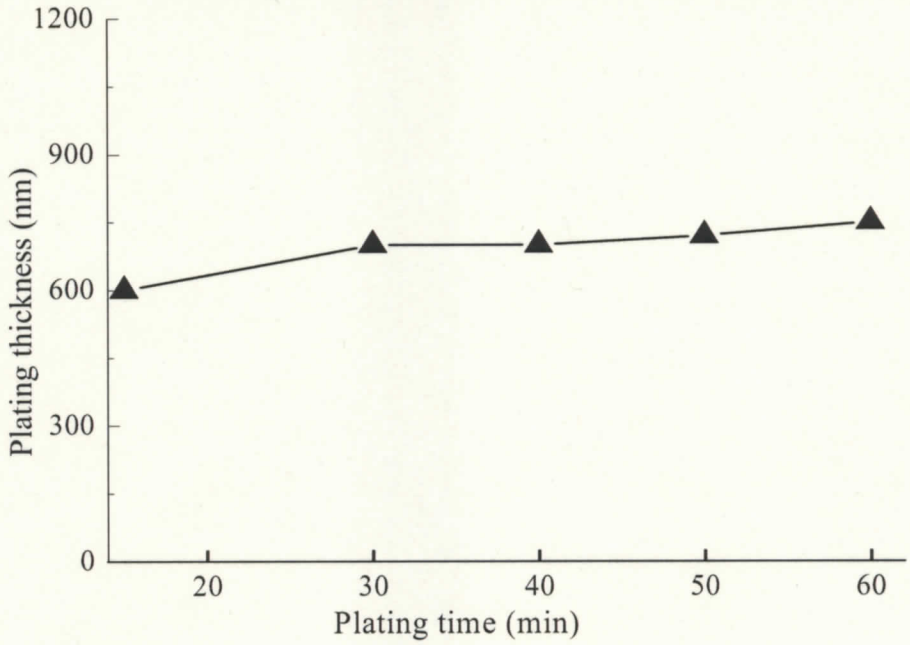

Fig. 4.14 SEM images of surface morphology of the Ni layer on PPTA as a function of plating time.

Concurrent with the improvement in uniformity was an increase in plating rate with temperature. It appears that at higher temperatures, the probability that two molecules will collide is higher. The plating rate increased almost linearly with increasing temperature, and a drastic increase was observed when the operating temperature rose to 90 °C from 80 °C with too much unfix Ni particles on fiber surface. It indicates that at higher temperatures,

the probability that the rapid reaction phenomenon of plate bath reactants causes some coagulation of Ni particles at plate bath and their subsequent deposition on fiber surface as unfix granules. Fig. 4.14 indicates that the time of plating is less significant for deposition rate than pH and temperature. However, longer time influences the smoothness of surface. The SEM image shows that 15 min plating time resulted a non-uniform layer of ca. 600 nm thickness, while increase of plating time stabilized the deposition rate with even deposition, but longer plating time resulted deposition of large Ni particles on fiber surface with bridge phenomenon. Further, increase of plating time to 60 min resulted almost same deposition rate with many micro holes on the plated surface.

The maintain of sufficient adhesive strength of plated layer by avoiding of formation of pits between plated layer and fiber as a result of the hydrogen evolution during the plating are an important concerns for the end use of electroless Ni plating. Stirring the plating solution or rotating objects being plated can lessen the problem but cannot provide a satisfactory resolution for the problem. Incorporation of the surface active compounds with suitable structure on fiber surface or into plate bath appears to be a promising remedy to diminish surface pinholes and enhancement of adhesion of plated layer. It has been reported that the use of anionic surfactant SDS influences on surface roughness and hardness of plated layer [42]. Also, hydrogen formed via the coupling of adsorbed hydrogen atoms has little chance to form into bubbles on the plating frontier in the presence of surfactant molecules [43]. The adsorption of tiny H_2 bubbles at the interface of the plated deposit is regarded as the root cause of pinholes or pits. Electroless Ni plating involves a complicated combination of several types of chemical reactions; therefore, the presence of small amount of surfactant on a fiber surface may affect these reactions in certain ways and lead to pit-free metal deposition. In principle, the surfactant molecules play a role in the removal of tiny hydrogen bubbles from the surface of the substrate through adsorption at the H_2-liquid interface. Therefore, water-soluble surfactants such as SDS have relatively lower hydrophilic-lipophilic balance (HLB) values and a stronger ability for the removal of H_2 bubbles from the Ni deposition frontier is anticipated. Therefore, I-PPTA was treated with a small amount of SDS (0.1 g/L aqueous solution) surfactant during the catalyzation process. It is clear that the anchoring of pore deposits is relatively weak and they may be

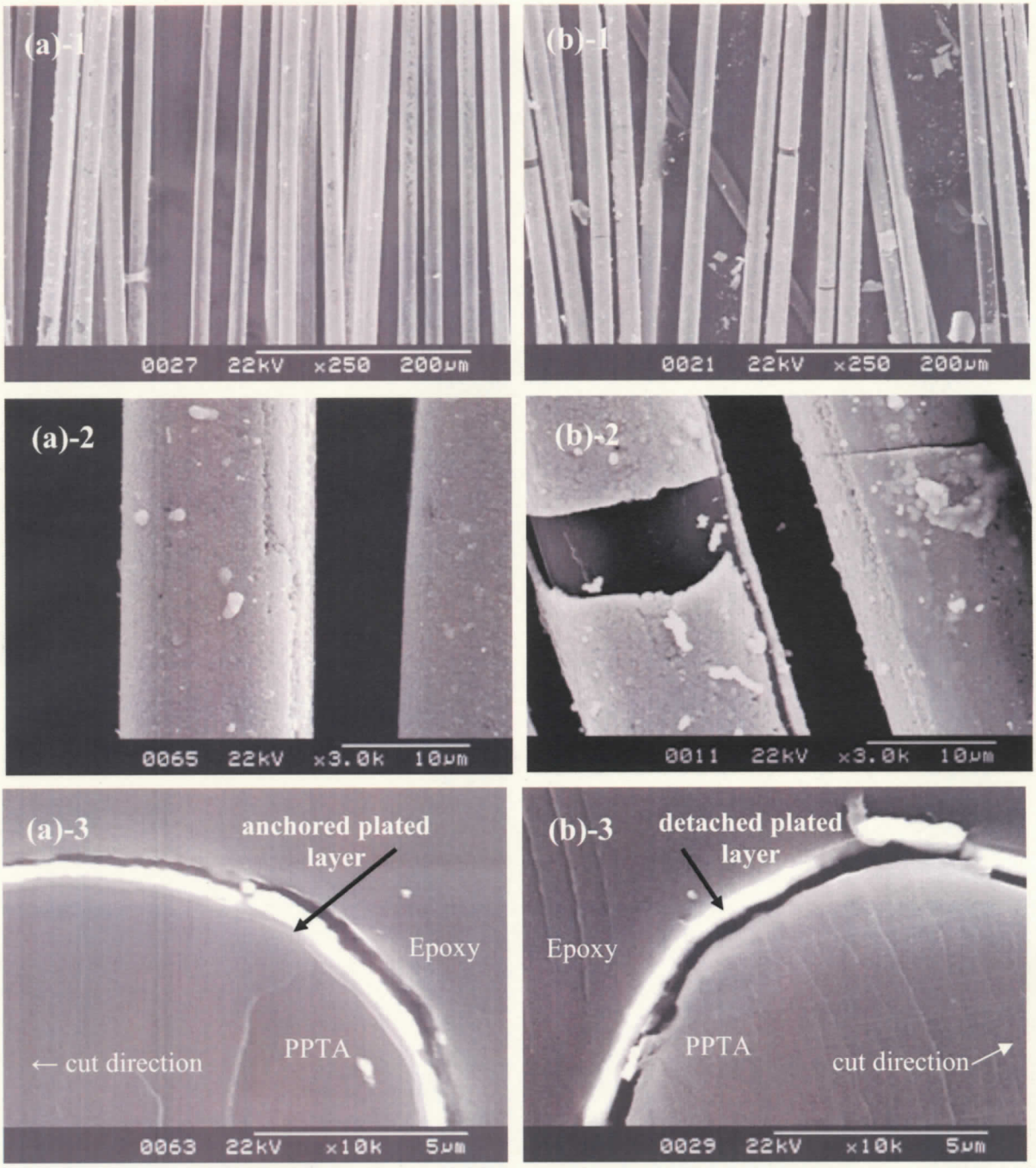

Fig. 4.15 SEM images of Ni-plated PPTA fibers after tape peel-off test. (Images (a)-1, 2, 3 and (b)-1, 2, 3 correspond to probe with and without use of SDS, respectively)

easily detached from the fiber surface during application. Therefore, the peeling performance of plated surfaces with and without the use of SDS was assessed using a tape peel-off test and the peeled surface was examined using SEM. The SEM images of Figs. 4.15(a) and 4.15(b) represent the represent the plated fibers with and without SDS, respectively. After the tape peel-off test, the plated fibers subjective to SDS treatment exhibited sufficient peeling resistance with a mostly intact plated layer as shown in Figs. 4.15(a)-1 and 4.15(a)-2. In contrast, the fibers without SDS treatment had cracks on the plated layer, which had a tendency for peeling, as shown in Figs. 4.15(b)-1 and 4.15(b)-2, due to insufficient anchoring force with the fiber surface. . In combination with the concept of H_2 bubble removal, the repulsion of charges on the hydrophilic groups of the surfactant and used silver complex, AgI formed near the PPTA fiber surface, which reduced subsequently to form catalyst Ag particles and facilitates the uniform deposition of Ni particles on the substrate and ensures a well-anchored plating layer. Cross-sectional SEM images of the plated layer adhesion, with and without the use of SDS, are shown in Fig. 4.15(a)-3 and Fig. 4.15(b)-3, respectively, the SDS plated layer remained strongly attached, even after the strong cutting force of trimming, while the plated layer without the use of SDS was easily detached from the fiber, which indicates weak anchoring strength against cutting stress. Thus, the use of surfactant during the catalyzation process enhances the adhesion of the electroless plated layer.

4. Conclusions

An efficient catalyzation process was explored using iodine pretreatment for the fabrication of a highly adhesive Cu, Ni and Ag-plating layer on high performance PBO and PPTA fibers. Iodine pretreatment followed by metal iodide formation on the fiber surfaces successfully catalyzed the fibers with metal particles (Pd or Ag) for subsequent electroless plating processes. The flexible metal plated fibers reflect a uniform lustrous appearance of respective metal with high durability. The anchoring effect of catalyst Pd or Ag particles ensures adhesion of the plated layer with fiber, which makes the plated layer resistant to tape peel-off, corrosion, and ultrasonic exposure. Also, the conditions of plate bath influence plate layer deposit rate and quality. Further investigation reveals that the use of the anionic SDS surfactant improves the adhesive durability of the plated layer. The

properties of the plated fibers will be discussed in detail in next chapter. The proposed pretreatment method has the potential for application to various electroless plating processes with different polymers.

5. References

[1] Ohta Y, Kajiwara K, in: Houck MM (Ed), High performance fibers: structure, characteristics and identification, Identification of textile fibers, Woodhead Pub Ltd, Cambridge, UK, (2009) p88–110.

[2] Hearly JWS, High performance fiber, Woodhead Pub Ltd., Cambridge, UK, (2001).

[3] Chae GH, Kumar S, Rigid rod polymeric structure, J Appl Polym Sci, 100, 791–802 (2006).

[4] Yang HH, Kevlar Aramid fiber, Wiley and Sons, USA, (1993).

[5] Kumar S, Dang TD, Arnold FE, Bhattacharya AR, Min BG, Zhang X et al., Synthesis and Properties of PBO/SWNT composites, Macromolecules, 35, 9039–9043 (2002).

[6] Kitagawa T, Murase H, Yabuki K, Morphological study on poly-p-phenylenebenzobisoxazole (PBO) fiber, J Polym Sci Part B Polym. Phys, 36, 39–48 (1998).

[7] Zylon technical information guide, Toyobo Co. Ltd., (2001).
http://www.toyobo.co.jp/e/seihin/kc/pbo/menu/fra_menu_en.htm

[8] Chin J, Forster A, Clerici C, Sung L, Oudina M, Rice K, Temperature and humidity aging of poly(p-phenylene-2,6-bemzobisoxazole) fibers: Chemical and physical characterization, Polym Degrad Stab, 92, 1234–1246 (2007).

[9] Gonzales AR, Schofield RB, Hart SB, Third status report to the attorney general on body armor safety initiative testing and activities, Special report (NCJ210418), National Institute of Justice, USA, August 24, 2005. (www.iop.usdoj.gov/nij)

[10] Forster AL, Pintus P, Messin GHR, Rilley MA, Petit S, Rossiter W, Chin J et al., Hydrolytic stability of polybenzobisoxazole and polyterephthalamide body armor, Polym Degrad Stab, (2010), doi:10.1016/polymdegradstab.2010.10.004.

[11] O'neil JM, Factors contributing to the degradation of poly(p-phenylene benzo-bisoxazole) (PBO) fibers under elevated temperature and humidity conditions, Master's thesis, Texas A&M University, (2006).

[12] Park ES, Sieber J, Guttman C, Rice K, Flynn S, Watson S et al., Methodology for detecting residual phosphoric acid in polybenzoxazole fibers, Anal Chem, 81, 9607–9617 (2009).

[13] Technical Guide: Kevlar® Aramid fiber, Dupont.

[14] Zhang H, Zhang J, Chen J, Hao X, Wang S, Feng X, Gua Y, Effects of solar irradiation on the tensile properties and structure of PPTA fiber, Polym Degrad Stab, 91, 2761–2767 (2006).

[15] Downing JW, Newell JA, Characterization of structural changes in thermally enhanced Kevlar-29 fiber, J Appl Polym Sci, 91, 417–424 (2004).

[16] Mallory GO, Hajdu JB, Electroless Plating-Fundamentals and Applications, William Andrew Pub/Noyes, New York, (1990).

[17] Ohno I, Electroplating chemistry of electroless plating, Mater Sci Eng A, 146, 39–49 (1991).

[18] Dini JW, Electrodeposition: The material science of coatings and substrates, Noyes Publications, New York (1993).

[19] Qui T, Chu PK, Self-selective electroless plating: An approach for fabrication of functional 1D nanomaterials, Mater Sci Eng R, 61, 59–77 (2008).

[20] Gabara V, Hsu CH, Electroless plated aramid surfaces and a process for making such surfaces, US Patent 5,302,415 (1994).

[21] Burch RR, Gould R, Lee KS, Phillips BR, Electroless plated Aramid surfaces, US Patent 5,370,934 (1994).

[22] Hsu CH, Process for making electroless plated aramid fibrids, US Patent 5,422,142, (1995).

[23] Schwarz A, Hakuzimana J, Kaczynska A, Banaszczyk J, Westbroek P, McAdams E et al., Gold coated para-aramid yarns through electroless deposition, Surf Coat Technol, 204(9–10), 1412–1418 (2010).

[24] Yuen CWM, Jiang SQ, Kan CW, Tung WS, Influence of surface treatment on the electroless nickel plating of textile fabric, Appl Surf Sci, 253(12), 5250–52557 (2007).

[25] Osaka T, Yoshino M, New formation process of plating thin films on several substrates by means of self-assembled monolayer (SAM) process, Electrochimica Acta, 53, 271–277 (2007).

[26] Martinez M, Hisada K, Tabata I, Hirogaki K, Yonezawa S, Hori T, The effectiveness of thermal treatment for development of conductive metalized aramid fiber using supercritical fluid carbon dioxide: Fiber-metal adhesive strength improvement, J Supercritical Fluids, 56(3), 22–329 (2011).

[27] Zhao X, Hirogaki K, Tabata I, Okubayashi S, Hori T, A new method of producing conductive aramid fibers using supercritical carbon dioxide , Surf Coat Technol, 201(3–4), 628–636 (2006).

[28] Belmas M, Tabata I, Hisada K, Hori T, Supercritical fluid-assisted electroless copper plating of aramid film: The influence of surface treatment, Sen'i Gakkaishi, 66(9), 215–219 (2010).

[29] Yang GH, Lim C, Tan YP, Zhang Y, Kang ET, Neoh KG, Electroless deposition of nickel on fluoropolymers modified by surface graft polymerization, European Polym J, 38, 2153–2160 (2002).

[30] Charbonnier M, Romand M, Tin-free electroless metallization of glass substrates using different PACVD surface treatment processes, Surf Coat Technol, 162, 19–30 (2002).

[31] Fujimori Y, Gotoh Y, Tamaki N, Ohkoshi Y, Nagura M, Introduction of copper iodide fineparticles into poly(acrylic acid) matrix via a complex of polymer-polyiodide ion, J Mater Chem, 15(45), 4816–4822 (2005).

[32] Yang W, Luo S, Bingjie Z, Huang Z, Tang X, Electroless preparation and characterization of magnetic Ni-plating on polyurethane foam, Appl Surf Sci, 254, 7427–7430 (2008).

[33] Jiang SQ, Kan CW, Yuen M, Wong WK, Electroless nickel plating of polyester fiber, J Appl Polym Sci, 108, 2630–2637 (2008).

[34] Huang Y, Shi K, Liao Z, Wang Y, Li W, Zhu F, Studies of electroless Ni-Co-P ternary alloy on glass fibers, Mater Lett, 61, 1742–1746 (2007).

[35] Tetsumoto T, Gotoh Y, Fabrication of silver plated nylon 6 nanofibers using iodine Sen'i Gakkaishi, 66(9), 222–227 (2010).

[36] Mizuno M, Tanaka J, Harada I, Electronic spectra and structures of polyiodide chain complexes, J Phys Chem, 85, 1789 (1981).

[37] Fatema UK, Tomizawa C, Harada M, Gotoh Y, Iodine-aided fabrication of hollow carbon fibers from solid poly(vinyl alcohol) fibers, Carbon, 49(6), 2158–2161 (2011).

[38] Wang L, Wang L, Tan E, Li L, Guo L, Flower-shaped PdI_2 nanomaterials with remarkable surface-enhanced Raman scattering activity, J Mater Chem, 21, 2369–2373 (2011).

[39] Inorganic material database, National Institute of Material science, Material database station, MatNavi. http://crystdb.nims.go.jp/index_en.html (last accessed Feb 10, 2011)

[40] Watanabe Y, Igawashi Y, Honma H, Evaluation of activation process for fine pattern deposition, J Japn Ins Intercon Pack ElectroCirc, 12(4), 231–235 (1997).

[41] Fujimori Y, Gotoh Y, Kawaguchi A, Ohkoshi Y, Nagura M, Conductivity and structure of a polyamide/silver iodide nanocomposite, J Appl Polym Sci, 108(5), 2814–2824 (2008).

[42] Elansezhein R, Ramamoorthy B, Nair PK, Effect of surfactant on the mechanical properties of electroless (Ni-P) coating, Surf Coat Technol, 203, 709-712 (2008).

[43] Chen BH, Hong L, Ma Y, Ko TM, Effect of surfactants in an electroless nickel-plating bath on the properties of Ni-P alloy deposits, Ind Eng Chem Res, 41, 2668–2678 (2002).

[44] Watanabe, Y, Igawashi, Y, Honma, H, Evaluation of activation process for fine pattern deposition, J Japn Ins Intercon Pack Electro Circ, 12(4), 231-235 (1997).

Chapter 5

Properties of metallized high performance fibers

1. Introduction

In previous Chapter 4, we discussed elaborately the metallization of high performance fibers (HPFs) of poly(*p*-phenylene benzobisoxazole) (PBO) and poly(*p*-phenylene terephthalamide) (PPTA) using iodine pretreatment and electroless plating with Cu, Ni and Ag metals. The functional properties of the metallized fibers were focused in this Chapter.

Iodine pretreatment effectively catalyzed PBO and PPTA fiber surface and a highly adhered plated layer was formed on the fiber surface. However, one of the difficulties in achieving successful electroless plating has reside in obtaining good adhesion between the plating substrate and the plated metals. While mere encapsulation may suffice for some applications and some articles, good adhesion of the plated metal is essential for most of the usage. Therefore, we focus on the performance of iodine treated and electroless plated fibers that determines their ability to withstand the forces of further processing and end use stresses. It is well known that, electroless coating on high performance fibers are functional coating, rarely used as decorative purpose. Therefore, the primary criterion of performance of plated fiber falls in the following categories [1-5]:

- Uniformity, appearance and flexibility
- Wear resistance
- Corrosion resistance
- Electrical conductivity (resistivity)
- Optical shielding properties
- Mechanical properties
- Magnetic properties etc.

This Chapter investigates the above mentioned criteria of metal plated fibers. Judging from the obtained results, a logical conclusion can be drawn about the effectiveness of iodine-aided catalyzation process and its feasibility on subsequent plating performances.

2. Experimental methods

The performance of plated fiber was evaluated based on the results of below mentioned tests.

Adhesion performance

The adhesive performance of the plating layer was evaluated using the following three

methods:

(i) Ultrasonic peeling was carried out by ultrasonic exposure in acetone at 50 °C with a Bransonic 2510J-DTH (42 kHz, 100 W). The ultrasonic exposure times were 60 min or 300 min.

(ii) Tape peel-off test was conducted on the basis of JIS H 8504-15-1999. A strip of Kokuyo T-SK18N cellophane tape was adhered to the plated surface by firmly pressing with thumbs followed by its pulling out from the plated surface.

(iii) The corrosion resistance of plated fiber was investigated in alkaline condition. First, fiber was immersed in a 3% NaCl solution with a pH of 7.0, and left for 24 h. After 24 h, the corroded fiber was washed with water and dried. Then the surface appearance was checked and condition of corroded surface was investigated under SEM.

Electrical Conductivity

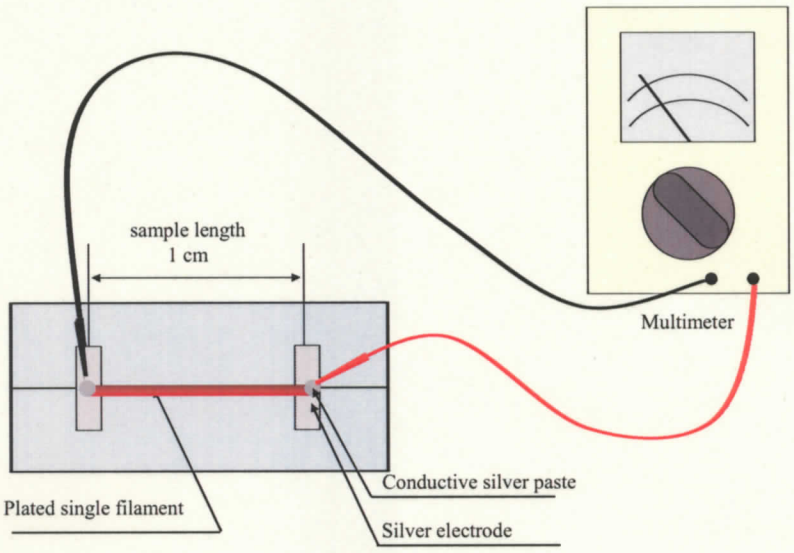

Fig. 5.1 Measurement of volume resistivity using two–terminal method.

The electrical conductivity of the plated fibers was assessed from their volume resistivity. The volume resistivity of plated fiber was calculated form their resistance; measured by conventional two-terminal method at ambient condition using a single fiber

attached to a silver electrode using silver paste as illustrated in Fig. 5.1 [6] and using the following formula:

$$R_v = R.A / l$$

where, R_v is the volume resistivity (Ω m), R is the resistance of fiber (Ω), A is the area of fiber tested (m^2) and l is the test length (m).

Mechanical properties

The mechanical properties of plated fibers were evaluated from their tensile strength and modulus value. The Young's modulus of single fiber was calculated from its stress-strain curve. The single fiber tensile test was measured using a Tensilon RTC-1250A tensile tester (A & D Co. Ltd., Japan) at room temperature. A cross head speed of 40 mm/min and a gauge length of 40 mm were used for all samples. For each sample, 30 to 40 specimens were tested.

Light resistance property

The light resistance of the pristine and plated PBO fibers was measured using a xenon weather meter (Table Sun XT 1-15, Suga Test Instruments Co. Ltd, Japan) under an illumination of 180 W/m^2 in ambient conditions. The xenon lamp was exposed only on PBO fiber that is more delicate to light sources like sunlight, UV, xenon and fluorescent lamps. The duration of exposure was 18 days for Cu-plated PBO fiber and 12 days for Ni-plated PBO fiber. After different intervals, samples were taken out and tensile strength was measured to investigate the influence on its mechanical properties.

Magnetic properties

The magnetic properties of Ni-plated PBO and PPTA fibers were assessed from a hysteresis loops measured at 300 K with a vibrating sample magnetometer (Mini plant VSM, Taiyo Toyo Sanso Co. Ltd.).

3. Results and discussion

3.1 Adhesion performances of the plated fibers

Sufficient adhesive forces between a substrate and the plated metal are required for good quality plating, because plating must be durable to withstand stresses accompanying further processing and end use. The adhesive durability of the plated layer was evaluated upon ultrasonic exposure, tape peeling-off, and corrosion tests.

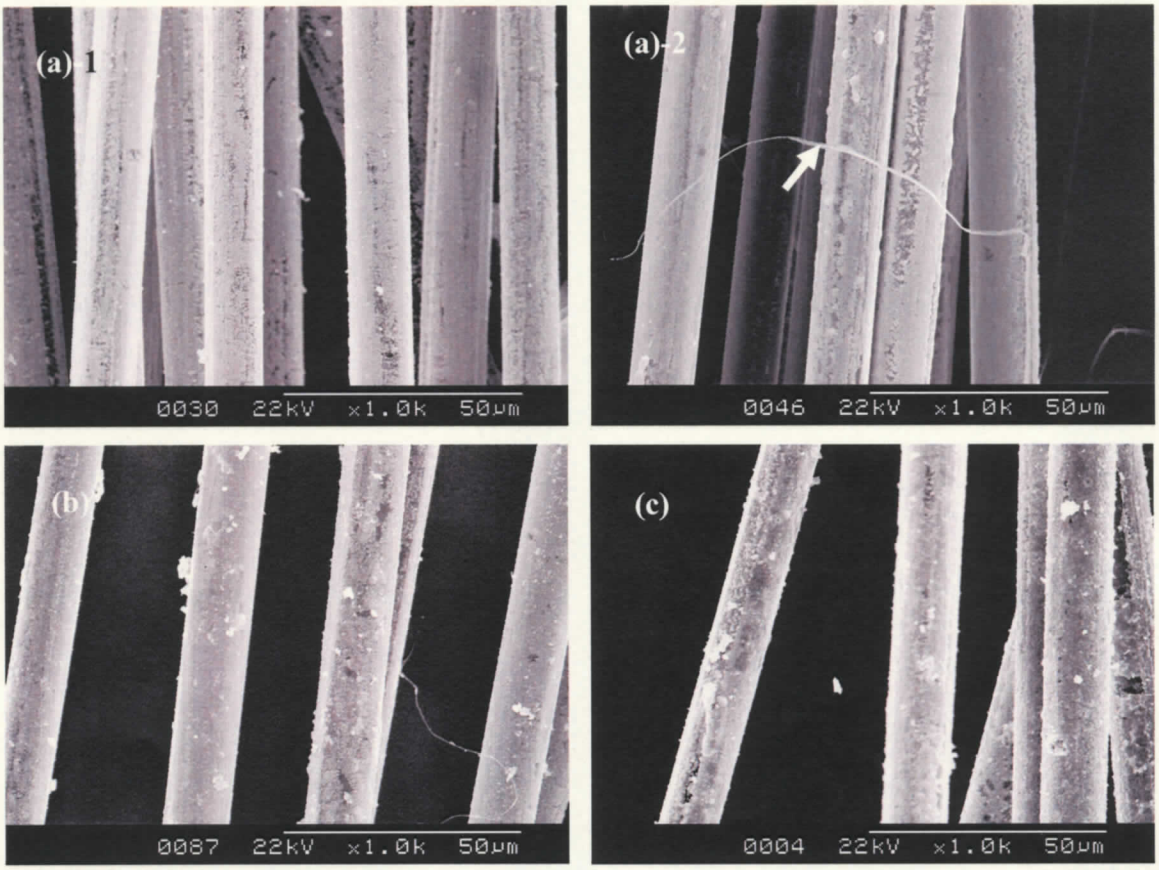

Fig. 5.2 SEM images of Cu-plated fibers after (a)-1 ultrasonic exposure for 60 min, (a)-2 for 300 min, (b) tape peeling-off, and (c) corrosion tests.

Fig. 5.2 shows the SEM images of Cu-plated fibers before and after the aforementioned durability tests. In Fig. 5.2(a)-1, a small section of the Cu plating layer was scraped because of ultrasonic exposure; however, the plated layer remained unaffected. After 300 min of exposure, fibrillation of the PBO fiber occurred, as indicated by the arrow shown in Fig.

5.2(a)-2, which refers that the filament was damaged by prolonged exposure, while distinct additional peeling was not observed. In Fig. 5.2(b), the adhesion resistance of the Cu-plated layer was also evaluated using a cellophane tape peeling-off test, which is commonly employed to determine the plating durability.

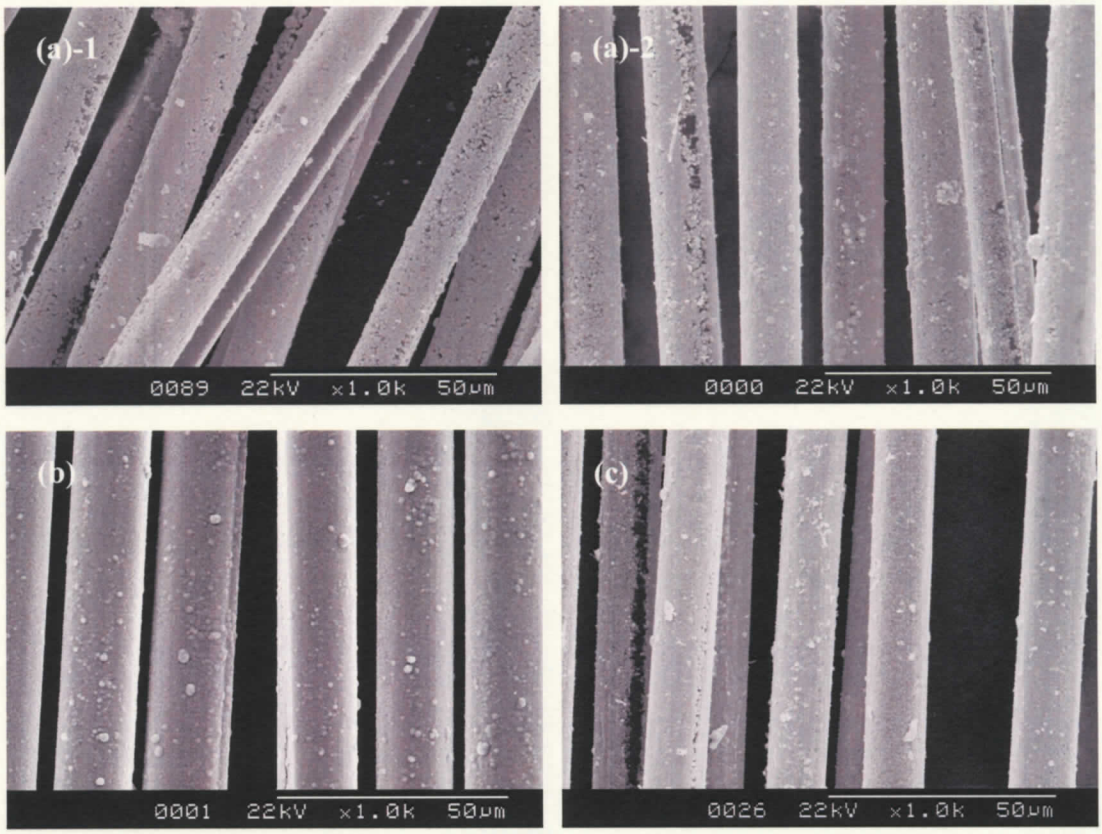

Fig. 5.3 SEM images of Ni-plated PBO fibers after (a)-1 ultrasonic exposure for 60 min, (a)-2 for 300 min, (b) tape peeling-off, and (c) corrosion tests.

The SEM investigation after the tape peeling-off test showed that the layer was intact and fewer cracks on the surface were observed. We visually evaluated the degree of adherence on the tape corresponding to the scraped residue on the tape. As a result, a small amount of small Cu particles was removed by the tape, and no large pits in the plated surface were observed. In addition, we studied the corrosion behavior of the plated layer. The plated PBO fiber was immersed in NaCl solution, and then the corroded specimen was observed using SEM. The surface somewhat roughened, but the Cu layer maintained its

texture, as shown in Fig. 5.2(c). Although some corrosion spots were observed and the luster of the plated layer became slightly dull because of the oxidation of Cu, high electrical conductivity was maintained, as described later. The aforementioned SEM observations of Fig. 5.2 imply that the robust Cu-plated layer formed on the PBO surface because of strong adhesion and dense metal layer having less pits.

Electroless Ni plating is characterized by its high wear and corrosion resistance properties. So we evaluated the same adhesion performance tests on Ni-plated PBO fiber. Fig. 5.3 shows the SEM images of Ni-plated PBO after each performance test. The test results evident that, Fig. 5.3(a)-1 and (a)-2, during ultrasonic exposure some of the plated layer was scraped off after initial ultrasonic exposure for 60 min, but after prolonged 300 min of exposure maintained the same surface appearance with few scraped plated area. However, after tape peel-off and corrosion tests, as shown in Fig. 5.3(b) and (c), respectively, maintained the intact plated layer which implies that Ni plating also formed a robust plated layer on PBO surface that is resistant against ultrasonic wear, peeling and alkaline corrosion.

Effect of catalyzation type on the adhesion property

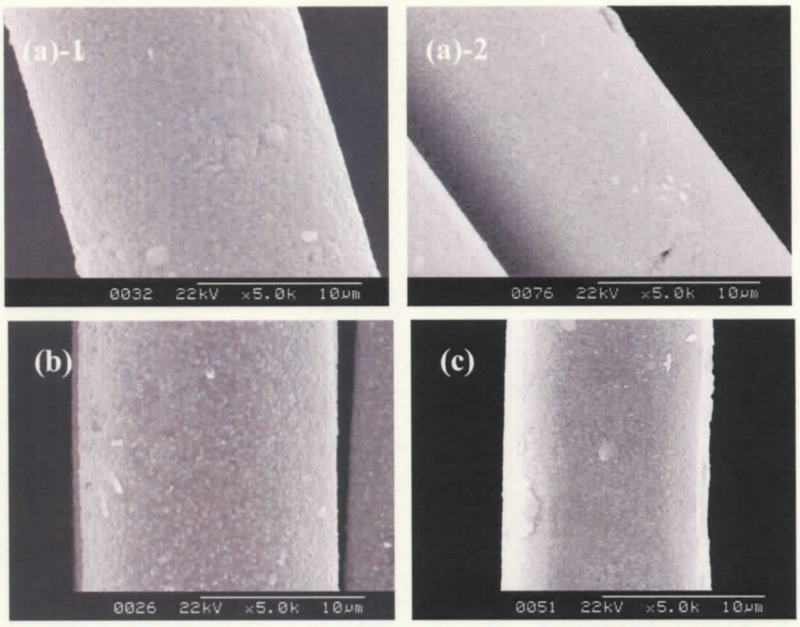

Fig. 5.4 SEM images of Pd activated and Ni-plated PPTA fibers after ultrasonic exposure for 60 min (a)-1, and 300 min (a)-2, tape peel-off test (b), and corrosion test (c).

As described in previous Chapter 4, iodine pretreatment assisted two types of catalyzation processes prior to electroless plating. Iodine treatment formed metal iodides on the fiber surface and their reduction generated Pd and Ag nuclei, which used as catalyst and as anchoring agents during electroless plating. However, electroless Ni plating was successfully conducted on both way catalyzed PPTA fibers with Pd and Ag catalyst particles. In an intention to investigate the influence of catalyst type on adhesion performance of resultant plated material, we performed all the performance tests on Ni-plated PPTA fibers followed both types catalyzation processes.

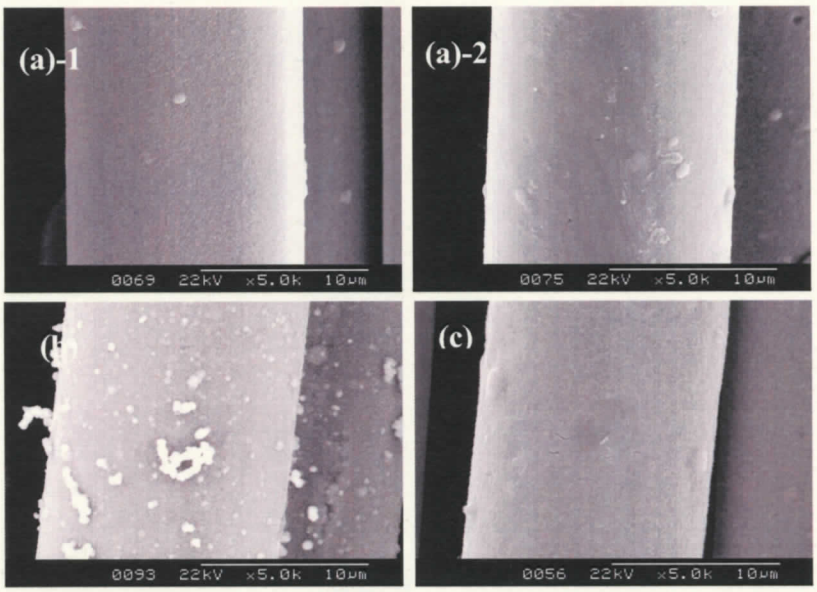

Fig. 5.5 SEM images of Ag activated and Ni-plated PPTA fibers after ultrasonic exposure for 60 min (a)-1, and 300 min (a)-2, tape peel-off test (b), and corrosion test (c).

Fig. 5.4 and Fig. 5.5 show the SEM images of Ni-plated PPTA fiber subjected to Pd and Ag activation process, respectively, after performance tests of ultrasonic exposure for 60 min in Figs. (a)-1 and 300 min in Figs. (a)-2, respectively, after tape peel-off Figs. (b) and corrosion test Figs. (c). The test results show that both way catalyzed PPTA fiber formed a highly adhered plated layer that remained unaffected after each of performance tests. In contrast to several expensive approaches, such as use of supercritical carbon dioxide or UV initiated graft polymerization to improve the adhesion of plated layer [7-9], our proposed method is simple, inexpensive and effective.

3.2 Electrical conductivity of the plated fibers

The volume resistivity means how strongly a material opposes the flow of electric current reflects the electrical conductivity of bulk. Electroless plated fibers are uniformly covered with different metals like Ag, Cu and Ni, which have conductive properties. Therefore, metal plated fiber also should exhibit some electrical properties. We measured the volume resistivity of single fiber plated with different metals, summarized and listed in the Table 5.1. It shows that electroless Cu, Ni and Ag plating process impart electrical conductivity on high performance fibers. The resistivity of the Cu-plated PBO fiber was 8.1 $\times$ 10^{-7} Ω m. Because the thickness of the plated layer was ca. 400–500 nm, the actual resistivity of the Cu layer was estimated to be 4 $\times$ 10^{-8} Ω m, which is slightly higher than that of the neat Cu metal (1.68 $\times$ 10^{-8} Ω m). Ni plated and Ag plated PBO fiber also exhibits electrical resistivity of 6.4 $\times$ 10^{-6} and 1.1 $\times$ 10^{-6} Ω m, respectively; which are lower than that of neat Ni and Ag metal (6.9 $\times$ 10^{-8} and 1.58 $\times$ 10^{-8} Ω m, respectively). Metallization of PBO and PPTA fiber functionalized these fibers with additional electrical properties.

Electrical resistivity after each performance test

As described in previous Section 3.1, several performance tests (ultrasonic exposure, corrosion resistance and tape peel-off) were performed on metal plated fibers to asses the durability of plated layer to fiber surface. The plated layer was found durable against each performance test and plated layer was found undamaged. Therefore, we measured the electrical resistivity of plated fibers after each performance test, which will reveals the actual condition of plated layer exposed to performance test conditions. Here Table 5.1 also summarizes the volume resistivities of the plated fibers subjected to different durability tests.

In case of Cu-plated PBO fiber, after ultrasonic exposure for 60 min or tape peeling-off, the conductivity was almost the same as that of the unexposed fiber. On the other hand, prolonged ultrasonic exposure for 300 min or the corrosion condition reduced the conductivity a bit, which implies that the Cu layer was slightly scraped off during these tests and the thickness of the layer was reduced. However, we did not observe significant detachment of the plating layer in the SEM images of Fig. 5.2. Therefore, it can be assumed

that the interfacial adhesion between the Cu plating layer and the PBO fiber was strong to withstand the influences of durability tests in this study. Ni plating and Ag plating on PBO fiber also result a durable plated layer with strong interfacial adhesion between the plating layer and fiber as evident from their resistivity values mentioned in of Table 5.1.

Similarly for PPTA fiber, the electrical resistivity of differently plated fiber and after different performance tests were measured as the same way, summarized and included in Table 5.1. Here, the changes of resistivity data correlates to the previous performance test results of PBO fiber. From the durability test results and electrical property data, it can be elucidated that strongly anchored plated layer on high performance fibers can withstand the performance tests used in this study.

Table 5.1

Electrical property of differently plated HPFs after different performance tests.
[Volume resistivities are in $\times 10^{-7}\ \Omega$ m]

Sample		After plating	After Ultrasonic exposure		After corrosion	After Tape Peel-off
			60 min	300 min		
PBO	Cu-plated	8.1	9	17	22	9.1
	Ni-plated	63	85	97	130	130
	Ag plate	11	27	110	150	36
PPTA	Cu-plated	9.8	17	35	31	14
	Ni-plated	120	240	330	240	160
	Ag-plated	45	70	210	240	120

* Volume resistivities of metals in $\times 10^{-7}\ \Omega$ m; Ni: 0.699 , Cu: 0.16, Ag: 0.158 [10, 11]

3.3 Mechanical properties of the plated fibers

As mentioned before, conventional electroless plating requires etching of fiber surface using strong chemicals, which causes strength deterioration of high strength fibers of PBO and PPTA. In our proposed technique, no surface etching was performed. So, investigation of mechanical properties will justify the efficacy of the applied method on high strength

fibers. The tensile strength of single fiber prior and after metal plating was investigated, and the mechanical properties are calculated from the typical stress-strain curves. The results of mean tensile strength and Young's modulus of pristine fibers and plated fibers were summarized in Table 5.2.

Table 5.2 demonstrates that the tensile strength after electroless plating is lower than that of pristine one in both fibers. The Cu-plated PBO fiber had a tensile strength of 4.9 GPa that was ca. 15% lower than that of the untreated fiber (5.8 GPa). We confirmed that the reduction of strength was mainly attributed to iodination and subsequent metal iodide formation process; the tensile strength of PBO fiber after iodination and after iodide formation was 5.4 and 5.1 GPa, respectively. Although PBO fiber exhibited decreased tensile strength after plating, but strength value was considerably higher than that (3.1 GPa) reported by Ishikawa et al. [12]. The higher tensile strength is attributed to the absence of a surface etching process. The tensile modulus of the plated PBO fiber was 190 GPa, which is comparable to that of the untreated one. Ni plating and Ag plating process on PBO fiber also maintained the tensile strength and Young's modulus value in the same range.

Table 5.2

Mechanical properties of pristine and plated fibers after different plating processes.

Sample		Tensile strength (GPa)	Young's modulus (GPa)	Elongation at break (%)
PBO	Pristine	5.8	200	4.25
	Cu-plated	4.9	190	3.50
	Ni-plated	4.9	180	3.25
	Ag-plated	4.8	175	3.00
PPTA	Pristine	3.6	75	4.30
	Cu-plated	3.0	70	3.50
	Ni-plated	2.9	95	2.80
	Ag-plated	2.7	70	3.00

After Cu plating, PPTA fiber showed a tensile strength of 3.0 GPa, and Ni- and Ag-plating process resulted the tensile strength of 2.9 and 2.7 GPa, respectively, which are also slightly lower than untreated one (3.6 GPa). However, tensile modulus of Ni-plated fiber (95 GPa) is little increased than that of the pristine one (75 GPa), because of high modulus on neat Ni (210 GPa) is also contributed to the modulus of the resultant plated fiber, and lessen flexibility of the fiber to some extent. The elongation of plated fiber; in every case, shows that the plated fibers exhibited less elongation at break, because of the influence of metal coated layer on fiber surface.

3.4 Light resistance of the plated fibers

The light degradation behavior of PBO fiber is a major drawback for its outdoor applications and storage. Many studies have revealed that the strength of PBO fiber decreased gradually on exposure to light sources such as UV, sunlight, xenon, and fluorescent lamps [13-16]. PPTA fiber also exhibits the same degradation phenomenon, but a bit lesser extent to PBO. The high optical reflectivity of metal layer on light sensitive fiber surface is expected to improve the light resistance of metallized fibers. Therefore, we investigated the influence of light exposure on the mechanical properties of untreated and metal plated PBO fibers under xenon lamp exposure for different periods.

Pristine and Cu-plated PBO fibers were exposed to xenon lamp for different periods and tensile strength of single filament was checked. Fig. 5.6(a) shows the dependence of the tensile strength of pristine and Cu-plated PBO fiber on different xenon lamp exposure time. The Cu-plated fiber exhibited improved light resistance. During the initial exposure time, a relatively drastic decrease in the strength was observed. After 2 days of exposure, the tensile strength of the plated fiber exceeded that of the pristine fiber. Further xenon lamp exposure resulted in a greater strength loss of the pristine PBO fiber compared with the plated fiber. After 18 days of exposure, the strength and modulus of the plated fiber were 3.6 GPa and 180 GPa, respectively. Fig. 5.6(b) shows the dependence of the tensile strength retention of the uncoated and Cu-plated PBO fibers on xenon lamp exposure time. The retention of the Cu-plated fiber is apparently higher than that of the uncoated PBO fiber after the same exposure time. After 18 days of exposure, the untreated fiber retained only 43% of its initial strength whereas the Cu-plated fiber retained 74%.

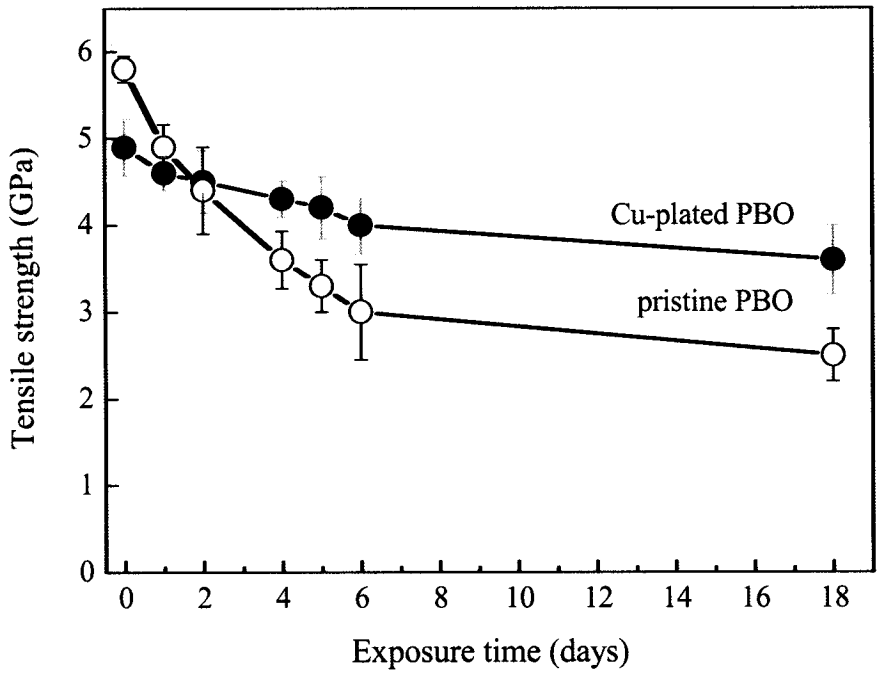

(a)

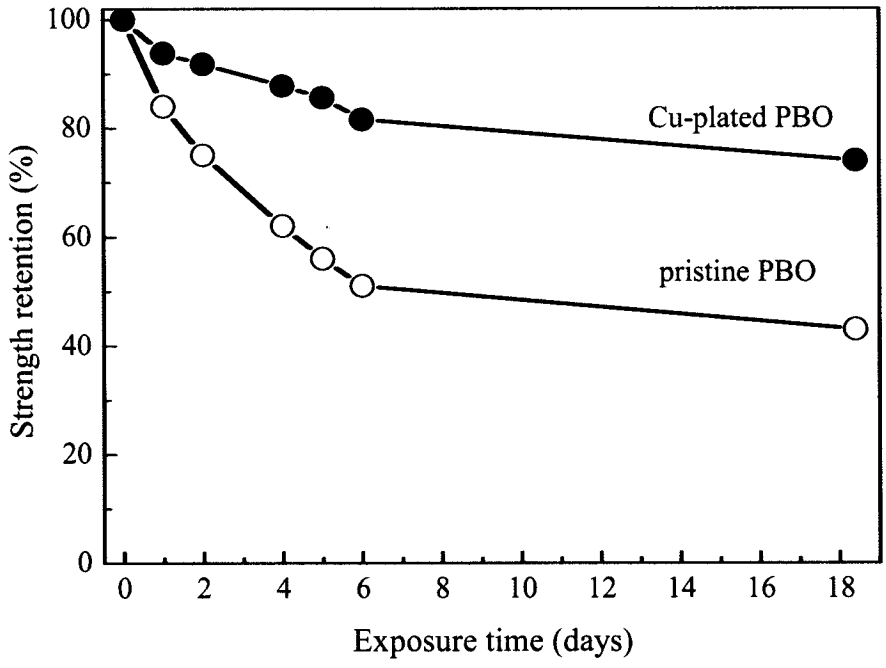

(b)

Fig. 5.6 Dependence of (a) tensile strength, and (b) strength retention of pristine and Cu-plated PBO fibers on xenon lamp exposure time.

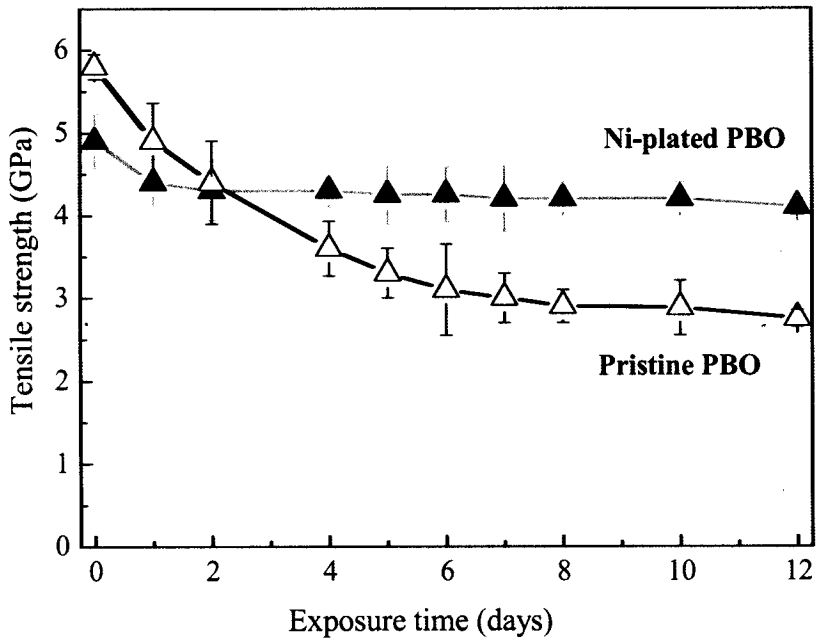

(a)

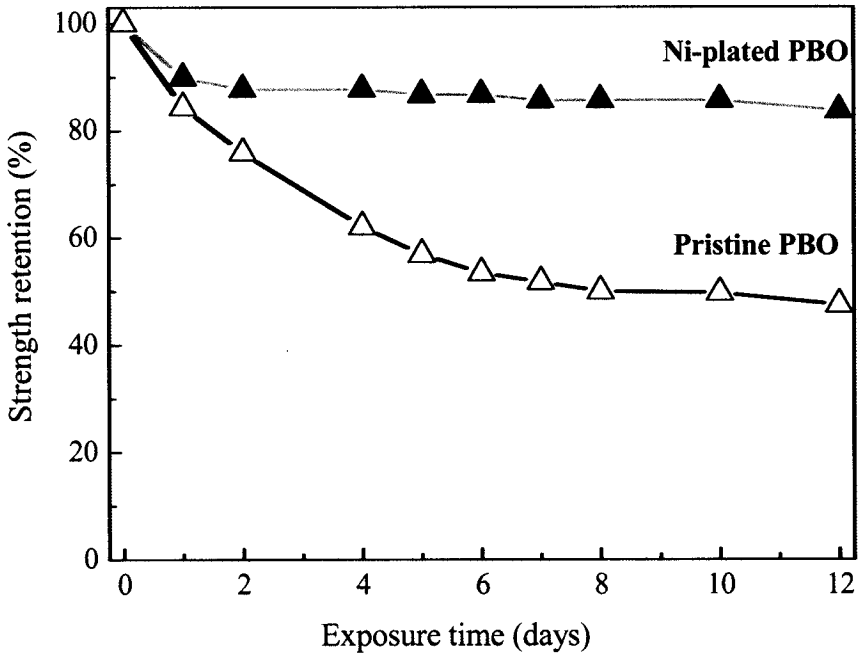

(b)

Fig. 5.7 Dependence of (a) tensile strength, and (b) strength retention of pristine and Ni-plated PBO fibers on xenon lamp exposure time.

Moreover, PBO fiber after Ni plating was exposed under xenon lamp and strength retention was calculated. The Ni-plated PBO fiber retained about 84% of its initial strength after 12 days of xenon lamp exposure, while untreated fiber retained only 47% of its initial strength on same exposure period. The coated layer of Cu and Ni metal prevent light from entering to the fiber; therefore, the degree of chain scission in the fiber surface was assumed to be reduced. Although complete prevention was not achieved, the availability of intact metal plating via the iodine pretreatment procedure was elucidated.

3.5 Magnetic properties of the plated fibers

The magnetic properties of the Ni-plated fibers are characterized using VSM. The magnetization hysteresis loops of Ni plated PBO and PPTA fibers measured at room temperature (300 K) revealed typical ferromagnetic behavior as shown in Fig. 5.8.

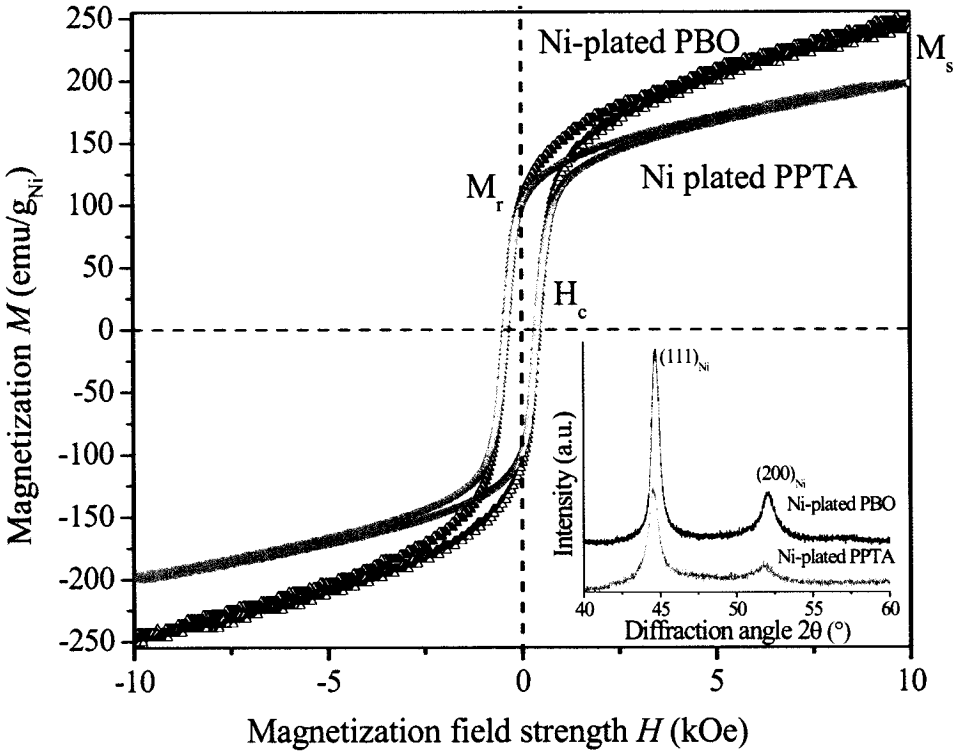

Fig. 5.8 Hysteresis loops of Ni-plated high performance fibers. (WAXD profiles of Ni plated PBO and PPTA fiber are in inset)

The ferromagnetism of Ni particles on plated fiber PPTA is clearly indicated by the value of coercivity (H_c), saturation magnetization (M_s) and remanent magnetization (M_r). For PPTA and PBO fibers, the H_c, M_s and M_r values are obtained as 389 Oe, 197.1 emu/g, 97.9 emu/g, and 400 Oe, 248.8 emu/g and 109.4 emu/g, respectively. The M_s of plated fibers is about one third and H_c is much higher than the respective value of bulk metals (58.57 emu/g and 0.7 Oe, respectively) [17]. The excellent saturation magnetization and high value of coercivity indicates its perfect crystalline structure and hard magnetic characteristics, respectively [18,19]. Though both plated fibers posses same plate layer thickness of 500-700 nm, the variation of saturation magnetization value indicates the most ordered structure of Ni (111) on the surface of plated PBO fiber (from inset image). Therefore, functional magnetic properties of plated fiber explore many special applications possibilities like in information storage module or flexible magnets and can broaden the application range of high performance PBO and PPTA fibers.

4. Conclusions

The performance of different electroless plating on PBO and PPTA fiber surface using Cu, Ni metal reflect a strongly adhered and durable plated layer, which verifies that the high durability of the plated layer was because of the Pd or Ag particles that serves as an anchor for the plated layer as well as a catalyst. Further, metal plated fibers showed a good electrical conductivity that sustained even after several durability tests. High values of tensile modulus and strength were also observed after each kinds of plating process. Although the tensile strength of the used fibers decreased a bit from their original strength after undergoing the pretreatment and plating processes, the light shielding effect improved the light resistance of the plated PBO fibers in terms of tensile properties. After 2 days of xenon lamp exposure, the tensile strength of the plated PBO fiber became higher than that of the unplated one. Finally, the plated fiber retained 74% of its initial strength for Cu-plated PBO, whereas the strength retention of the untreated fibers decreased to 43% after 18 days of exposure. Ni-plated PBO fiber also showed improved light resistance characteristics upon exposure to xenon lamp for a period of 12 days. So, light shielding by the metal layer protected the PBO fiber against light degradation, which enhances the

credibility of the high-performance fibers in terms of mechanical properties. Furthermore, nickel plated fibers shows excellent magnetic properties.

5. References

[1] Ohno I, Electroplating chemistry of electroless plating, Mater Sci Eng A, 146, 39–49 (1991).

[2] Jack WD, Electrodeposition: the material science of coatings and substrates, Noyes Pub, New York, USA (1993).

[3] June JB, Seo MS, Cho SH, Synthesis of monodisperse nickel-coated polymer particles by electroless plating method utilizing functional polymeric ligands, J Appl Polym Sci Phys, 44(6), 3801 (2005).

[4] Mallory GO, Hajdu JB, Electroless Plating-Fundamentals and Applications, William Andrew Pub/Noyes, New York, USA (1990).

[5] Chen BH, Hong L, Ma Y, Ko TM, Effect of surfactants in an electroless nickel-plating bath on the properties of Ni-P alloy deposits, Ind Eng Chem Res, 41, 2668–2678 (2002).

[6] Line up catalogue, Resistivity meter series, Mitsubishi Chemicals Group, 2007 p.3–4. http://www.dins.jp/dins_e/1prdcts/pdf/Cat%200704-LP2000US_em.pdf (last accessed Feb 10, 2011)

[7] Martinez M, Hisada K, Tabata I, Hirogaki K, Yonezawa S, Hori T, The effectiveness of thermal treatment for development of conductive metallized aramid fiber using supercritical fluid carbon dioxide: Fiber-metal adhesive strength improvement, J Supercritical Fluids, 56(3), 22–329 (2011).

[8] Zhao X, Hirogaki K, Tabata I, Okubayashi S, Hori T, A new method of producing conductive aramid fibers using supercritical carbon dioxide , Surf Coat Technol, 201(3–4), 628–636 (2006).

[9] Belmas M, Tabata I, Hisada K, Hori T, Supercritical fluid-assisted electroless copper plating of Aramid film: The influence of surface treatment, Sen'i Gakkaishi, 66(9), 215–219 (2010).

[10] books.mcgraw-hill.com/EST10/site/.../ElectricalConductivityOfMetals.pdf, Macgraw-hill, pp.207-211. (last accessed March 1, 2011)

[11] Rossiter PL, The Electrical Resistivity of Metals and Alloys, Cambridge solid state science series, Monash University, Victoria p.137–271 (1987).

[12] Ishikawa H, Chen Q, Bin Y, Komatsu K, Matsu M, High electrical conductivity and high corrosion resistance fibers with high modulus and high strength prepared by electroless plating of gold on the surface of poly (p-phenylene benzo-bisoxazole) (PBO), J Mater Sci, 42, 7772–7779 (2007).

[13] Zylon technical information guide, Toyobo Co. Ltd., (2001).
http://www.toyobo.co.jp/e/seihin/kc/pbo/menu/fra_menu_en.htm (last accessed Jan 22, 2011)

[14] Technical Guide: Kevlar® Aramid fiber, Dupont.

[15] Chin J, Forster A, Clerici C, Sung L, Oudina M, Rice K, Temperature and humidity aging of poly(p-phenylene-2,6-bemzobisoxazole) fibers: Chemical and physical characterization, Polym Degrad Stab, 92, 1234–1246 (2007).

[16] Forster AL, Pintus P, Messin GHR, Rilley MA, Petit S, Rossiter W, Chin J, Rice K, Hydrolytic stability of polybenzobisoxazole and polyterephthalamide body armor, Polym Degrad Stab, (2010) doi:10.1016/polymdegradstab.2010.10.004

[17] Wohlfatrh EP, Ferromagnetic Materials, North-Holland, Amsterdam, 1, p.20 (1980).

[18] Chikazumi S, Physics of magnetism, Chapter 1, Wiley & Sons, New York, USA, p19 (1964).

[19] Wu H, Zhang R, Lui X, Lin D, Wei P, Electrospinning of Fe, Co, and Ni nanofibers: synthesis, assembly, and magnetic properties, Chem Mater, 19, 3506–3511 (2007).

Chapter 6

Conclusions

This dissertation deals with the utilization of iodine for the fabrication of functional carbon fiber and the functionalizations of high performance fibers. Carbon nanofibers and hollow carbon fiber (H-CFs) were fabricated from poly(vinyl alcohol) (PVA) fibers using iodine pretreatment. Further, iodine pretreatment was utilized for the metallization of high performance fibers (HPFs) such as poly(p-phenylene benzobisoxazole) (PBO) and poly(p-phenylene terephthalamide) (PPTA) to incorporate new functionalities and protect existing properties as well. The functionality of the resultant HPFs defines their properties and applications in many advance fields. The concept of fabrication and functionalization technique of high performance fibers using iodine were explored in different chapters of this thesis and the main results are summarized as follows.

First of all, an overview of iodine and functionalization processes are described in brief as general introduction in Chapter 1. It also discloses the strategies of iodine utilization techniques for fabrication of carbon fibers from PVA fibers and functionalizations of HPFs.

Chapter 2 reports the manufacture of neat PVA nanofibers by electrospinning and subsequent fabrication of carbon fibers from the electrospun PVA nanofibers. First, electrospun PVA nanofibers were treated with iodine vapor for different periods, and followed by carbonization at different temperatures, and then structural changes of the derived carbon fibers were investigated. The optimization of the pretreatment process was performed to form carbon fibers with graphite structure. The PVA nanofiber iodinated for 24 h at 80 °C and carbonized at 1200 °C leads to a stable carbon fiber with good carbon yield. The influence of metal nanoparticles on the fabrication of carbon fiber and its properties was also investigated by addition of metal salt, nickel (II) acetate tertrahydrate, to the PVA spinning solution. Incorporation of metal Ni nanoparticles developed the graphitic structure at lower carbonization temperature and .improved the yield of resultant carbon fiber.

In Chapter 3, the author explores the idea of previous chapter and focuses on the fabrication of carbon hollow fibers from solid PVA fibers. Iodination converted the chemical structure of PVA to polyene form due to promotion of dehydration reaction, and stabilization of heat treatment at 200 °C in air provided infusibilization of iodinated PVA fibers. These processes extremely enhanced the carbon yield and enabled to obtain carbon fiber. The hollow structure was formed by selective iodination and subsequent stabilization

of the precursor PVA fiber close to the fiber surface followed by carbonization. The influence of heating conditions on the structure of hollow carbon fibers (H-CFs) during their fabrication from solid poly(vinyl alcohol) (PVA) fibers is reported. The broadening of X-ray diffraction peaks due to disorder and the small-size effects of the (002) plane decreased significantly as the heat treatment temperature (HTT) increased from 800 to 3000 °C, but the asymmetric shape of the (10) and (110) reflections suggests turbostratic layer stacking. The increase of HTT to 3000 °C increased the degree of graphitization, as evidenced by the decrease in the interplanar spacing from 0.360 to 0.338 nm and in the intensity ratio of D to G bands in the Raman spectra from 0.93 to 0.58. The crystallite size, orientation and electrical conductivity of the resultant H-CFs also improved with increasing HTT. Furthermore, the size of the hollow was influenced by the HTT, and both the wall thickness and carbon yield decreased with increasing HTT. The core of the H-CFs could be easily filled with polymer by bulk polymerization of the monomer.

Chapter 4 illustrates a highly durable electroless plating process on PBO and PPTA fibers through iodine pretreatment process is reported. The catalyzation processes using Pd or Ag nuclei were investigated. First, iodine components were selectively doped into the inner part near the fiber surface using aqueous solution or iodine vapor treatment. Doped iodine resided as polyiodide ions such as I_3^- and I_5^- and converted to respective metal iodide particles by treating with palladium chloride or silver nitrate solution. After reduction of metal iodides to respective metals, electroless plating was carried out and a highly adhesive and durable plated layer was achieved on fiber surface. The metal particles formed at the inner part near the fiber surface function as an anchor for the plated layer as well as a catalyst for electroless plating. Investigation of plate bath conditions showed that the pH and temperature of plating solution determine the plating rate and the morphology of the layer. Further investigation revealed that the use of an anionic surfactant during the catalyzation process enhanced the adhesion of the plated layer.

In Chapter 5, the performances of differently metal plated PBO and PPTA fibers were evaluated. The adhesion durability of plated layer was investigated in terms of ultrasonic peeling, tape peel-off and corrosion resistance in NaCl solution. The electrical conductivity and magnetic properties of plated super fibers were also evaluated. Although the tensile strength of the plated HPFs somewhat decreased after undergoing the pretreatment and

plating processes, the light shielding effect improved the light resistance of the plated fibers in terms of tensile properties. The Cu- and Ni-plated PBO fibers showed significant improvement of light resistance against xenon lamp exposure.

Parts of this thesis are published, submitted to be published or presented at conferences:

List of publications

1. Iodine-aided fabrication of hollow carbon fibers from solid poly(vinyl alcohol) fibers. Ummul Khair Fatema, Chiemi Tomizawa, Masaru Harada, Yasuo Gotoh. Carbon, 49(6), p2158–2161 (2011).
2. Fabrication of carbon fibers from electrospun poly(vinyl alcohol) nanofibers. Ummul Khair Fatema, Ahmed Jalal Uddin, Keita Uemura, Yasuo Gotoh. Textile Research Journal, 81(7), p659–672 (2011).
3. Highly adhesive metal plating to Zylon® fiber utilizing iodine pretreatment. Ummul Khair Fatema, Yasuo Gotoh. Applied Surface Science, under revision.
4. Influence of heat-treatment conditions on the structure of hollow carbon fibers prepared from solid PVA fibers using iodine pretreatment. Ummul Khair Fatema, Fujio Okino, Yasuo Gotoh. Carbon, submitted.
5. A new electroless Ni plating procedure on iodine treated Aramid fiber. Ummul Khair Fatema, Yasuo Gotoh. Journal of Coatings Technology and Research, submitted.
6. Iodine-aided palladium-free catalyzation process for durable electroless nickel plating on Kevlar® fiber. Ummul Khair Fatema, Yasuo Gotoh. Surface and Coatings Technology, submitted.

Conference presentations

1. Functionalization of high strength super fibers using metal iodide. Ummul Khair Fatema, Yasuo Gotoh. The 2nd international workshop of the DAAD alumni network, Dhaka, Bangladesh, 3 (February 16, 2010).
2. Metal plating on high performance fibers using iodine. Ummul Khair Fatema, Terutoshi Ishikawa, Yasuo Gotoh. Fiber Preprints, The society of fiber science and technology, Japan , 65(1), 243 (June 16, 2010).